Characterization of thylakoid membrane in a heterocystous cyanobacterium and green alga with dual-detector fluorescence lifetime imaging microscopy with a systematic change of incident laser power

Shuho Nozue[1], Akira Mukuno[1], Yumi Tsuda[1],Takashi Shiina[2], Masahide Terazima[1], and Shigeichi Kumazaki[1]*

[1] Department of Chemistry, Graduate School of Science, Kyoto University, Kyoto, 606-8502, Japan.

[2]Graduate School of Life and Environmental Sciences, Kyoto Prefectural University , Sakyo-ku, Kyoto 606-8522 , Japan.

*Corresponding author: e-mail: (S.K.) kumazaki@kuchem.kyoto-u.ac.jp

Corresponding author

Shigeichi Kumazaki, Ph.D.

Department of Chemistry, Graduate School of Science, Kyoto University

Kyoto 606-8502, Japan

Tel: +81-75-753-4023

Fax: +81-75-753-4000

E-mail: kumazaki@kuchem.kyoto-u.ac.jp

Biochimica et Biophysica Acta 1857 (2016) 46–59

http://dx.doi.org/10.1016/j.bbabio.2015.10.003

Article history:

Received 3 June 2015

Received in revised form 29 September 2015

Accepted 11 October 2015

Available online 22 October 2015

Keywords:
Photosystem II, Photosystem I, Chlorophyll fluorescence, Fluorescence lifetime imaging microscopy, Heterocystous cyanobacteria, Green algae

Abbreviations:

APC: allophycocyanin, light-harvesting subunit of phycobilisome.
CF: chlorophyll fluorescence.
CFL: chlorophyll fluorescence lifetime.
Chla, Chlb: chlorophyll a, chlorophyll b.
CP26, CP29; light-harvesting complex of photosystem II.
FL: fluorescence lifetime.
FLIM: Fluorescence Lifetime Imaging Microscopy.
FWHM: full width at half maximum.
IRF: instrument-response function.
LHCI: light-harvesting complex of photosystem I.
LHCII: light-harvesting complex of photosystem II.
NPQ: nonphotochemical quenching.
PAM: Pulse-amplitude-modulation fluorometry.
PBS: phycobilisome.
PC: phycocyanin, light-harvesting subunit of phycobilisome
PEC: phycoerythrocyanin, light-harvesting subunit of phycobilisome.
PSI, PSII: photosystem I, photosystem II.
Q_A: electron acceptor quinone in photosystem II.

A**bstract**

Fluorescence Lifetime Imaging Microscopy (FLIM) has been applied to plants, algae and cyanobacteria, in which excitation laser conditions affect the chlorophyll fluorescence lifetime due to several mechanisms. However, the dependence of FLIM data on input laser power has not been quantitatively explained by absolute excitation probabilities under actual imaging conditions. In an effort to distinguish between photosystem I and photosystem II (PSI and PSII) in microscopic images, we have obtained dependence of FLIM data on input laser power from a filamentous cyanobacterium *Anabaena variabilis* and single cellular green alga *Parachlorella kessleri*. Nitrogen-fixing cells in *Anabaena variabilis*, heterocysts, are mostly visualized as cells in which short-lived fluorescence (≤ 0.1 ns) characteristic of PSI is predominant. The other cells in *Anabaena variabilis* (vegetative cells) and *Parachlorella kessleri* cells show a transition in the status of PSII from an open state with the maximal charge separation rate at a weak excitation limit to a closed state in which charge separation is temporarily prohibited by previous excitation(s) at a relatively high laser power. This transition is successfully reproduced by a computer simulation with a high fidelity to the actual imaging conditions. More details in the fluorescence from heterocysts were examined to assess possible functions of PSII in the anaerobic environment inside the heterocysts for the nitrogen-fixing enzyme, nitrogenase. Photochemically active PSII:PSI ratio in heterocysts is tentatively estimated to be typically below our detection limit or at most about 5 % in limited heterocysts in comparison with that in vegetative cells.

(246 words)

1. Introduction

All chemical energy in the biosphere on Earth is mostly attributable to photosynthesis, the primary step of which is a conversion from a solar photon to transmembrane charge separation in chloroplasts of plants and algae or some photosynthetic prokaryotes including cyanobacteria. Although most of the absorbed photons by photosynthetic pigments are used to drive the charge separation and subsequent synthesis of energy-rich chemicals, some minor portion of photons are reemitted as autofluorescence or dissipated as heat. Autofluorescence of photosynthetic pigments, especially that of chlorophyll *a* (Chla), has been thus widely and extensively monitored as an index of photosynthetic reactions in oxygenic photosynthetic organisms [1, 2]. Microscopic fluorescence images of Chla is also useful for understanding the structures and photochemical functions of thylakoid membrane in chloroplasts of plants and cyanobacterial cells under physiological conditions [3-5]. Fluorescence spectral acquisition in microscopic imaging has also been successful to obtain images of important photosynthetic molecular components like photosystem I (PSI), photosystem II (PSII), and light-harvesting molecules [4, 6-12]. However, fluorescence intensity suffers from attenuation due to absorption, refraction and scattering during transmission through the samples between focus plane of interest and microscope objective. This leads to deformation of fluorescence spectra, because the attenuation of signals is dependent on fluorescence wavelength [11].

Fluorescence lifetime (FL) measurement function has been recently implemented in laser scanning confocal fluorescence microscopy in order to obtain an image with fluorescence decay parameters in all pixels (Fluorescence Lifetime Imaging Microscopy, FLIM) [4] [13]. Time constants of fluorescence decay are robust parameters against attenuation, because they are just determined by the nature of distribution of the delay time between absorption of excitation photon and emission of fluorescence photon. The nature of the distribution is unchanged by the attenuation of the number of fluorescence photons, as far as attenuation is in a linear regime, under which propagation and transmission of the fluorescence does not depend on the fluorescence intensity.

Fluorescence decay on a picosecond to nanosecond time scale of thylakoid membrane reflects the time scales of energy conversion and/or dissipation from photons to chemical energy and/or heat. It is thus expected that FLIM can be used to a wide range of studies on thylakoid membrane in plants, algae and cyanobacteria. There are already a substantial number of applications of FLIM to study many aspects of thylakoid membrane in vivo by visible short pulses [14-17]. Two-photon excitation has also been tested in the application of FLIM to chloroplasts [18-21]. However, there still remain several uncertainties in the potential and limitations in the FLIM measurements. First, excitation power dependence of the FLIM data has not been sufficiently documented. There are hundreds of photosynthetic pigments that can exchange electronic excitation energy. It is thus possible that annihilations between multiple excited pigments (singlet-singlet, singlet-triplet etc.) can lead to an abnormally fast decay of fluorescence [18, 22, 23][24]. It is also well known that strong pulse and/or continued illumination on the same sample region can temporarily convert substantial portion of reaction centers of PSII into charge-separated state that cannot perform primary charge separation (closed PSII). The closed PSII shows a longer fluorescence lifetime (about 0.7 - 2 ns) than PSII that is ready for the primary charge separation (about 0.17 -0.4 ns, open PSII) [15, 18] [21, 25-29] [30, 31]. The effects of annihilation and the open-closed status of PSII to the actual FLIM images can be predicted only if scanning parameters of the excitation laser, absorption cross section of PSII and transition rate from closed PSII to open PSII are all properly considered. Second, contribution of PSI to the chlorohyll fluorescence (CF) at physiological temperature has not been sufficiently characterized. PSI fluorescence is most conventionally measured at cryogenic temperatures, because fluorescence quantum yield from PSI and/or its closely associated antenna like light-harvesting complex I (LHCI) in chloroplasts are relatively enhanced in comparison with that of PSII [1]. However, PSI fluorescence at physiological temperatures is not negligible [26][32, 33]. The lifetime of PSI

fluorescence (about 0.025 - 0.12 ns) is generally reported to be independent of excitation light intensity and shorter than that of PSII [26, 28, 34-36]. It is then likely that the image of PSII/PSI ratio in various chloroplasts/cells can be potentially obtained if dependence of fluorescence lifetimes on laser power is obtained. It is thus desirable to accumulate examples of FLIM measurements on various types of thylakoid membranes with different ratios of PSI/PSII.

Based on the above background, we have conducted FLIM measurements of an algal chloroplast and cyanobacterial cells with systematically varied excitation laser power. Our FLIM system has two channels of rigorously simultaneous fluorescence detection, largely corresponding to PSII and PSI. As a first test, we have avoided multicellular organisms in which it is difficult to estimate excitation power reaching a target focal plane. We have selected a filamentous diazotroph, *Anabaena variabilis (A. variabilis)*, which contains differentiated cell, heterocyst. It is well known that the PSII content in matured heterocyst is far lower than that of vegetative cells in the same filament [9, 10, 37]. It is thus expected that FL of PSI-rich thylakoid membrane in the heterocyst can be obtained and compared with that of vegetative cells having substantial PSII in addition to PSI. As a second example, a unicellular green alga, *Parachlorella kessleri* (*P. kessleri*) was selected, because it lacks motility and has chlorophyll-based light-harvesting complexes [38, 39]. Our available excitation wavelength was 404 nm, at which chlorophyll-based light-harvesting systems show far greater absorption cross section than phycobilin-based antenna, phycobilisome (PBS), of cyanobacteria. It is then likely that multiple excitation effects in the single PSI and/or PSII units are more sensitively observed in the *P. kessleri* than in *A. variabilis*. In addition, we have composed a numerical simulation that almost fully reflects all relevant parameters: absorption cross section of PSII and its associated light-harvesting complexes, decay time constants of closed PSII (recovery time constant of open PSII) and laser-scanning parameters in the actually employed FLIM conditions. The simulation can largely reproduce experimental sensitivity of the FL to the absolute laser power. As an application example of our methodology, possible indication of functional PSII in the PSI-rich heterocyst was examined in detail. There have been reports on the presence of transcripts and proteins of PSII reaction centers in isolated heterocysts [40-42]. PSII activity in heterocysts in filaments in vivo was also reported by single cell variable fluorescence intensity [5]. These observations raised a question of how oxygen-sensitive nitrogenase for the nitrogen-fixation is compatible with the function of PSII in the heterocysts. Our methodology will hopefully add one more experimental observation on this interesting issue on a single cell basis in intact filaments.

2. Experimental

A. variabilis cells (strain NIES-2095) were purchased from the microbial culture collection at the National Institute of Environmental Studies (Tsukuba, Ibaraki, Japan). The cell filaments were grown photoautotrophically in nitrogen-free BG-11 medium (removing $NaNO_3$ and replacing ferric ammonium citrate with ferric citrate in the BG-11 formulation [43]) for 3, 24, or 90 days at 29°C under a 15-h light/9-h dark photoperiod after an inoculation. The same nitrogen-free BG-11 medium was also used before the inoculation. The photosynthetic photon flux density at the sample position in an incubator was about 20 μmol photons m^{-2} s^{-1}. A cell suspension after a suitable dilution was transferred to glass-bottom dish (D111505, Matsunami, Osaka, Japan). One piece of agar was put on the cell suspension in order to immobilize cells at the surface of the cover glass. All microspectroscopic measurements were started after 15 - 20 min of dark adaptation period on the microscope stage (Table S1).

P. kessleri cells were purchased from the IAM culture collection as IAM C-531 (now maintained as NIES-2160 in the microbial culture collection, at the National Institute of Environmental Studies, Tsukuba, Ibaraki, Japan). The cells used for measurement were grown photoautotrophically in 40 cm^3 of BG-11 incubation medium in the same incubator as *A.*

variabilis for 15 or 29 days after an inoculation. The preparation for the microscopic observation was also the same as used for *A. variabilis* cells. All microspectroscopic measurements were started after 15 - 20 min of dark adaptation period on the microscope stage (Table S1).

Autofluorescence images and lifetimes of the cells were obtained by a laser-scanning confocal imaging system (DCS-120, Becker & Hickl GmbH) with time-correlated single photon counting (TCSPC) boards (SPC-152, Becker & Hickl GmbH). The glass-bottom dish containing cells was mounted on an inverted microscope (IX-71, Olympus), with which the confocal scanner (DCS-120) was coupled. Photosynthetic pigments were excited by the second harmonic beam (404 nm) of a mode-locked Ti:Sapphire oscillator (Coherent) with a repetition rate of 75.5 MHz. Two detection channels with band-path filters (673 − 698 nm and 703 − 740 nm) were simultaneously used to see mainly CF, which largely corresponds to PSII and PSI. The wavelength regions were optically selected by combinations of a long-wavelength-passing beam splitter (with an edge wavelength at 700 nm) and two band-pass filters. Residual laser light was rejected by long-wavelength-passing filter with an edge wavelength at about 500 nm. The obtained datasets of FL images were analyzed using image analysis software (SPCImage, Becker & Hickl GmbH), and some kinetic traces of selected regions were fitted by Igor Pro (version 6, e.g., Fig. S1−S5). Images at different depth positions were obtained by using a piezo actuator for changing the focus of an oil-immersion microscope objective (Olympus UPLSAPO, 100XO, NA = 1.40). The excitation intensity of the laser was automatically controlled by a filter wheel with neutral density filters of different transmissions. A laser power of 20 nW at the sample position was confirmed by a power meter (PD-300-SH & NOVA, Ophir), and weaker laser powers were achieved by the filters of known transmission at 404 nm. Confocal pinhole sizes for the two fluorescence bands were manually changed between FLIM acquisitions at different laser powers (Table S1), by which the maximal probability of detection of fluorescence photons per single excitation pulse was limited to at most 3×10^{-3} at the brightest spot in fluorescence images. It is thus to be noted that fluorescence counts at different laser powers cannot be directly compared. (Figs. S2− S5). The instrument-response function (IRF) was 0.08±0.015 ns at 689 nm and 0.10±0.015 ns at 716 nm in full width at half maximum (FWHM). One test on time resolution is shown in Fig. S1. The curve with a time constant of 0.084 ns obtained in the constraint-free fitting is clearly better than that in the constrained fitting with a fixed time constant of 0.050 ns. As far as our data analysis is based on data with a comparable s/n or better, the distinguishability of the time constant is at worst about 0.03 ns (30 ps).

3. Results

3.1. *Fluorescence lifetime imaging*

FLIM measurements at varied laser intensities of *A. variabilis* were performed on 22 filaments of cells (or trichomes) including a total of about 190 vegetative cells and 22 heterocysts. One set of data is shown in Fig. 1. The cells in the image panels are all vegetative cells except one heterocyst indicated by white (Figs. 1(a) - 1(o)) or black (Fig. 1(s)) arrow heads. Three levels of excitation laser power, 0.08, 1.1 and 20 nW at the sample position were employed in this order (Table S1) in one set of experiments on 6 filaments containing 6 heterocysts that were 90 days after inoculation (Tables S2,S3). Five levels of excitation laser power, 0.08, 0.30, 1.1, 5.3 and 20 nW at the sample position were also analogously employed in this order in the other two independent sets of experiments on filaments harvested 3 and 24 days after inoculation (7 and 9 filaments containing 7 and 9 heterocysts, respectively)(Tables S2, S3). In order to check damage or any long-lived actinic effects of previous laser scans on the sample, a FLIM measurement with the lowest power at 0.08 nW was

always repeated after the measurement at the highest laser power (Fig. S2,S3**,** Table S1). Average FL at each pixel,$<\tau>$, was calculated according to the following formulae,

$$F(t) \approx \int_{-\infty}^{+\infty} IRF(s) \left\{ \begin{array}{ll} A_0 + A_1 \exp\left[-\frac{(t-s)}{\tau_1}\right] + A_2 \exp\left[-\frac{(t-s)}{\tau_2}\right] & , \quad t \geq s \\ 0 & , \quad t < s \end{array} \right\} ds \quad , \quad \text{(eq. 1)}$$

$$\langle \tau \rangle = (A_1\tau_1 + A_2\tau_2)/(A_1 + A_2), \quad \tau_1 < \tau_2 \ , \qquad \text{(eq. 2)}$$

where temporal profile of fluorescence intensity at the pixel, *F*(t), was fitted by convolution of a sum of two exponential functions with the instrument-response function, *IRF*(*s*), (as eq. 1). The fitting yielded exponential decay time constants, τ_1 and τ_2, and their amplitudes, A_1 and A_2, in addition to a non-decaying component, A_0. Our measurement time window was only between minus 0.3 ns and plus 2.7 ns, and the pulse-to-pulse interval in the excitation laser was 13.24 ns. The amplitude of A_0 thus suggests a long-lived fluorescence with an approximate lifetime between 2 and 13 ns. A_0 was always set to be zero in the SPCimage analysis program. When fluorescence decay profiles were later extracted from certain specified areas of cells, amplitude of A_0 were set to be non-negative and they were typically 0 −1 % or at most 2− 3% in a very few cases with a relatively poor s/n, which does not affect our following discussion (Tables 1−3 and S2 − S4). In using the SPCimage analysis program for *A. variabilis*, a binning of pixels was performed in which photon data in 11 × 11 raw pixels (square region of about 1.94 × 1.94 μm) were all included to obtain a fluorescence decay profile at the center pixel. This binning was employed at all the laser power levels, which enabled us to obtain the color-coded images of average FL of cells even at the weakest laser power employed. However, it caused degradation of apparent spatial resolution in the average FL map. As the laser power is increased, the lifetimes in the whole filament except the heterocyst are elongated. At the weakest laser power of 0.08 nW, the most frequent average FL obtained at 689 nm is around 200 ps (Fig. 1(p)). The average FL at 689 nm given by the middle (1.1 nW) and strongest laser power (20 nW) are 300 and 570 ps, respectively (Figs. 1(q) and 1(r)). This elongation of average FL is evident in all the vegetative cells in both the two detection channels (689 and 716 nm). The FL of the heterocysts does not show obvious elongation. It is to be noted that contribution of the heterocyst to the lifetime histogram is recognized as a small peak around 0.08 − 0.09 ns and 0.12 − 0.13 ns in the cases of 689 nm and 716 nm, respectively (Figs. 1(q) and 1(r)).

Multi-exponential nature of the fluorescence decay is not visualized in the map of average FL like Fig.1. Photon counting data, which are photon counts versus arrival times, were separately collected from the vegetative cells and heterocyst, which gave fluorescence decay traces (Figs. 2(a)-2(c), S2-S4). Before the curve fitting by eq. 1, average photon counts in the sufficiently negative time region (For example, 5 −10 and 3 − 19 counts per time channel in the 689 and 716 nm wavelength channels, respectively, for the traces shown in Fig. S2) was subtracted. It is thus possible that artificially negative photon counts arise (Figs. 2, S2−S5). These counts at negative times remained in the above-mentioned range even when the laser power was increased by 200 times. It is thus unlikely that the subtracted counts are attributable to short-lived laser-induced transient phenomena in samples (<10 s). These small signals are thus not considered in this work. All types of fluorescence traces in the two cellular types (heterocysts or vegetative cells), with the two center wavelengths of detection (689 or 716 nm), and with the three or five different laser intensities were fitted by the sum of two

decaying exponential components (eq. 1, Table 1, 2, Figs. 2, S2-S4). When the two exponential time constants are not separated well due to intrinsic nature of the decay and/or signal-to-noise, single decaying exponential function was used. The judgment was also supported by the reduced chi square values (Fig. S2-S4). Although some reduced chi square values are substantially larger than 1, we focus on the approximate description of the whole data by at most two exponential functions, which is mainly for the consistency with the simulation framework (See section 3.2 and 4.6). It is to be noted that the short lifetime component of vegetative cell is limited in a very narrow range (0.22 - 0.26 ns in Table 1), which seems to be independent of the center wavelength of the fluorescence detection and the excitation laser powers employed, even though we did *not* impose any linkage of parameters (so-called globally common parameters) in the curve fitting between the different fluorescence traces. This lifetime is in good agreement with the most dominant component observed in an ensemble of cells of *A. variabilis* (0.22 ns and 85 %) [44]. It is also largely comparable to CFL observed in other cyanobacteria at room temperatures (Table S6)[34, 36, 45-47]. The average FL of the vegetative cell gradually increases as the excitation power is raised, which is caused by the increase of the long lifetime component with time constants of 0.74 - 1.09 ns and 0.85 - 1.13 ns at the detection wavelengths of 689 and 716 nm, respectively (Fig. 2(a), Table 1, Fig. S2). These behaviors are largely consistent with those reported in another cyanobacterium *Synechococcus* 6301 by raising the level of closed PSII [46].

In the sum of FLIM data of all 22 heterocysts, at least 94 % of its fluorescence decays with a time constant of 0.080 - 0.089 ns and 0.14 ns at 689 and 716 nm, respectively, at all the excitation powers (Table 2, Fig. S2). There is a minor long-lived component with a time constant of 0.86 - 1.03 ns. Since single-cell fluorescence spectra and photochemical behavior changes during differentiation process [5, 9, 10, 48, 49], it is likely that FLIM data from randomly selected heterocyst are heterogeneous, which may reflect developmental stage or age of each heterocyst. The 22 heterocysts that we analyzed were classified into two subsets (17 and 5 heterocysts) based on an approximate single-exponential curve fittings of the 689 nm fluorescence kinetics of individual heterocysts at the highest laser power (20 nW). The lifetimes of 689 nm fluorescence kinetics of the first subset (17 heterocysts) are shorter than those of the second one (5 heterocysts). The former and the latter subsets are designated as subset/w/o (without a substantial long-lived component) and subset/w/ (with a substantial long-lived component). Sum of photon data were separately prepared from the two subsets (Fig. 2(b) and (c), Table 2, Fig. S4). The subset/w/ has a long-lived component even at the weakest laser power (0.57 ns, 8%) that was distinguishable from infinitely long-lived component (with an approximate time constant of 2 - 13 ns) and the amplitude of the long-lived component was constantly greater than those of the subset/w/o at all power levels (Table 2).

Excitation power dependence of FLIM in the case of *P. kessleri* were obtained for 32 cells at excitation laser powers that were about one order of magnitude weaker than those of *A. variabilis* (Figs. 2(d), 3, S5, Table 3). Example of one data set, in which three cells were imaged at the same time, is shown in Fig. 3. The color-coded average FL image for the *P. kessleri* cells was obtained with a binning of 21 × 21 raw pixels (square region of about 3.7 × 3.7 μm). Three or five levels of excitation laser power, (4, 55 and 1.0×10^3 pW or 4, 15, 55, 265 and 1.0×10^3 pW) at the sample position were employed in this order (Table S1). In order to check damage or any long-lived actinic effects of previous laser scans on the sample, FLIM measurement with the lowest power at 4 pW was repeated after the measurement at the highest laser power (Fig. S5), which have shown essentially the same results as the first ones with the same power. One of the three cells (cell no. 2 in Fig. 3(m)) showed clearly longer average FL than the other two cells (cell no. 1 and 3 in Fig. 3(m)). Such a cell with exceptional lifetime was not included as the target cells of fine analysis on the fluorescence decay profiles. An elongation of the average FL was evident especially between 55 and 265 pW (Tables 3 and S4). The shortest lifetime observed in the

case of *P. kessleri* was about 0.28-0.33 ns at 689 nm, which was always longer than that of the vegetative cells of *A. variabilis* (0.22-0.26 ns) (Figs. 1, 2, and Table 1).

3.2. *Simulation on open-closed state of PSII under the FLIM imaging conditions*

Although it seems to be well established that open and closed PSII show relatively short (0.1 - 0.4 ns) and long fluorescence lifetimes (0.8 - 2 ns), [15, 21, 25, 28] [29][26, 27, 31] [30] (See also Table S5 and S6 for more references), how the components appear in fluorescence kinetics under actual FLIM experimental conditions has remained unexplained in a sufficiently quantitative manner. The purpose of the computer simulation described here is to quantitatively support our hypothesis that double exponential decay observed in our FLIM measurements in vegetative cells of *A. variabilis* and *P. kessleri* (Tables 1, 3, S2, S4) is a result of observing fluorescence from both open and closed PSII. Only an outline of the simulation is presented below and the details are fully described in Text S1.

The experimentally obtained fluorescence decay is made of fluorescence from many PSII units in the cells, but this situation is equivalently expressed by a single representative PSII unit at the position (x,y,z) = (0,0,0) with full description on the probability of open/closed status (Fig. S6 and Text S1). In the simulation, a laser beam focus is moved in a manner of raster scan around the PSII, as in the experiments. Excitation probability of the PSII unit by a single laser pulse is assumed to be given by the single pulse laser energy, a Gaussian laser intensity profile, position of the laser focus, and an effective absorption cross section of PSII at the laser wavelength (404 nm) (Fig. S6 and Text S1). Once the PSII in the open state is optically excited, it is converted into a closed PSII with a probability of the photosynthetic charge separation. The time-dependent populations of open PSII and closed PSII in a unit volume, $N_{\mathrm{open}}(t_{\mathrm{m}})$ and $N_{\mathrm{closed}}(t_{\mathrm{m}})$, or their proportional quantities that are probabilities for the PSII to be open or closed, $p_{\mathrm{open}}(\mathrm{t})$ or $p_{\mathrm{closed}}(\mathrm{t})$, are calculated as follows (Text S1).

$$\begin{aligned}\begin{bmatrix} N_{\mathrm{open}}(t_{m+1}) \\ N_{\mathrm{closed}}(t_{m+1}) \end{bmatrix} &= \begin{bmatrix} N_{\mathrm{PSII}} p_{\mathrm{open}}(t_{m+1}) \\ N_{\mathrm{PSII}} p_{\mathrm{closed}}(t_{m+1}) \end{bmatrix} = N_{\mathrm{PSII}} \begin{bmatrix} p_{\mathrm{open}}(t_{m+1}) \\ 1 - p_{\mathrm{open}}(t_{m+1}) \end{bmatrix} \\ &= N_{\mathrm{PSII}} \begin{bmatrix} 1 - 0.80\, p_f(j_y(t_m), j_x(t_m)) & \{1 - \exp[-(t_{m+1} - t_m)/\tau_{\mathrm{R}}]\} \\ 0.80\, p_f(j_y(t_m), j_x(t_m)) & \exp[-(t_{m+1} - t_m)/\tau_{\mathrm{R}}] \end{bmatrix} \begin{bmatrix} p_{\mathrm{open}}(t_m) \\ 1 - p_{\mathrm{open}}(t_m) \end{bmatrix}, \end{aligned} \qquad \text{(eq. 3)}$$

where t_{m} and $t_{\mathrm{m+1}}$ represent a time in the simulation and its subsequent time, respectively, N_{PSII} the total population of PSII in a unit volume (assumed to be constant), $p_{\mathrm{f}}(j_{\mathrm{y}}(t_{\mathrm{m}})$ and $j_{\mathrm{x}}(t_{\mathrm{m}}))$ the probability for the PSII to be excited by the laser pulses between t_{m} and $t_{\mathrm{m+1}}$, $j_{\mathrm{y}}(t_{\mathrm{m}})$ and $j_{\mathrm{x}}(t_{\mathrm{m}})$ are x (horizontal-axis) and y (vertical-axis) interger coordinates with a unit length of 25 nm of the laser beam at the time t_{m}, respectively, τ_{R} the time constant for the closed PSII to be converted back into open state. The excitation probability function, p_{f} in eq. 3 (and in eqs 4 - 5 (*vide infra*)), is set to be two-dimensional Gaussian and non-zero only when $-10 \leq j_{\mathrm{y}}(t_{\mathrm{m}}) \leq +10$ and $-10 \leq j_{\mathrm{x}}(t_{\mathrm{m}}) \leq +10$. This means that PSII is excited only when the laser spot resides in the square of a side length of 500 nm that is centered at PSII (See Supplemental Fig. S6 and Text S1). Closed PSII is set to be generated from the optically excited PSII supercomplex with a probability of 0.80, which is the most typical parameter $F_{\mathrm{v}}/F_{\mathrm{m}}$ of dark adapted chloroplasts in the pulse-amplitude-modulation fluorometry (PAM)[50-52]. The same yield was also applied to the case of *A. variabilis*, because similar $F_{\mathrm{v}}/F_{\mathrm{m}}$ values are obtained in phycobilisome-lacking and/or PSII-enriched cyanobacterial mutants [53, 54]. The numbers of fluorescence photons from open and closed PSII units are proportional to the populations of open PSII and closed PSII before each excitation, respectively. Thus, the

experimentally obtained ratios of short-lived and long-lived fluorescence components were compared with the following time-integrated sum of the product between excitation probability and populations of open and closed PSII units at each simulation time, respectively.

$$F_{\text{open, accum}} \propto \sum_{s=1}^{2\text{or}3}\sum_{k=1}^{29}\sum_{i=N_{y1}}^{N_{y2}}\sum_{j=-N_x}^{+N_x} p_f\left(7i+\left\{\Delta_{\text{offset}}/25\right\}, j\right) N_{\text{PSII}}\, p_{\text{open}}(t_{j,i,k,s}) = N_{\text{PSII}}\sum_{s=1}^{2\text{or}3}\sum_{k=1}^{29}\sum_{i=N_{y1}}^{N_{y2}}\sum_{j=-N_x}^{+N_x} p_f\left(7i+\left\{\Delta_{\text{offset}}/25\right\}, j\right) p_{\text{open}}(t_{j,i,k,s}) \quad \text{(eq. 4)}$$

$$F_{\text{closed, accum}} \propto \sum_{s=1}^{2\text{or}3}\sum_{k=1}^{29}\sum_{i=N_{y1}}^{N_{y2}}\sum_{j=-N_x}^{+N_x} p_f\left(7i+\left\{\Delta_{\text{offset}}/25\right\}, j\right) N_{\text{PSII}}\left\{1-p_{\text{open}}(t_{j,i,k,s})\right\} = N_{\text{PSII}}\sum_{s=1}^{2\text{or}3}\sum_{k=1}^{29}\sum_{i=N_{y1}}^{N_{y2}}\sum_{j=-N_x}^{+N_x} p_f\left(7i+\left\{\Delta_{\text{offset}}/25\right\}, j\right)\left\{1-p_{\text{open}}(t_{j,i,k,s})\right\} \quad \text{(eq. 5)}$$

where the previously used index m and time t_m in eq 3 is replaced with a new set of indices j, i, k, s that reflect actual raster scan of the laser. The index j corresponds to different horizontal positions of the laser focus at a constant vertical position, i to different vertical positions of the laser focus in a single focal plane, k to different frames for accumulation in the same focal plane, and s to different focal planes. The integer coordinates, $7i+(\Delta_{\text{offset}}/25)$ and j corresponding to j_y and j_x in the previous notations (eq. 3) indicate the relative location of the laser focus with respect to the position of PSII (at the origin). The parameter Δ_{offset} (varied between 0 and 175 nm with a step size of 25 nm for averaging) represents a relative vertical offset in nm between the origin (location of PSII) and one of the horizontal lines that are fastest scan axes of the laser. The actual ranges of j, i, k and s ($-N_x \le j \le +N_x$, $N_x=10$, $N_{y1} \le j \le N_{y2}$, $N_{y2}-N_{y2}=1$ or 2) are given by the finite size of the laser spot (with a diffraction-limited size of 176 nm for the excitation wavelength of 404 nm) and the other actual scanning parameters (See Text S1 for more details). When PSII is located in the exact focal plane, laser focus in the simulation is set to move by 25 nm along the x axis by the single step in the index j ($j \rightarrow j+1$). The single step in the index i ($i \rightarrow i+1$) is set to move the laser focus by 176 nm, which gives the rounded integer 7 in the eqs. 4 and 5 ($176/25 \approx 7$). One should take into account the weights (w_1, w_2, w_3) of the three different time constants, $\tau_{R,1}$, $\tau_{R,2}$, $\tau_{R,3}$, for the recovery of open PSII from closed PSII [55, 56]. The experimentally obtained dependence of FLIM on the laser power should be compared with a weighted average as follows (cf. Fig. S8).

$$\left\langle F_{\text{open, accum}}(P_{\text{laser}})\right\rangle = \sum_{i=1}^{3} w_i F_{\text{open, accum}}(P_{\text{laser}}, \tau_{R,i})$$

$$\left\langle F_{\text{closed, accum}}(P_{\text{laser}})\right\rangle = \sum_{i=1}^{3} w_i F_{\text{closed, accum}}(P_{\text{laser}}, \tau_{R,i}) \quad \text{(eqs. 6)}$$

More details of this simulation is fully described in Text S1.

Relatively long-lived components (>0.6ns) show greater weights at 689 nm than at 716 nm (Table 1-3), which is understandable because PSII and PSI show maximum CF intensity near 689 and 716 nm, respectively [8, 9][7, 11, 32][26]

and because the FL of only PSII shows an elongation due to increase of the laser power [26][27]. It is thus reasonable that our simulation on PSII is compared with the amplitude ratio of the long-lived components at 0 ps ($A_2/(A_0+ A_1+ A_2)$ in eq. 2) in the 689 nm CF kinetics (Fig. 4). Contribution of PSI CF is not considered from the beginning in the simulation, but it will be later considered if its contribution is unavoidable, especially in the case of a cyanobacterium *A. variabilis* that is generally more rich in PSI than in green algae (including *P. kessleri*) [57].

One essential parameter in the simulation is the absorption cross section of PSII supercomplex, to which the excitation probability function, p_f in eqs 3-5, is proportional. The pigments of PS II monomer of *A. variabilis* was assumed to be the same as those in the core of the PSII complex from *Thermosynechococcus vulcanus* [58], in which 35 molecules of Chla, 2 molecules of pheophytin *a* and 11 molecules of β-carotene are contained. Absorption coefficients of these molecules at 404 nm (6.11×10^5 $cm^{-1}mol^{-1}dm^3$, 1.07×10^6 $cm^{-1}mol^{-1}dm^3$, and 5.59×10^5 $cm^{-1}mol^{-1}dm^3$ for Chla, pheophytin *a* and β-carotene, respectively) were obtained with the help of absorption spectra in several references [59-61]. When only the pigments in the monomer units are considered, the total absorption coefficient of PSII monomer at 404 nm thus amounts to 2.97×10^6 $cm^{-1}mol^{-1}dm^3$ (Text S2, Table S7). Cyanobacterial PSII is assumed to be in the state 2 since we have given a dark period of 15 - 20 min before each set of measurements (Table S1) [62][63][64]. One simulation was thus carried out with a minimal light-harvesting ability for PSII, where there is no PBS transferring energy to PSII. The reopening time constants of PSII in *A. variabilis* (the transition from closed state to open state) were assumed to be the same as those in another cyanobacterium, *Synechocystis* sp. PCC 6803 [55], in which there are three time constants (0.22 ms (68 %), 2.9 ms (23 %) and 13 s (9%)). The simulation yielded ratios of the accumulated number of excitations of closed PSII to the total accumulated number of excitations of PSII in *A. variabilis* at varied excitation laser power (PSII alone, dashed line in Fig, 4(a)). The possible association of PBS to PSII makes the effective absorption coefficient of PSII even larger, although the energy transfer efficiency from phycocyanin in PBS to PSII was reported to be 78 % in an red alga *Porphyridium cruentum* and 86 % in an cyanobacterium *Anacystis nidulans*, which was found to be substantially lower than about 100 % in the transfer from Chlb to Chla in an green alga *Chlorella pyrenoidosa* [65]. The energy transfer from PBS to PSII lifts the simulation curve to the upper side, which results in an even greater gap between experimental and simulation plots (PSII + full PBS, solid line in Fig. 4(a)). On the other hand, the deviation of the simulation from experimental data can be alleviated if one considers contribution of PSI. Contribution of PBS fluorescence is not considered here, because the excitation wavelength at 404 nm was relatively preferential for Chla and the cyanobacterium was set to be state II (See also section 4.3 and Table S7). In the modified simulation to better reproduce the experimental plot, the CF from PSI is assumed to contribute to 33 % of the total amplitude at the weak excitation limit, and its lifetime (about 0.025 - 0.12 ns) [26, 28, 34-36] are safely in the short lifetime range (<0.25 ns) at all excitation laser power levels (PSII alone×(2/3), dashed and dotted line in Fig. 4(a), cf. Table 1).

In the case of *P. kessleri*, a green alga, the initial state of the thylakoid membrane before each set of FLIM measurements is state 1, because the dark period of 15 - 20 min was also given (Table S1) [66]. The organization of PS II supercomplex of *P. kessleri* was assumed to be the same as that proposed in the case of *Chlamydomonas reinhardtii* [67]. When light-harvesting ability per PSII is largest (state 1), there are three trimers of LHCII, one CP26 and one CP29 per PSII monomer in the model PSII complex (Text S2). The total number of pigments per monomer PSII were largely based on a reference [68]. In addition to the above-mentioned absorption coefficients for the pigments common to cyanobacterial PSII, absorption coefficients of the other pigments at 404 nm (1.45×10^5 $cm^{-1}mol^{-1}dm^3$, 4.75×10^5 $cm^{-1}mol^{-1}dm^3$, 6.01×10^5 $cm^{-1}mol^{-1}dm^3$, and 5.69×10^5 $cm^{-1}mol^{-1}dm^3$ for Chl *b*, neoxanthin, violaxanthin, lutein) were obtained with the help of several references reporting their absorption spectra and absorption coefficients at representative peaks (Table S8) [59, 60,

69-71]. Given the sum of all pigments per PSII monomer (124.5 Chla, 62.5 Chlb, 10 neoxanthin, 6.3 violaxanthin, 24.7 lutein, 11 β-carotene, 2 pheophytin molecules), the total absorption coefficient amounts to 1.16×10^7 $cm^{-1}mol^{-1}dm^3$, which yields a simulation curve designated as the equivalent number of Chla of 190 (Fig. 4(b)). We also added another simulation curve in the case where effective absorption cross section is twice (380 Chla) [72]. The decay of the closed state of PSII in *P. kessleri*, (reopening of PSII) was assumed to be the same as that in *Chlamydomonas reinhardtii*, in which there are three time constants (0.23 ms (73 %), 46 ms (16 %) and 7.5 s (11%)) [56]. We also performed an extra FLIM experiments with an excessively strong excitation power, which yielded a decay profile to be fitted by a sum of two exponential functions with time constants of 0.60 ns (33 %) and 1.42 ns (67%) (Fig. S6), although the target cells measured for the Fig. S6 on a longer time scale were different from those analyzed as in Tables 3 and S4. This result is also added to the Fig. 4(b and c). The relatively short time constant of 0.60 ns at 6 nW excitation is clearly longer than those at the lower excitation powers (Tables 3 and S4). Possible presence of more than two decay time constants in the CF decay suggests that the open-closed PSII model (two-state model) is not sufficient. Given the current simulation framework and the signal-to-noise ratio, not the amplitude ratio of relatively long-lifetime component, but the average lifetime (eq. 2) is tentatively fitted by the simulation results as a compromise (Fig. 4(c)). The average FL at the weak limit and longest FL observed as a slowly-decaying component was averaged with weights of open and closed PSII that were given by the simulations at varied laser intensities, which nicely reproduces the experimental average FLs.

4. Discussion

4.1. *Contribution of PSI fluorescence*

Chlorophyll FL (CFL) of PSI (about 0.025 - 0.12 ns in the previous works) in live cells have been reported by careful decomposition/deconvolution in wild type cells [26, 31, 35] or from PSII-deficient mutant cells that were grown heterotrophically [34, 36, 73]. To the best of our knowledge, the CF obtained from single heterocysts of *A. variabilis* in this work is probably a rare example in that CF in wild-type intact cells is almost purely attributable to PSI. However, it should be noted that PSI in heterocyst may be associated with the so-called rod part of PBS (consisting of phycocyanin (PC) and phycoerythrocyanin (PEC)) [9, 41, 74-76]. The high purity of the PSI (nearly negligible contribution by PSII) in the heterocysts is supported by several features, although possible minor contribution of PSII is also analyzed in the next section 4.2. First, there is almost no increase of slowly-decaying component in heterocyst by the increase of laser power (Table 2, Figs. 2(b), 2(c), S3, S4). Even in the selected subset of heterocysts (subset/w) (Table 2), the increase of the long-lived component at 689 nm is from 8% to at most 12% in the amplitude while the corresponding long-lived component in vegetative cells increases in the amplitude from 2.5 % to 37 % between 0.08 and 20 nW. Second, the CFLs at both 689 and 716 nm in heterocyst are clearly shorter than those in vegetative cells (Table 1). This reflects higher abundance of PSI in heterocyst as CFL of PSI is widely reported to be shorter than that of PSII [18, 28, 36, 77]. Third, the CFL at 689 nm of heterocyst is shorter than that at 716 nm. This is in contrast to the very similar CFL of the short-lived component (0.22 -0.26 ns) in the vegetative cells between 689 and 716 nm (Table 1). This feature is consistent with the observation in purified PSI complexes (PSI or PSI-LHCI) or in mutants lacking PSII and its associated antenna system, in which there are one relatively fast decay around the main peak of the Qy band (major spectral forms of Chla in PSI, with fluorescence wavelength < 700nm) and one relatively slow decay of the so-called minor long-wavelength-absorbing form (>700 nm) [36, 77]. For example, one of the above-cited time-resolved spectroscopic study reported two main fluorescence decay

lifetimes of 15 ps and 50 ps that are attributable to net loss of fluorescence (trapping) in isolated PSI from a cyanobacterium *Spirulina platensis* [77]. In their work, the fast trapping component (15 ps) is centered around 700 nm with an approximate FWHM of 46 nm, whereas the slow component (50 ps) is centered around 730 nm with an approximate FWHM of 57 nm. Although our IRFs (0.08 ns at 689 nm and 0.10 ns at 716 nm in FWHM) and the signal-to-noise ratio are presumably not sufficient to resolve the two trapping components at a single wavelength alone, the relatively slow decay at 716 nm (0.13 - 0.14 ns) than at 689 nm (0.084 - 0.096 ns) of the CF in heterocyst is most plausibly attributable to the presence of the two trapping dynamics with different spectra and lifetimes in PSI. This trend would not be easily observed if there was a substantial contribution from PSII to the wavelength region around the main Qy peak (around 689 nm), as the CFL of PSII is generally even slower than the slow trapping component in PSI.

Contribution of PSI in the vegetative cells of *A. variabilis* is noticeable as a decreased amplitude of the long-lived CF due to closed PSII around 716 nm (16 % at 20 nW) than that around 689 nm (37 % at 20 nW in Table 1). The decreased amplitude of the long-lived component at 716 nm than at 689 nm can be at least in part attributable to higher spectral weight of PSI at 716 nm than at 689 nm. Contribution of PSI in *P. kessleri* was also noticeable in the varied amplitude of the long-lived components (28 % at 716 nm vs. 53 % at 689 nm with 1.0×10^3 pW in Table 3). These suggest that not only the dependence of FL on laser power but also dual-wavelength detection can be helpful for imaging PSI/PSII .

4.2. *Long-lived fluorescence and possible presence of PSII in heterocysts*

In one selected subset of heterocysts (subset/w, 5 among 22 heterocysts), a long-lived fluorescence with a lifetime of 0.57 -0.74 ns was found with a substantial amplitude larger than 8 % at all laser intensities (Table 2, Fig. S4). However, its increase in amplitude by the rise of laser power was only from 8 to at most 12 % (Table 2, Fig. S4), which is about one-order of magnitude smaller than that in vegetative cells (from 2.5 to 37 %, Table 1). The amplitude of 8 % at the weakest excitation should be thus attributed to long-lived fluorescence other than closed PSII. One possibility is that these indicate phycobilisomes or parts of phycobilisomes that are uncoupled from both PSII and PSI [78]. In our random selection of heterocysts, it is impossible to avoid premature heterocysts, which temporarily contain substantial number of uncoupled highly fluorescent phycobilisome [9, 49, 79]. Given this possibility, the small increase of the long-lived component from 8 to 11-12 % in the subset of heterocyst (subset/w) by the rise of laser intensity (Table 2) may also be attributable not to stable presence of functional PSII but to residual but photochemically active PSII that is not yet decomposed during the heterocyst differentiation. It should be noted that the substantial amplitude of the long-lived component was observed only in the minor subset (subset/w): 3 heterocysts in filaments harvested 24 days after the inoculation (total was 9 heterocysts) , 2 heterocysts in filaments harvested 90 days after the inoculation (total was 6 heterocysts) , and none in filaments harvested 3 days after the inoculation (total was 7 heterocysts). All these inoculations were *not* step-down of the nitrogen, but simply dilutions of cells from cell-rich nitrogen-deficient media to new nitrogen-deficient media. As far as randomly sampled 22 heterocysts in this study are concerned, we tentatively estimated that photochemically active PSII:PSI ratio in heterocysts are estimated to be typically below our detection limit and at most about 5 % in limited cases in comparison with that in vegetative cells (See Text S3 for the details of this estimation). This number was given on an assumption that effective light-harvesting abilities of PSII in vegetative cells and heterocysts are the same under the experimental conditions in this work (state II and 404 nm excitation). To further clarify the molecular entity of the long-lived fluorescence, it is thus desirable to carry out a FLIM-based time-lapse observation on heterocyst differentiation, which will be described in our next publications.

4.3. *Fluorescence lifetime when PSII is in the open state*

Most obvious mission of FLIM should be to obtain absolute values of CFLs in a wide spatial region including three dimensional objects like plant leaves. Straightforward comparison of CFLs between different organisms or different cells is generally meaningful, but only when CFLs to be compared should be obtained at well-defined excitation and preillumination conditions, e.g., at weak excitation limits after dark adaptation that are generally attained at different laser powers for different organisms/tissues, as demonstrated in Fig. 4. The average FL at 689 nm seems to reach a weak limit below 0.30 nW and 55 pW in the cases of *A. variabilis* vegetative cells and *P. kessleri* cells, respectively (Table 1 and 3, Fig. 4), although double exponential curve fitting did not give constant results due probably to the limited s/n ratio in the relatively weak excitation powers. The average FL with PSII in the open state thus seems to be 0.25 ns and 0.36 - 0.39 ns in the cases of *A. variabilis* vegetative cells and *P. kessleri* cells, respectively, which are largely consistent with previous reports (Tables S5, S6). Even if the primary charge separation in the isolated core PSII dimer is intrinsically common between *P. kessleri* and *A. variabilis*, the different CFLs between *A. variabilis* and *P. kessleri* at the weak limit (0.25 and 0.36 - 0.39 ns, respectively) observed in this study can be caused by the difference in the organization of light-harvesting system. With the 404 nm excitation in our PSII models, 63 % and 26 % of the excitation at 404 nm is estimated to initially reside in the PSII dimer in *A. variabilis* and *P. kessleri*, respectively (Table S7 and S8), when any excitation in the whole PSII supercomplex including associated phycobilisome is set to be 100%. In addition, back energy transfer from the PSII dimer to light-harvesting systems in the *P. kessleri* (PSII ⟶ LHCII, CP26 and CP29) seems to be far more significant than that in *A. variabilis* (PSII ⟶ APC, PC, PEC). This is supported by the estimation of number of pigments weighted by the thermal excitation probability in both the core PSII dimer and associated light-harvesting systems (Table S7 and S8). It should be also noted that PBS tends to be associated with PSI rather than with PSII in the dark adapted state (state 2 in the case of cyanobacteria) [2, 62, 63]. It thus seems very reasonable that average FL at the weak limit in *A. variabilis* is shorter than in *P. kessleri* upon the 404 nm excitation. However, it should be certainly noted that contribution of PSI, which has a CFL of largely 0.08 -0.09 ns at 689 nm in heterocyst in *A. variabilis* (Table 2), should also make the apparent CFL of vegetative cells around 689 nm shorter than that of pure PSII to some extent. The contribution of PBS to the lifetime of vegetative cells of *A. variabilis* at 689 is likely less substantial than that of PSI, since substantial part of PBS is dissociated from PSII by the state II conditions and the excitation wavelength at 404 nm is more preferential for Chla than phycobilin (Table S7).

4.4. *Transition from open to closed state of PSII as observed by varied excitation laser power*

The transition from open to closed state in the majority of PSII of *A. variabilis* is observed at about one-order of magnitude higher excitation power than that of *P. kessleri*. The recovery dynamics of open PSII from closed PSII in cyanobacteria (0.22 ms (68 %), 2.9 ms (23 %) and 13 s (9%) in *Synechocystis* sp. PCC 6803 [55]) seems to be largely similar to that in green algae (0.23 ms (73 %), 46 ms (16 %) and 7.5 s (11%) in *C. reinhardtii* [56]). The difference in the laser power necessary to close most PSII thus seems to be primarily attributable to the difference in the absorption coefficient at 404 nm for PSII. In *P. kessleri*, as one of green algae, PSII possess an antenna system that contains Chla and chlorophyll *b* (Chlb) as main antenna pigments exhibiting strong absorption mainly in the blue-green and red regions [80, 81]. For the simulation, we have assumed the same molecular organization of PSII supercomplex as in *C. reinhardtii* [67], the total absorption coefficient per PSII monomer in state 1 (Text S2) is equivalent to about 191 Chla molecules per monomer PSII (Fig. 4(b)).

The simulation curve for the light-harvesting ability equivalent to 380 Chla may give a slightly improved fit to the experiment. Absolute absorption cross section of PSII in *Chlorella vulgaris* was reported to be equivalent to 130 - 400 Chla [72]. It should be also noted that there remains a certain long-lived component (≥0.6 ns) even at the weak limit, which is similar to the situations in some references reporting such minor long-lived component (See Table S5 for references) [26, 35]. Given this possibility, the estimated ratio of closed PSII based on the amplitude of the long-lived component (closed circles in Fig. 4(b)) may have to be modified. On an assumption that 12 % of the amplitude at zero time (the amplitude of the 0.82 ns component at 689 nm, 4 pW in Table 3) is intrinsically given by the open PSII, our experimental data yield another plot for the ratio of closed PSII (open circles) in Fig. 4(b). This modified experimental plot matches well with the simulation. In the case of *A. variabilis*, the experiment was best reproduced by the simulation if all PBS components are dissociated from PSII and if PSI contribute to the short-lived component (≤0.23 ns) at 689 nm by about 33 % in the amplitude ratio at t = 0 ps (the simulation curve: PSII alone×(2/3) in Fig. 4(a)), as explained in section 3.2.

The rise in FL with the increase of laser power is sensitively influenced by both the antenna size of PSII and recovery dynamics of open PSII from its closed states (Fig. S8(b)). Although the two factors of antenna size and the recovery rate of open PSII are inseparable in the input-power dependence of FLIM alone, FLIM will be certainly helpful for obtaining a new type of images on antenna size and/or recovery rate of open PSII. For example, about 3-4 cells near the heterocyst cell in *A. variabilis* (part A of the filament in Fig. 1(f)) show an average FL of about 0.25 ns, and about 2 cells in the same filament (part B of the filament in Fig. 1(f)) show an average FL of about 0.4 ns at the same excitation power. Such a difference is not yet generalized, but it may suggest differently regulated light-harvesting abilities and/or redox conditions of plastoquinone pool affecting electron transfers from Q_A [53, 64]. Properties of individual vegetative cells as well as heterocysts will be analyzed based on FLIM data in our next publications.

4.5. *Relevance of FLIM to PAM parameters*

Pulse-amplitude-modulation fluorometry (PAM) of CF is probably the most popular chlorophyll fluorometry on photosynthetic organisms [51, 52]. There have been extensive reports demonstrating microscopic images for PAM-related parameters from individual chloroplasts and cyanobacterial cells [5, 82-85]. FLIM data with varied excitation power also contains information directly related to the PAM. Since the simulation based on open-closed status of PSII in this study largely reproduced the experimental results in terms of ratio of closed PSII included in the FLIM data (Fig. 4), the maximum yield of PSII charge separation under dark-adapted chloroplasts or cyanobacteria in PAM analysis is related to the CFL as follows.

$$\frac{\left\langle \tau_{open} \right\rangle^{-1} - \tau_{closed}{}^{-1}}{\left\langle \tau_{open} \right\rangle^{-1}} = \frac{(0.38)^{-1} - (1.42)^{-1}}{(0.38)^{-1}} \approx 0.73 \quad \text{(eq. 6)} \quad \text{for } \textit{P. kessleri} \quad \text{(cf. Table3, Text S6, Fig. S7)}$$

$$\frac{\left\langle \tau_{open} \right\rangle^{-1} - \tau_{closed}{}^{-1}}{\left\langle \tau_{open} \right\rangle^{-1}} = \frac{(0.25)^{-1} - (0.79)^{-1}}{(0.25)^{-1}} \approx 0.69 \quad \text{(eq. 7)} \quad \text{for vegetative cells of } \textit{A. variabilis}$$

(cf. Table 1, Text S6)

The above $<\tau_{open}>$ and τ_{closed} are set to be the average fluorescence lifetime at 689 nm at the weakest laser power and the time constant of the slowly-decaying component at 689 nm at the highest laser power, respectively. In the above estimation, we assume that the average fluorescence lifetime at a sufficiently high laser power to close all PSII should be equal to the CFL of the most long-lived component that we observed. In the case of *P. kessleri*, this value is slightly lower than the typical value of $(F_M - F_0)/F_M = F_V/F_M$ (about 0.8) in dark-adapted state in the PAM fluoromerty on green algae including *Chlorella* [62, 86], although the two values should be ideally the same in the simple two-state model (Text S6). Possible activation of protective quenching against excess excitation (so-called nonphotochemical quenching, NPQ) during the scanning laser illumination may decrease the apparent maximum yield of PSII charge separation through shortening of τ_{closed}. However, such a scenario is unlikely in this study, because the average intensity of the excitation laser at 1 nW (strongest laser power in the consecutive FLIM measurements in the case of *P. kessleri* summarized in Table 3) for 45×45 μm scanning area is estimated to be about 1.7 μ mol photons $m^{-2}s^{-1}$ (Text S4) This is about one or two order of magnitude smaller than that used for actinic light in most PAM measurements to induce NPQ [51, 52]. Moreover, consecutive FLIM measurements for a total exposure time of 45 s at even higher excitation laser at 6 nW (the other experimental conditions are unchanged from those used in the results of the main text) did not show noticeable changes in CF decay profile from the first 4.5 s to the last 4.5 s in the case of *P. kessleri* cells (Fig. S7). The above discrepancy in the maximum quantum yield (between 0.73 and about 0.8) may suggest an underestimation of the amplitude of some short-lived component in the fluorescence decay due to our limited time-resolution (FWHM of IRF was 80 ps at 689 nm) and/or s/n. On the other hand, the above value of $(<\tau_{open}>^{-1} - \tau_{closed}^{-1})/ \tau_{open}^{-1}$ is higher than typical values of F_V/F_M of dark-adapted cyanobacteria [53, 62, 64]. This is caused by the contribution of at least PSI and also PBS to the short lifetime component with the FL of about 0.23 ns (See section 3.2 and Fig. 4(a)). The PSI/PSII ratio in cyanobacteria are generally higher than those in green algae [57]. It is thus likely that CFL of pure PSII is longer than 0.25 ns in *A. variabilis*. For a direct comparison with actual PAM measurements on cyanobacteria, τ_{closed} in eq. 7 may have to be replaced with $<\tau_{closed}>$ as follows.

$$\frac{\left\langle \tau_{open} \right\rangle^{-1} - \left\langle \tau_{closed} \right\rangle^{-1}}{\left\langle \tau_{open} \right\rangle^{-1}} = \frac{(0.25)^{-1} - (0.44)^{-1}}{(0.25)^{-1}} \approx 0.43 \qquad \text{(eq. 8)}$$

for vegetative cells of *A. variabilis*

(cf. Table 1, Text S6)

$$\frac{\left\langle \tau_{open} \right\rangle^{-1} - \left\langle \tau_{closed} \right\rangle^{-1}}{\left\langle \tau_{open} \right\rangle^{-1}} = \frac{(0.087)^{-1} - (0.129)^{-1}}{(0.087)^{-1}} \approx 0.33 \qquad \text{(eq. 9)}$$

for all 22 heterocysts of *A. variabilis*

(cf. Table 2, Text S6)

These are comparable to and largely consistent with the values of F_V/F_M reported for vegetative cells and heterocysts in *Anabaena* sp. strain PCC7120 by time-lapse microscopic PAM (or fluorescence kinetic microscopy, FKM) [5]. The estimation on heterocysts based on our results, however, critically depends on the two subsets, subset/w/o and subset/w, for which the eq. 9 gives 0.07 and 0.27 based on Table 2, respectively. According to the time-dependent F_V/F_M values after the nitrogen step-down in the reference [5], the value of 0.07 for the subset/w/o corresponds to a late "stress period" (about 30 h after the nitrogen step-down). The value of 0.27 for the subset/w corresponds to an early "stress period" (about 20 - 25 h after the nitrogen step-down) or "acclimation period" (about 120 h after the nitrogen step-down). In the former case, the

relatively minor subset of heterocysts (subset/w having a substantial long-lived fluorescence) is indeed understandable as a transient state during the heterocyst development. However, it should be noted that our estimation is critically dependent on the accuracy of the curve fitting at the weak excitation limit and that we need to increase the number of sampling in order to reach a definite conclusion.

4.6. *Limitations of current simulation model and data analysis*

Some previous studies have suggested a need to introduce the so-called three-state model of the charge separation assuming open, semi-closed, and closed states, which reflect redox states of at least two sequential electron acceptors (Text S5) [87, 88]. Semi-closed state is suggested to show lower fluorescence quantum yield than that in fully closed state [87], which may be consistently observed in this study as the slightly shorter CFLs of the "closed" state at the medium laser powers (0.63 - 0.82 ns at 4 -265 pW in *P. kessleri*) than those at the highest laser power (1.24-1.42 ns at 1.0 - 6.0×10^3 pW in *P. kessleri*) (Table 3, Fig. S5). The need for the three-state model is also supported by the residuals and chi square values of the curve fitting in Fig. S2-S5, which show that the single or double exponential function are sufficient only at weak - medium excitation powers that we employed. Presence of more than two exponential components at the relatively high laser powers should be explained in an improved model in our next publications.

Moreover, even at low laser powers where most PSII are open, the intrinsic fluorescence decay of PSII is generally multiexponential with at least 3 - 5 lifetimes in both green algae [25, 31, 35] and cyanobacteria [36, 45-47] especially when the decay of CF is observed from many cells by non-FLIM TCSPC with a high s/n (See also Table S5, S6). The sufficiency of single or double components especially at the relatively weak laser powers in our case is just given by our limited s/n. The relatively low s/n is inevitable as far as we primarily concern imaging in order to resolve individual cells within a short time. Our contribution is thus focusing on the overall reproduction of the experimental results, which are approximately described as sum of at most two exponential functions at all power levels, by the relatively crude but elaborate two-state model for the PSII status. Improvement of the simulation model together with the more accurate analysis on the experimental results will be carried out in our next studies with more focus on differences between individual cells.

4.7. *Comparison with other FLIM studies in terms of open-closed status of PSII and laser power dependence*

A brief overview is given to the laser power levels and/or excitation probabilities that are employed in previously reported FLIM-based imaging of chloroplasts and cyanobacteria. In some cases, NPQ processes were mainly studied at light levels that seem to close substantial fraction of PSII [14, 16]. In one of the studies [16], the major CFL in avocado plants was about 1.5 ns (probably from closed PSII) and activation of NPQ was observed as appearance of CFL around 0.5 ns. A certain oligomeric state of LHCII was suggested to show a CFL of 0.4 ns when NPQ was induced in *Arabidopsis* leaves [89]. In other cases, average CFL was found to be in the range between 0.15 and 0.5 ns at relatively weak laser power [15, 21, 36, 90]. On the other hand, CF with two-photon excitation has been reported to decrease in lifetime by raising incident laser power [18, 19], which has been ascribed to singlet-singlet and/or singlet-triplet annihilation. This is a qualitatively different trend than those reported with visible excitation including this work [34]. Singlet-singlet annihilation can be operative only when a single laser pulse excites multiple pigments in the same or nearby PSII unit(s) among which at least multi-step energy transfer to each other is possible, because typical pulse-to-pulse interval of about 10 ns or longer (13.2 ns in this work) is sufficiently longer than lifetime of fluorescence (lifetime of singlet excited state of

Chls). Our estimation of the excitation probability of PSII in *P. kessleri* by a single laser pulse of 1 nW power (at 404 nm, and highest laser power in Table 3) is only about 5×10^{-3}, by which singlet-singlet annihilation should be virtually negligible (Text S5). If prepared concentration of excited PSII at the focus and detection efficiency of CF in the references ([18, 19]) are comparable to our conditions, singlet-singlet annihilation can thus be safely excluded. Singlet-triplet annihilation may be operative, since formation of triplet state(s) of Chls and/or carotenoids is certainly enhanced when substantial portion of PSII is closed at high input laser power and their lifetimes are in the range of μs to ms [91-94]. The long-lived triplet states may thus interact with singlet excited state prepared in the subsequent laser pulses, which leads to shortening of fluorescence lifetime. Lifetime shortening in the FLIM by NPQ and singlet-triplet annihilation may be differentiated on a more quantitative basis if one performs a numerical simulation to estimate the transient accumulation of the triplet states during FLIM imaging, as shown in this work.

5. Conclusions

FLIM data of a single cellular green alga *P. kessleri* and nitrogen-fixing filamentous cyanobacterium *A. variabilis* were obtained at varied excitation powers. At weak excitation limits, fluorescence lifetimes of the thylakoid membrane with mostly open PSII can be obtained, although it takes a long total exposure time to obtain a high quality image. The transition in FLIM data from the weak excitation limits to higher powers that close a substantial fraction of PSII can be successfully explained by a numerical model considering the open-closed status of PSII based on absolute laser powers. The difference in FLIM between *P. kessleri* and cyanobacterium *A. variabilis* can be largely explained by the difference in the light-harvesting ability of the PSII supercomplex at the excitation wavelength at 404 nm. The fluorescence decay in nitrogen-fixing heterocysts is largely independent of the excitation power. This reflects a high purity of PSI in the unique heterocyst thylakoid lacking PSII. Among heterocysts that were randomly sampled, photochemically active PSII/PSI ratio in heterocysts is at most about 5 % in comparison with that of vegetative cells. Heterogeneous properties of individual heterocysts were found, but accurate determination of their physiological states should await further studies.

A whole plant leaf can be a target of FLIM, but special care should be taken when comparing chloroplasts in deep regions with those close to the surface, because it is in general difficult to estimate absolute laser power reaching deep individual chloroplasts. The dependence of FLIM on laser power is sensitively influenced by at least the antenna size of PSII and recovery rates of open PSII from its closed states. A simulation fully reflecting laser scanning conditions, as shown in this work, will potentially help one to interpret observed features of FLIM images in terms of important parameters of photochemistry in individual chloroplasts, cyanobacterial cells and thylakoid domains.

Funding

This work was supported in part by the Japan Science and Technology Agency (the Precursory Research for Embryonic Science and Technology, "Chemical conversion of light energy", to S.K.), the Ministry of Education, Culture, Sports, Science and Technology in Japan (MEXT) (grant no. 24657036 to T. S. & S.K.), MEXT-Supported Program for the Strategic Research Foundation at Private Universities (2015 - 2018, no. S1511025 partly to S.K.), the Murata Science Foundation (to S.K.), and Shorai Foundation for Science and Technology (to S.K.).

Disclosures

Dr. Kumazaki reports grants and personal fees from Japan Science and Technology Agency, grants from The Murata Science Foundation, grants from Shorai Foundation for Science and Technology, grants from the Ministry of Education, Culture, Sports, Science and Technology in Japan during the conduct of the study.

Acknowledgements

We thank Profs. Haruo Inoue (Tokyo Metropolitan University) for many valuable advice and Mr. Masashi Akari, Mr. S. Fukuda, Mr. K. Tamamizu, Mr. K. Kodama for their contributions at preliminary stages of this work.

Figure captions

Figure 1. Characteristics of average fluorescent lifetime images *A. variabilis* at different laser powers and detection wavelengths in the FLIM measurements. Excitation laser power at the sample position was 0.08 nW (weak), 1.1 nW (med.) and 20 nW (str.) in (a - c), (d - i) and (j - o), respectively. The laser powers and detection wavelength (centered at 689 nm or 716 nm) are shown on the left. (a),(d),(g),(j),(m): Photon count-based fluorescent images. (b),(e),(h),(k),(n): Corresponding average fluorescent lifetime images with intensity-dependent brightness adjustment. (c), (f), (i), (l),(o): Corresponding average fluorescent lifetime images without the brightness adjustment. (p), (q) ,(r): distributions of average fluorescence lifetime at the three different laser intensities. (s): Bright-field image of the same area. Scale bar in (d) is equal to 10 μm and applicable to all the image panels. The effective spatial resolution in the color-coded average FL images is about 1.94 μm due to the binning of 11 × 11 pixels.

Figure 2. Effects of incident excitation laser power on decay profiles of fluorescence centered at 689 nm. Dots represent normalized fluorescence intensities based on photon count data from which average photon counts in the sufficiently negative time region was subtracted. It is thus possible that artificially negative fluorescence intensities arise. (a) Photon count data from all vegetative cells in 22 filaments (about 8 - 13 cells per filament) of *A. variabilis* at single focal planes were used. (b) Selected 17 heterocysts of *A. variabilis* at two or three focal planes were used. These heterocysts were selected as having relatively low level of long-lived fluorescence at the highest laser power (See Table 2). (c) Selected 5 heterocysts of *A. variabilis* at two or three focal planes were used. These heterocysts were selected as having relatively high level of long-lived fluorescence at the highest laser power (See Table 2). (d) Photon count data from 32 cells of *P. kessleri* at 1 - 3 focal planes were used. Solid lines represent fitting curves made by convolution of the instrument-response function with a sum of one or two exponential functions. The parameters obtained through the curve fitting are shown in Table 1-3. The plots in black and red represent data and fitting curves in the cases of weakest and strongest laser power levels, respectively. More examples of fluorescence decay profiles of fluorescence at both 689 and 716 nm at all employed laser power levels are shown in Figs. S2- S5.

Figure 3. Characteristics of average fluorescent lifetime images *P. kessleri* at different laser powers and detection wavelengths in the FLIM measurements. Excitation laser power at the sample position was 4 pW (weak), 55 pW (med.) and 1×10^3 pW (str.) in (a - c), (d - i) and (j - o), respectively. The laser powers and detection wavelength (centered at 689 nm or 716 nm) are shown on the left. (a),(d),(g),(j),(m): Photon count-based fluorescent images. (b),(e),(h),(k),(n): Corresponding average fluorescent lifetime images with intensity-dependent brightness. (c), (f), (i), (l),(o): Corresponding average fluorescent lifetime images without the adjustment of brightness. (p), (q) ,(r): distributions of average fluorescence lifetime. (s): Bright-field image of the same area. Scale bar in (a) is equal to 10 μm and applicable to all the image panels. The effective spatial resolution in the color-coded average FL images is about 3.7 μm due to the binning of 21 × 21 pixels.

Figure 4. Comparison between simulation and experimental parameters derived from fluorescence at 689 nm. (a) Amplitude ratios of long-lived fluorescence (> 0.6 ns) at 689 nm for vegetative cells of *A. variabilis* (open circles (○), cf. Table 1). Simulated probabilities of detecting fluorescence from its closed PSII in the cases of PSII with fully extended PBS (solid line, PSII+full PBS), PSII without extra antenna (broken line, PSII alone). The dashed and dotted line (— - — - —, PSII alone ×(2/3)) represent a modified plot that is a simple multiplication of the broken line (− − − −) by a factor of 0.666. This means a situation where PSI and/or PBS fluorescence is always contributing to one third of the total fluorescence at t=0 ps and its fluorescence lifetime is always included in the relatively short lifetime (≤ 0.25 ns). (b) Amplitude ratios of long-lived fluorescence (> 0.6 ns) at 689 nm for *P. kessleri* (closed circles (●), cf. Table 3). The data point at 6 nW ($\log_{10}(6000)$ ~3.78, closed square (■)) was obtained from a separate measurement on different cells described in Supplemental Fig. S7(e). Modified estimation of ratio of closed PSII (○), which are made from the corresponding closed circles at the same excitation power by postulating that there is a relatively long-lived component with a lifetime of 0.60 - 0.83 ns intrinsically from open PSII with a ratio of 12 % in amplitude relative to that of the short-lived component (cf. Table 3). Solid and broken lines are ratios of closed PSII simulated in the cases of PSII having light-harvesting abilities equivalent to 190 and 380 Chla molecules, respectively. (c) Dependence of average lifetime on laser power in the vegetative cells of *A. variabilis* and *P. kessleri* cells. The solid line is given by a formula $0.36\times(1-R_{closed})+ 1.42\times R_{closed}$, which is an average fluorescence lifetime in ns given by the weighted sum of those from open and closed PSII in the case of *P. kessleri*. The ratio of closed PSII, R_{closed}, is the same as the simulated curve of solid line in (b). The broken line is given by a formula $0.23\times(1-R_{closed})+ 0.79\times R_{closed}$, which is an average fluorescence lifetime in ns given by the weighted sum of those from open and closed PSII in the case of vegetative cells of *A. variabilis*. The ratio of closed PSII in the total fluorescence signal, R_{closed}, is the same as the simulated curve (dashed and dotted line (— - — - —)) in (a).

Table 1.

Parameters yielded by curve fitting of the FLIM data of vegetative cells of *A. variabilis*.

λ_{fl} [nm]	P_{laser} [nW]	τ_1[ns] (amplitude in %)	τ_2 [ns] (amplitude in %)	∞ (amplitude in %)	Average lifetime [ns]
689[a]	0.08	0.22[a]±0.01[c] (97.5[a](+2.5/-1.5)[c])	1.09[a](±0.00/-0.34)[c] (2.5[a]±2.5)[c]	(0.0[a](+1.5/-0.0)[c])	0.25[a](+0.00/-0.03)[c]
	0.30	0.23(+0.00/-0.01) (96)	0.88(+0.00/-0.09) (4)	(0)	0.25
	1.1	0.23(+0.01/-0.02) (85(+3/-5))	0.74(+0.03/-0.12) (15(+5/-3))	(0)	0.31(+0.03/-0.04)
	5.3	0.26(+0.00/-0.02) (67(+5/-10))	0.80(+0.00/-0.08) (33(+10/-5))	(0)	0.43±0.05
	20	0.25±0.02 (62(+8/-9))	0.75±0.05 (37(+10/-7))	(0.5±0.5)	0.44(+0.03/-0.05)
716[b]	0.08	0.225[b]±0.005[c] (99.5[b]±0.5[c])	n.d.	(0[b])	0.225[b]±0.005[c]
	0.30	0.225±0.005 (100)	n.d.	(0)	0.225±0.005
	1.1	0.23 ±0.01 (95.5 ±2.5)	1.13±0.18 (4.5±2.5)	(0)	0.25
	5.3	0.23 (85 ±3)	0.88±0.05 (15±3)	(0)	0.33±0.03
	20	0.225±0.015 (84±3)	0.85±0.05 (16±3)	(0)	0.34

[a]These parameters in the case of fluorescence at 689 nm were given by the curve fitting of the sum of all available data (3 independent experiments) at the same laser excitation power to the double exponential function convoluted with the IRF. See Table S2 for the parameters separately obtained for the three sets of experiments.

[b]These parameters in the case of fluorescence at 716 nm are given as the average values obtained by the curve fitting for the two or three independent experiments (See Table S2). .

[c]All error bars in this table are given so as to cover the differences between the multiple data sets that were acquired independently (See Table S2).

Table 2.

Parameters yielded by curve fitting of the FLIM data of heterocysts of *A. variabilis*.

λ_{fl} [nm]	P_{laser} [nW]	τ_1[ns] (amplitude in %)	τ_1[ns] of the subsets[c] (amplitude in %) upper :w/o lower:w/	τ_2 [ns] (amplitude in %)	τ_2[ns] of the subsets[c] (amplitude in %) upper :w/o lower:w/	∞ (amplitude in %)	Average lifetime [ns]	Average lifetime of the subsets[c] upper :w/o lower:w/ [ns]
689[a]	0.08	0.087[a]±0.009[b] (99[a]±1[b])	0.084(99)	n.d.	n.d.	(1[a]±1[b])	0.087	0.084
			0.072(91)		0.57(8)			0.112
	0.30	0.089±0.005 (99.5±0.5)	0.084 (100)	n.d.	n.d.	(0.5±0.5)	0.089	0.084
			0.088(88)		0.69(11)			0.155
	1.1	0.080±0.002 (96±2)	0.078(98)	0.86 ±0.25 (4±2)	0.64(2)	(0)	0.112	0.089
			0.092(89)		0.74(10)			0.157
	5.3	0.081±0.002 (96.5±1.5)	0.075(98)	0.855 ±0.25 (3.5±1.5)	0.67(2)	(0)	0.108	0.087
			0.088(87)		0.70(12)			0.162
	20	0.081±0.003 (94.5±3.5)	0.075(98)	1.03 ±0. 39 (5±3)	0.70(2)	(0.5±0.5)	0.129	0.088
			0.085(88)		0.70(11)			0.153
716[a]	0.30	0.145±0.005 (100)	n.a.	n.d.	n.a.	(0)		
	1.1	0.14±0.01 (100)	n.a.	n.d.	n.a.	(0)		
	5.3	0.14 (100)	n.a.	n.d.	n.a.	(0)		
	20	0.14±0.01 (100)	n.a.	n.d.	n.a.	(0)		

[a]These parameters in the two wavelength regions are given as the average values between maximum and minimum obtained by the curve fitting for the three independent experiments (See Table S3).

[b]All error bars in this table are given so as to cover the differences between the multiple data sets that were acquired independently (See Table S3).

[c]One of the subsets of heterocysts (subset/w) includes 5 heterocysts with a substantial amplitude of long-lived fluorescence (>0.6 ns). The other subset of heterocysts (subset/w/o) includes 17 heterocysts with a relatively small amplitude of long-lived fluorescence (>0.6 ns).

Table 3.

Parameters yielded by curve fitting of FLIM data of *P. kessleri*.

λ_{fl} [nm]	P_{laser} [pW]	τ_1[ns] (amplitude in %)	τ_2 [ns] (amplitude in %)	∞ (amplitude in %)	Average lifetime [ns]
689[a]	4	0.32[a](+0.08/-0.04)[c] (88 (+11/-5)[c])	0.82[a](+0.00/-0.20)[c] (12(+5/-12)[c])	(0(+1/-0)[c])	0.38[a] (+0.02/-0.02)[c]
	15	0.28 (77)	0.63 (23)	(0)	0.36
	55	0.29(+0.00/-0.00) (75(+1/-9))	0.70(+0.00/-0.02) (25(+9/-1))	(0)	0.39 (+ 0.03/-0.01)
	265	0.29 (61)	0.83 (39)	(0)	0.50
	1.0 $\times 10^3$	0.33± 0.01 (47± 1)	1.24± 0.06 (53± 1)	(0)	0.81 (± 0.04)
716[b]	15	0.32[b] (95)	0.87[b](5)	(0)	0.34[b]
	55	0.37±0.03 (100)	n.d.	(0)	0.37
	265	0.36 (90)	1.3(10)	(0)	0.45
	1.0 - 1.2 $\times 10^3$	0.365± 0.005 (72)	1. 4 ± 0.1 (28)	(0)	0.655± 0.025

[a]These parameters in the case of fluorescence at 689 nm were given by the curve fitting of the sum of all available data (2 independent experiments) at the same laser excitation power to the double exponential function convoluted with the IRF. See Table S4 for the parameters separately obtained for the two experiments.

[b]These parameters in the case of fluorescence at 716 nm are given as the average values obtained by the curve fitting for the two independent experiments (See Table S4).

[c]These error bars are given so as to cover the ranges of the parameters separately obtained for the multiple data sets that were acquired independently (See Table S4).

Reference list

[1] Govindjee, Chlorophyll a Fluorescence: A Bit of Basics and History, in: C. Papageorgiou, Govindjee (Eds.) Chlorophyll a Fluorescence a Signature of Photosynthesis, Springer, Netherland, 2004, pp. 1-42.

[2] G.C. Papageorgiou, M. Tsimilli-Michael, K. Stamatakis, The fast and slow kinetics of chlorophyll a fluorescence induction in plants, algae and cyanobacteria: a viewpoint, Photosynthesis Research, 94 (2007) 275-290.

[3] V. Sarafis, Chloroplasts: a structural approach, Journal of Plant Physiology, 152 (1998) 248-264.

[4] K. Harter, A.J. Meixner, F. Schleifenbaum, Spectro-Microscopy of Living Plant Cells, Molecular Plant, 5 (2012) 14-26.

[5] N. Ferimazova, K. Felcmanova, E. Setlikova, H. Kupper, I. Maldener, G. Hauska, B. Sediva, O. Prasil, Regulation of photosynthesis during heterocyst differentiation in Anabaena sp strain PCC 7120 investigated in vivo at single-cell level by chlorophyll fluorescence kinetic microscopy, Photosynthesis Research, 116 (2013) 79-91.

[6] W.F.J. Vermaas, J.A. Timlin, H.D.T. Jones, M.B. Sinclair, L.T. Nieman, S.W. Hamad, D.K. Melgaard, D.M. Haaland, In vivo hyperspectral confocal fluorescence imaging to determine pigment localization and distribution in cyanobacterial cells, Proceedings of the National Academy of Sciences of the United States of America, 105 (2008) 4050-4055.

[7] M. Hasegawa, T. Shiina, M. Terazima, S. Kumazaki, Selective Excitation of Photosystems in Chloroplasts Inside Plant Leaves Observed by Near-Infrared Laser-Based Fluorescence Spectral Microscopy, Plant and Cell Physiology, 51 (2010) 225-238.

[8] M. Hasegawa, T. Yoshida, M. Yabuta, M. Terazima, S. Kumazaki, Anti-Stokes Fluorescence Spectra of Chloroplasts in Parachlorella kessleri and Maize at Room Temperature as Characterized by Near-Infrared Continuous-Wave Laser Fluorescence Microscopy and Absorption Microscopy, Journal of Physical Chemistry B, 115 (2011) 4184-4194.

[9] S. Kumazaki, M. Akari, M. Hasegawa, Transformation of Thylakoid Membranes during Differentiation from Vegetative Cell into Heterocyst Visualized by Microscopic Spectral Imaging, Plant Physiology, 161 (2013) 1321-1333.

[10] K. Sugiura, S. Itoh, Single-cell confocal spectrometry of a filamentous cyanobacterium Nostoc at room and cryogenic temperature. Diversity and differentiation of pigment systems in 311 cells., Plant Cell Physiology, 53 (2012) 1492-1506.

[11] E. Kim, T.K. Ahn, S. Kumazaki, Changes in Antenna Sizes of Photosystems during State Transitions in Granal and Stroma-exposed thylakoid membrane of Intact Chloroplasts in Arabidopsis mesophyll protoplasts, Plant and Cell Physiology, 56 (2015) 759-768.

[12] Y. Shibata, W. Katoh, Y. Tahara, Study of cell-differentiation and assembly of photosynthetic proteins during greening of etiolated Zea mays leaves using confocal fluorescence microspectroscopy at liquid-nitrogen temperature, Biochimica et Biophysica Acta (BBA)-Bioenergetics, 1827 (2013) 520-528.

[13] C.A. Buecherl, A. Bader, A.H. Westphal, S.P. Laptenok, J.W. Borst, FRET-FLIM applications in plant systems, Protoplasma, 251 (2014) 383-394.

[14] O. Holub, M.J. Seufferheld, C.G. Govindjee, G.J. Heiss, R.M. Clegg, Fluorescence lifetime imaging microscopy of Chlamydomonas reinhardtii: non-photochemical quenching mutants and the effect of photosynthetic inhibitors on the slow chlorophyll fluorescence transient, Journal of Microscopy-Oxford, 226 (2007) 90-120.

[15] M. Iwai, M. Yokono, N. Inada, J. Minagawa, Live-cell imaging of photosystem II antenna dissociation during state transitions, Proceedings of the National Academy of Sciences of the United States of America, 107 (2010) 2337-2342.

[16] S. Matsubara, Y.-C. Chen, R. Caliandro, Govindjee, R.M. Clegg, Photosystem II fluorescence lifetime imaging in avocado leaves: Contributions of the lutein-epoxide and violaxanthin cycles to fluorescence quenching, Journal of Photochemistry and Photobiology B: Biology, 104 (2011) 271-284.

[17] C. Unlu, B. Drop, R. Croce, H. van Amerongen, State transitions in Chlamydomonas reinhardtii strongly modulate the functional size of photosystem II but not of photosystem I, Proceedings of the National Academy of Sciences of the United States

of America, 111 (2014) 3460-3465.
[18] K. Broess, J.W. Borst, H. van Amerongen, Applying two-photon excitation fluorescence lifetime imaging microscopy to study photosynthesis in plant leaves, Photosynthesis Research, 100 (2009) 89-96.
[19] Y. Zeng, Y. Wu, D. Li, W. Zheng, W.X. Wang, J.N.Y. Qu, Two-photon excitation chlorophyll fluorescence lifetime imaging: a rapid and noninvasive method for in vivo assessment of cadmium toxicity in a marine diatom Thalassiosira weissflogii, Planta, 236 (2012) 1653-1663.
[20] Y. Wu, Y. Zeng, J.A.Y. Qu, W.X. Wang, Mercury effects on Thalassiosira weissflogii: Applications of two-photon excitation chlorophyll fluorescence lifetime imaging and flow cytometry, Aquatic Toxicology, 110 (2012) 133-140.
[21] A.S. Kristoffersen, O. Svensen, N. Ssebiyonga, S.R. Erga, J.J. Stamnes, O. Frette, Chlorophyll a and NADPH Fluorescence Lifetimes in the Microalgae Haematococcus pluvialis (Chlorophyceae) under Normal and Astaxanthin-Accumulating Conditions, Applied Spectroscopy, 66 (2012) 1216-1225.
[22] T. Kolubayev, N.E. Geacintov, G. Paillotin, J. Breton, DOMAIN SIZES IN CHLOROPLASTS AND CHLOROPHYLL-PROTEIN COMPLEXES PROBED BY FLUORESCENCE YIELD QUENCHING INDUCED BY SINGLET-TRIPLET EXCITON ANNIHILATION, Biochimica Et Biophysica Acta, 808 (1985) 66-76.
[23] V. Barzda, V. Gulbinas, R. Kananavicius, V. Cervinskas, H.v. Amerongen, R.v. Grondelle, L. Valkunas, Singlet-singlet annihilation kinetics in aggregates and trimers of LHCII, Biophys. J., 80 (2001) 2409-2421.
[24] V. Barzda, C.J. de Grauw, J. Vroom, F.J. Kleima, R. van Grondelle, H. van Amerongen, H.C. Gerritsen, Fluorescence lifetime heterogeneity in aggregates of LHCII revealed by time-resolved microscopy, Biophys. J., 81 (2001) 538-546.
[25] R.J. Gulotty, L. Mets, R.S. Alberte, G.R. Fleming, Picosecond fluorescence study of photosynthetic mutants of Chlamydomonas reinhardii: origin of the fluorescence decay kinetics of chloroplasts, Photochemistry and Photobiology, 41 (1985) 487-496.
[26] A.R. Holzwarth, J. Wendler, W. Haehnel, Time-resolved picosecond fluorescence spectra of the antenna chlorophylls in Chlorella vulgaris. Resolution of Photosystem I fluorescence, Biochimica et Biophysica Acta (BBA)-Bioenergetics, 807 (1985) 155-167.
[27] I. Moya, M. Hodges, J. Briantais, G. Hervo, Evidence that the variable chlorophyll fluorescence in Chlamydomonas reinhardtii is not recombination luminescence, Photosynthesis Research, 10 (1986) 319-325.
[28] G.H. Krause, E. Weis, CHLOROPHYLL FLUORESCENCE AND PHOTOSYNTHESIS - THE BASICS, Annual Review of Plant Physiology and Plant Molecular Biology, 42 (1991) 313-349.
[29] H.J. Keuper, K. Sauer, Effect of photosystem II reaction center closure on nanosecond fluorescence relaxation kinetics, Photosynthesis Research, 20 (1989) 85-103.
[30] K. Amarnath, J. Zaks, S.D. Park, K.K. Niyogi, G.R. Fleming, Fluorescence lifetime snapshots reveal two rapidly reversible mechanisms of photoprotection in live cells of Chlamydomonas reinhardtii, Proceedings of the National Academy of Sciences of the United States of America, 109 (2012) 8405-8410.
[31] F. Rizzo, G. Zucchelli, R. Jennings, S. Santabarbara, Wavelength dependence of the fluorescence emission under conditions of open and closed Photosystem II reaction centres in the green alga Chlorella sorokiniana, Biochimica et Biophysica Acta (BBA)-Bioenergetics, 1837 (2014) 726-733.
[32] F. Franck, P. Juneau, R. Popovic, Resolution of the Photosystem I and Photosystem II contributions to chlorophyll fluorescence of intact leaves at room temperature, Biochimica Et Biophysica Acta-Bioenergetics, 1556 (2002) 239-246.
[33] N. Moise, I. Moya, Correlation between lifetime heterogeneity and kinetics heterogeneity during chlorophyll fluorescence induction in leaves:: 1. Mono-frequency phase and modulation analysis reveals a conformational change of a PSII pigment

complex during the IP thermal phase, Biochimica et Biophysica Acta (BBA)-Bioenergetics, 1657 (2004) 33-46.
[34] L.J. Tian, S. Farooq, H. van Amerongen, Probing the picosecond kinetics of the photosystem II core complex in vivo, Phys. Chem. Chem. Phys., 15 (2013) 3146-3154.
[35] J. Wendler, A.R. Holzwarth, State transitions in the green alga Scenedesmus obliquus probed by time-resolved chlorophyll fluorescence spectroscopy and global data analysis, Biophys. J., 52 (1987) 717.
[36] S.B. Krumova, S.P. Laptenok, J.W. Borst, B. Ughy, Z. Gombos, G. Ajlani, H. van Amerongen, Monitoring Photosynthesis in Individual Cells of Synechocystis sp. PCC 6803 on a Picosecond Timescale, Biophys. J., 99 (2010) 2006-2015.
[37] R. Haselkorn, HETEROCYSTS, Annual Review of Plant Physiology and Plant Molecular Biology, 29 (1978) 319-344.
[38] R. Grotjohann, M.S. Rho, W. Kowallik, INFLUENCES OF BLUE AND RED-LIGHT ON THE PHOTOSYNTHETIC APPARATUS OF CHLORELLA-KESSLERI - ALTERATIONS IN PIGMENT-PROTEIN COMPLEXES, Botanica Acta, 105 (1992) 168-173.
[39] I. Ikegami, A. Kamiya, Presence of the photoactive reaction-center chlorophyll of PSI (P700) in dark-grown cells of a chlorophyll-deficient mutant of Chlorella kessleri, Plant and Cell Physiology, 39 (1998) 1087-1092.
[40] S.Y. Ow, T. Cardona, A. Taton, A. Magnuson, P. Lindblad, K. Stensjo, P.C. Wright, Quantitative shotgun proteomics of enriched heterocysts from Nostoc sp. PCC 7120 using 8-plex isobaric peptide tags, Journal of Proteome Research, 7 (2008) 1615-1628.
[41] T. Cardona, N. Battchikova, P. Zhang, K. Stensjo, E.M. Aro, P. Lindblad, A. Magnuson, Electron transfer protein complexes in the thylakoid membranes of heterocysts from the cyanobacterium Nostoc punctiforme, Biochimica et biophysica acta, 1787 (2009) 252-263.
[42] J.-J. Park, S. Lechno-Yossef, C.P. Wolk, C. Vieille, Cell-specific gene expression in Anabaena variabilis grown phototrophically, mixotrophically, and heterotrophically, Bmc Genomics, 14 (2013).
[43] R.Y. Stanier, R. Kunisawa, M. Mandel, Cohenbaz.G, PURIFICATION AND PROPERTIES OF UNICELLULAR BLUE-GREEN ALGAE (ORDER CCHROOCOCCALES), Bacteriological Reviews, 35 (1971) 171-&.
[44] E. Bittersmann, A. Holzwarth, G. Agel, W. Nultsch, PICOSECOND TIME‐RESOLVED EMISSION SPECTRA OF PHOTOINHIBITED AND PHOTOBLEACHED Anabaena variabilis, Photochemistry and Photobiology, 47 (1988) 101-105.
[45] E. Bittersmann, W. Vermaas, Fluorescence lifetime studies of cyanobacterial photosystem II mutants, Biochimica et Biophysica Acta (BBA)-Bioenergetics, 1098 (1991) 105-116.
[46] C.W. Mullineaux, A.R. Holzwarth, Effect of photosystem II reaction centre closure on fluorescence decay kinetics in a cyanobacterium, Biochimica et Biophysica Acta (BBA)-Bioenergetics, 1183 (1993) 345-351.
[47] J. Veerman, F.K. Bentley, J.J. Eaton-Rye, C.W. Mullineaux, S. Vasil'ev, D. Bruce, The PsbU subunit of photosystem II stabilizes energy transfer and primary photochemistry in the phycobilisome-photosystem II assembly of Synechocystis sp. PCC 6803, Biochemistry, 44 (2005) 16939-16948.
[48] L. Ying, X. Huang, B. Huang, J. Xie, J. Zhao, X.S. Zhao, <Ying_2002_Anabaena_sp PCC7120_spectral_confocal.pdf>, Photochemistry and Photobiology, 76 (2002) 310-313.
[49] S. Ke, R. Haselkorn, Fluorescence spectroscopy study of heterocyst differentiation in Anabaena PCC 7120 filaments, Microbiology-Sgm, 159 (2013) 253-258.
[50] S.W. Hogewoning, E. Wientjes, P. Douwstra, G. Trouwborst, W. van Ieperen, R. Croce, J. Harbinson, Photosynthetic Quantum Yield Dynamics: From Photosystems to Leaves, The Plant Cell, 24 (2012) 1921-1935.
[51] K. Roháček, M. Barták, Technique of the modulated chlorophyll fluorescence: basic concepts, useful parameters, and some applications, Photosynthetica, 37 (1999) 339-363.

[52] U. Schreiber, Pulse-amplitude-modulation (PAM) fluorometry and saturation pulse method: an overview, in: Chlorophyll a Fluorescence, Springer, 2004, pp. 279-319.
[53] D. Campbell, V. Hurry, A.K. Clarke, P. Gustafsson, G. Oquist, Chlorophyll fluorescence analysis of cyanobacterial photosynthesis and acclimation, Microbiology and Molecular Biology Reviews, 62 (1998) 667-+.
[54] K. El Bissati, D. Kirilovsky, Regulation of psbA and psaE expression by light quality in Synechocystis species PCC 6803. A redox control mechanism, Plant Physiology, 125 (2001) 1988-2000.
[55] I. Vass, D. Kirilovsky, A.L. Etienne, UV-B radiation-induced donor- and acceptor-side modifications of photosystem II in the cyanobacterium Synechocystis sp PCC 6803, Biochemistry, 38 (1999) 12786-12794.
[56] A. Volgusheva, G. Kukarskikh, T. Krendeleva, A. Rubin, F. Mamedov, Hydrogen photoproduction in green algae Chlamydomonas reinhardtii under magnesium deprivation, Rsc Advances, 5 (2015) 5633-5637.
[57] Y. Hihara, K. Sonoike, Regulation, inhibition and protection of photosystem I, in: Regulation of Photosynthesis, Springer, 2001, pp. 507-531.
[58] Y. Umena, K. Kawakami, J.-R. Shen, N. Kamiya, Crystal structure of oxygen-evolving photosystem II at a resolution of 1.9 Å, Nature, 473 (2011) 55-60.
[59] T. Watanabe, A. Hongu, K. Honda, M. Nakazato, M. Konno, S. Saitoh, PREPARATION OF CHLOROPHYLLS AND PHEOPHYTINS BY ISOCRATIC LIQUID-CHROMATOGRAPHY, Analytical Chemistry, 56 (1984) 251-256.
[60] E.W. Chappelle, M.S. Kim, J.E. McMurtrey, RATIO ANALYSIS OF REFLECTANCE SPECTRA (RARS) - AN ALGORITHM FOR THE REMOTE ESTIMATION OF THE CONCENTRATIONS OF CHLOROPHYLL-A, CHLOROPHYLL-B, AND CAROTENOIDS IN SOYBEAN LEAVES, Remote Sensing of Environment, 39 (1992) 239-247.
[61] S.L. Ustin, A.A. Gitelson, S. Jacquemoud, M. Schaepman, G.P. Asner, J.A. Gamon, P. Zarco-Tejada, Retrieval of foliar information about plant pigment systems from high resolution spectroscopy, Remote Sensing of Environment, 113 (2009) S67-S77.
[62] U. Schreiber, T. Endo, H.L. Mi, K. Asada, QUENCHING ANALYSIS OF CHLOROPHYLL FLUORESCENCE BY THE SATURATION PULSE METHOD - PARTICULAR ASPECTS RELATING TO THE STUDY OF EUKARYOTIC ALGAE AND CYANOBACTERIA, Plant and Cell Physiology, 36 (1995) 873-882.
[63] S. Joshua, C.W. Mullineaux, Phycobilisome diffusion is required for light-state transitions in cyanobacterial, Plant Physiology, 135 (2004) 2112-2119.
[64] T. Ogawa, T. Harada, H. Ozaki, K. Sonoike, Disruption of the ndhF1 Gene Affects Chl Fluorescence through State Transition in the Cyanobacterium Synechocystis sp PCC 6803, Resulting in Apparent High Efficiency of Photosynthesis, Plant and Cell Physiology, 54 (2013) 1164-1171.
[65] G. Tomita, E. Rabinowitch, Excitation energy transfer between pigments in photosynthetic cells, Biophys. J., 2 (1962) 483.
[66] J.F. Allen, PROTEIN-PHOSPHORYLATION IN REGULATION OF PHOTOSYNTHESIS, Biochimica Et Biophysica Acta, 1098 (1992) 275-335.
[67] B. Drop, M. Webber-Birungi, S.K.N. Yadav, A. Filipowicz-Szymanska, F. Fusetti, E.J. Boekema, R. Croce, Light-harvesting complex II (LHCII) and its supramolecular organization in Chlamydomonas reinhardtii, Biochimica Et Biophysica Acta-Bioenergetics, 1837 (2014) 63-72.
[68] S. Caffarri, T. Tibiletti, R.C. Jennings, S. Santabarbara, A Comparison Between Plant Photosystem I and Photosystem II Architecture and Functioning, Current Protein & Peptide Science, 15 (2014) 296-331.
[69] G. Britton, UV/visible spectroscopy, in: G. Britton, Liaaen-Jensen, S. and Pfander, H. (Ed.) Carotenoids: Spectroscopy, Birkhauser, Basel, 1995, pp. 13 - 62.

[70] B.H. Davies, K**ö**st H.-P., Carotenoids, in: K. H.-P. (Ed.) Handbook of Chromatography; Plant Pigments, CRC Press, Boca Raton, 1998, pp. 1-185.

[71] H.A. Frank, J.A. Bautista, J.S. Josue, A.J. Young, Mechanism of nonphotochemical quenching in green plants: Energies of the lowest excited singlet states of violaxanthin and zeaxanthin, Biochemistry, 39 (2000) 2831-2837.

[72] A.C. Ley, D.C. Mauzerall, Absolute absorption cross-sections for photosystem II and the minimum quantum requirement for photosynthesis in Chlorella vulgaris, Biochimica et Biophysica Acta (BBA)-Bioenergetics, 680 (1982) 95-106.

[73] M. Werst, Y. Jia, L. Mets, G.R. Fleming, Energy transfer and trapping in the photosystem I core antenna. A temperature study, Biophys. J., 61 (1992) 868.

[74] R.B. Peterson, E. Dolan, H.E. Calvert, B. Ke, Energy transfer from phycobiliproteins to photosystem I in vegetative cells and heterocysts of Anabaena variabilis, Biochimica et Biophysica Acta (BBA)-Bioenergetics, 634 (1981) 237-248.

[75] M. Watanabe, D.A. Semchonok, M.T. Webber-Birungi, S. Ehira, K. Kondo, R. Narikawa, M. Ohmori, E.J. Boekema, M. Ikeuchi, Attachment of phycobilisomes in an antenna–photosystem I supercomplex of cyanobacteria, Proceedings of the National Academy of Sciences, 111 (2014) 2512-2517.

[76] G. Yamanaka, A. Glazer, Phycobiliproteins in Anabaena 7119 heterocysts, Photosynthetic Prokaryotes: Cell Differentiation and Function. Elsevier Science Publishing, Amsterdam, (1983) 69-90.

[77] B. Gobets, R. van Grondelle, Energy transfer and trapping in photosystem I, Biochimica Et Biophysica Acta-Bioenergetics, 1507 (2001) 80-99.

[78] A.M. Acuña, J.J. Snellenburg, M. Gwizdala, D. Kirilovsky, R. van Grondelle, I.H. van Stokkum, Resolving the contribution of the uncoupled phycobilisomes to cyanobacterial pulse-amplitude modulated (PAM) fluorometry signals, Photosynthesis Research, (2015) 1-12.

[79] M. Toyoshima, N.V. Sasaki, M. Fujiwara, S. Ehira, M. Ohmori, N. Sato, Early candidacy for differentiation into heterocysts in the filamentous cyanobacterium Anabaena sp. PCC 7120, Archives of microbiology, 192 (2010) 23-31.

[80] A.B. Juarez, L. Barsanti, V. Passarelli, V. Evangelista, N. Vesentini, V. Conforti, P. Gualtieri, In vivo microspectroscopy monitoring of chromium effects on the photosynthetic and photoreceptive apparatus of Eudorina unicocca and Chlorella kessleri, Journal of Environmental Monitoring, 10 (2008) 1313-1318.

[81] M.M. Saleh, D.N. Matorin, B.K. Zayadan, D.A. Todorenko, E.P. Lukashov, M.M. Gaballah, Differentiation between two strains of microalga Parachlorella kessleri using modern spectroscopic method, Botanical Studies, 55 (2014) 53.

[82] B. Osmond, O. Schwartz, B. Gunning, Photoinhibitory printing on leaves, visualised by chlorophyll fluorescence imaging and confocal microscopy, is due to diminished fluorescence from grana, Australian Journal of Plant Physiology, 26 (1999) 717-724.

[83] H. Kupper, I. Setlik, M. Trtilek, L. Nedbal, A microscope for two-dimensional measurements of in vivo chlorophyll fluorescence kinetics using pulsed measuring radiation, continuous actinic radiation, and saturating flashes, Photosynthetica, 38 (2000) 553-570.

[84] K. Oxborough, Using chlorophyll a fluorescence imaging to monitor photosynthetic performance, in: Chlorophyll a Fluorescence, Springer, 2004, pp. 409-428.

[85] K. Omasa, A. Konishi, H. Tamura, F. Hosoi, 3D Confocal Laser Scanning Microscopy for the Analysis of Chlorophyll Fluorescence Parameters of Chloroplasts in Intact Leaf Tissues, Plant and Cell Physiology, 50 (2009) 90-105.

[86] W.I. Gruszecki, K. Wojtowicz, Z. Krupa, K. Strzalka, A DIRECT MEASUREMENT OF THERMAL-ENERGY DISSIPATION IN THE PHOTOSYNTHETIC APPARATUS DURING INDUCTION OF FLUORESCENCE, Journal of Photochemistry and Photobiology B-Biology, 22 (1994) 23-27.

[87] W.J. Vredenberg, A three-state model for energy trapping and chlorophyll fluorescence in photosystem II incorporating radical pair recombination, Biophys. J., 79 (2000) 26-38.
[88] W. Vredenberg, O. Prasil, On the polyphasic quenching kinetics of chlorophyll a fluorescence in algae after light pulses of variable length, Photosynthesis Research, 117 (2013) 321-337.
[89] Y. Miloslavina, A. Wehner, P.H. Lambrev, E. Wientjes, M. Reus, G. Garab, R. Croce, A.R. Holzwarth, Far-red fluorescence: A direct spectroscopic marker for LHCII oligomer formation in non-photochemical quenching, Febs Letters, 582 (2008) 3625-3631.
[90] S.B. Krumova, S.P. Laptenok, L. Kovács, T. Tóth, A. van Hoek, G. Garab, H. van Amerongen, Digalactosyl-diacylglycerol-deficiency lowers the thermal stability of thylakoid membranes, Photosynthesis Research, 105 (2010) 229-242.
[91] J. Durrant, L. Giorgi, J. Barber, D. Klug, G. Porter, Characterisation of triplet states in isolated Photosystem II reaction centres: oxygen quenching as a mechanism for photodamage, Biochimica et Biophysica Acta (BBA)-Bioenergetics, 1017 (1990) 167-175.
[92] A. Telfer, Singlet Oxygen Production by PSII Under Light Stress: Mechanism, Detection and the Protective role of beta-Carotene, Plant and Cell Physiology, 55 (2014) 1216-1223.
[93] L. Zhang, T.B. Melo, H. Li, K.R. Naqvi, C. Yang, The inter-monomer interface of the major light-harvesting chlorophyll a/b complexes of photosystem II (LHCII) influences the chlorophyll triplet distribution, Journal of Plant Physiology, 171 (2014) 42-48.
[94] D.A. Hartzler, D.M. Niedzwiedzki, D.A. Bryant, R.E. Blankenship, Y. Pushkar, S. Sayikhin, Triplet Excited State Energies and Phosphorescence Spectra of (Bacterio)Chlorophylls, Journal of Physical Chemistry B, 118 (2014) 7221-7232.

Supplemental information for

Characterization of thylakoid membrane in a heterocystous cyanobacterium and green alga with dual-detector fluorescence lifetime imaging microscopy with a systematic change of incident laser power

Shuho Nozue[1], Akira Mukuno[1], Yumi Tsuda, Takashi Shiina[2], Masahide Terazima[1] and Shigeichi Kumazaki[1]*

1 Department of Chemistry, Graduate School of Science, Kyoto University, Kyoto, 606-8502

2Graduate School of Life and Environmental Sciences, Kyoto Prefectural University , Sakyo-ku, Kyoto 606-8522 , Japan.

*Corresponding author: e-mail: (S.K.) kumazaki@kuchem.kyoto-u.ac.jp

Corresponding author

Shigeichi Kumazaki, Ph.D.

Department of Chemistry, Graduate School of Science, Kyoto University

Kyoto 606-8502, Japan

Tel: +81-75-753-4023

Fax: +81-75-753-4000

E-mail: kumazaki@kuchem.kyoto-u.ac.jp

Supplemental Table S1

Experimental scheme to systematically measure FLIM data at three different incident laser powers.

samples	order	tasks	duration (seconds)	relative distance from the microscope objective
	1	dark adaptation	900-1200	
ROI-1[b] (1st group of cells)	2	FLIM measurement at a weakest laser power	40	z = 0.0 μm,
				z = + 1.0 μm
				z = −1.0 μm
	3	change of pinhole sizes and laser power [a]	< 30	
	4	FLIM measurement at an intermediate laser power	40	z = 0.0 μm
				z = + 1.0 μm
				z = −1.0 μm
	5	change of pinhole sizes and laser power[a]	< 30	
	6	FLIM measurement at a strongest laser power[a]	40	z = 0.0 μm
				z = + 1.0 μm
				z = −1.0 μm
	7	change of pinhole sizes and laser power[a]	< 30	
	8	FLIM measurement at a weakest laser power[a]	40	z = 0.0 μm
				z = + 1.0 μm
				z = −1.0 μm
	9	dark adaptation for the next region of interest	900 -1200	
ROI-2[b] (2nd group of cells that do not include previously measured cells)	10	FLIM measurement at a weakest laser power	40	z = 0.0 μm
				z = + 1.0 μm
				z = −1.0 μm
	11	change of pinhole sizes and laser power[a]	< 30	
	. . .	. . .	. . .	. . .

[a] The sizes of confocal pinholes for the two detectors (centered at 689 and 716 nm) were manually changed in order to limit maximum photon count rates, but the incident laser power was automatically changed by a filter wheel controlled by the measurement program.

[b]When the dependence of FLIM data on laser power was measured at five laser powers, six FLIM measurements were carried out for a single ROI in an analogous manner.

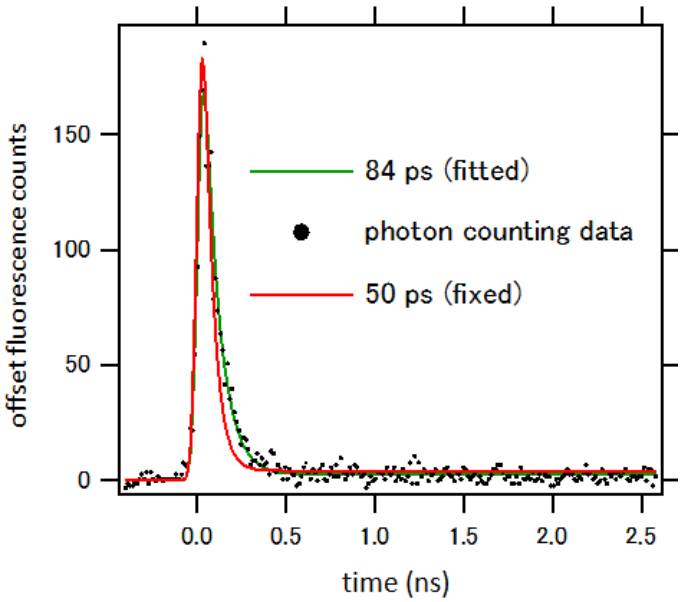

Supplemental Fig. S1

One test of time resolution at a relatively low s/n ratio. The photon counting data is the same as plotted in Fig. S4(a). The green solid line indicates a fitted curve of convolution between the instrument response function (IRF) and a single exponential function. The red solid line indicates a fitted curve of convolution between the IRF and a single exponential function with a constraint that the time constant is fixed at 50 ps.

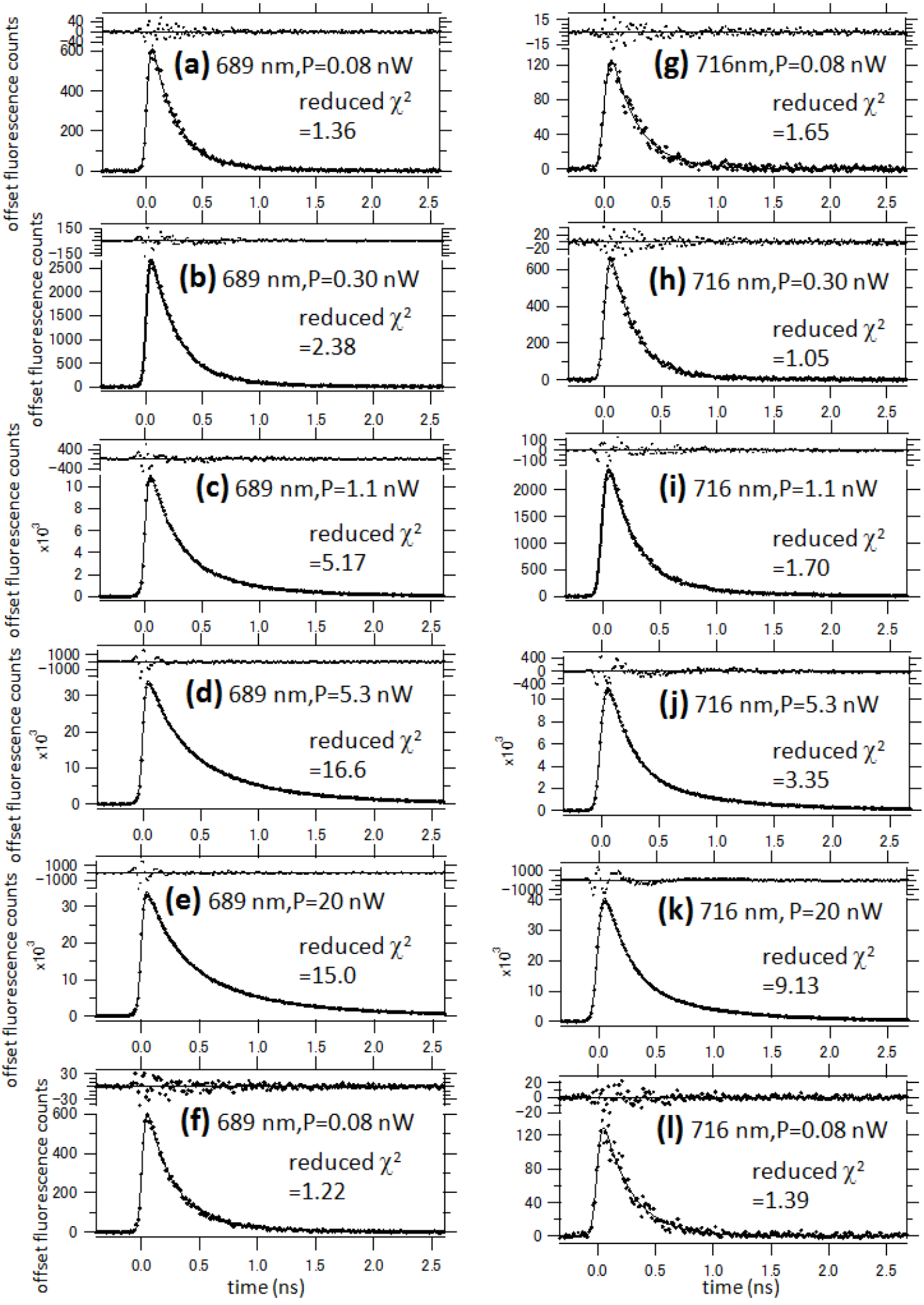

Supplemental Figure S2.

Legend for Supplemental Figure S2. Fluorescence decay profiles of vegetative cells in *A. variabilis.* Detection wavelength range was centered at 689 nm (a, b, c, d,e,f) or 716 nm (g, h,i,k,j,k,l). Fluorescence from all vegetative cells in one data set (7 filaments with about 8 - 13 cells in the image per filament, 3 days after the inoculation) at single focal planes were collected. Dots represent detected photons, but average photon counts in the sufficiently negative time region (5 -10 and 3 - 19 counts per time channel in the 689 and 716 nm wavelength channels, respectively) was subtracted. It is thus possible that artificially negative photon counts arise. Solid lines represent fitting curves made by convolution of the instrument-response function with a sum of one or two exponential functions. The parameters obtained through the curve fitting are shown in Table S2. Although both the residuals and reduced chi square values indicate that more exponential components are necessary to achieve sufficient fit to the data especially at relatively high laser powers, we are here focusing on an approximate description of the whole data sets by at most two exponential decaying components. This basic policy is consistent with the use of two-state model to reproduce open-closed status of PSII in the FLIM.

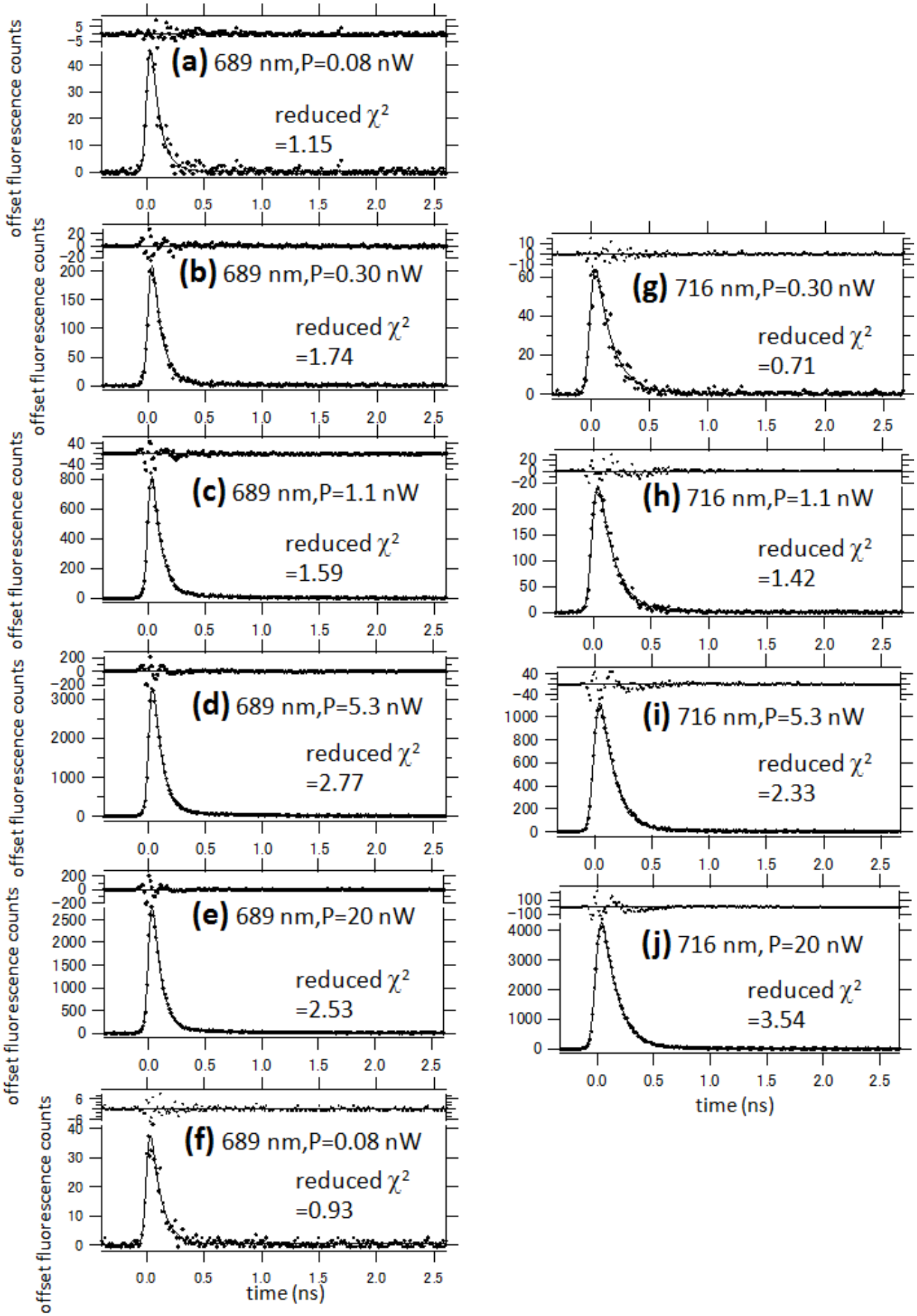

Supplemental Figure S3.

Legend for Supplemental Figure S3. Fluorescence decay profiles of heterocysts in *A. variabilis.* Detection wavelength range was centered at 689 nm (a, b, c, d, e, f) or 716 nm (g, h, i, j). Fluorescence counts from 7 heterocysts were collected and summed. These heterocysts were in the same filaments as the vegetative cells shown in Fig. S2, which were harvested 3 days after an inoculation. Dots represent detected photons, but average photon counts in the sufficiently negative time region was subtracted. It is thus possible that artificially negative photon counts arise. Solid lines represent fitting curves made by convolution of the instrument-response function with a sum of one or two exponential functions. The parameters obtained through the curve fitting are shown in Table S3. Although both the residuals and reduced chi square values indicate that more exponential components may be necessary to achieve sufficient fit to the data especially at relatively high laser powers, we are here focusing on an approximate description of the whole data sets by at most two exponential decaying components. This basic policy is consistent with the use of two-state model to reproduce open-closed status of PSII in the FLIM.

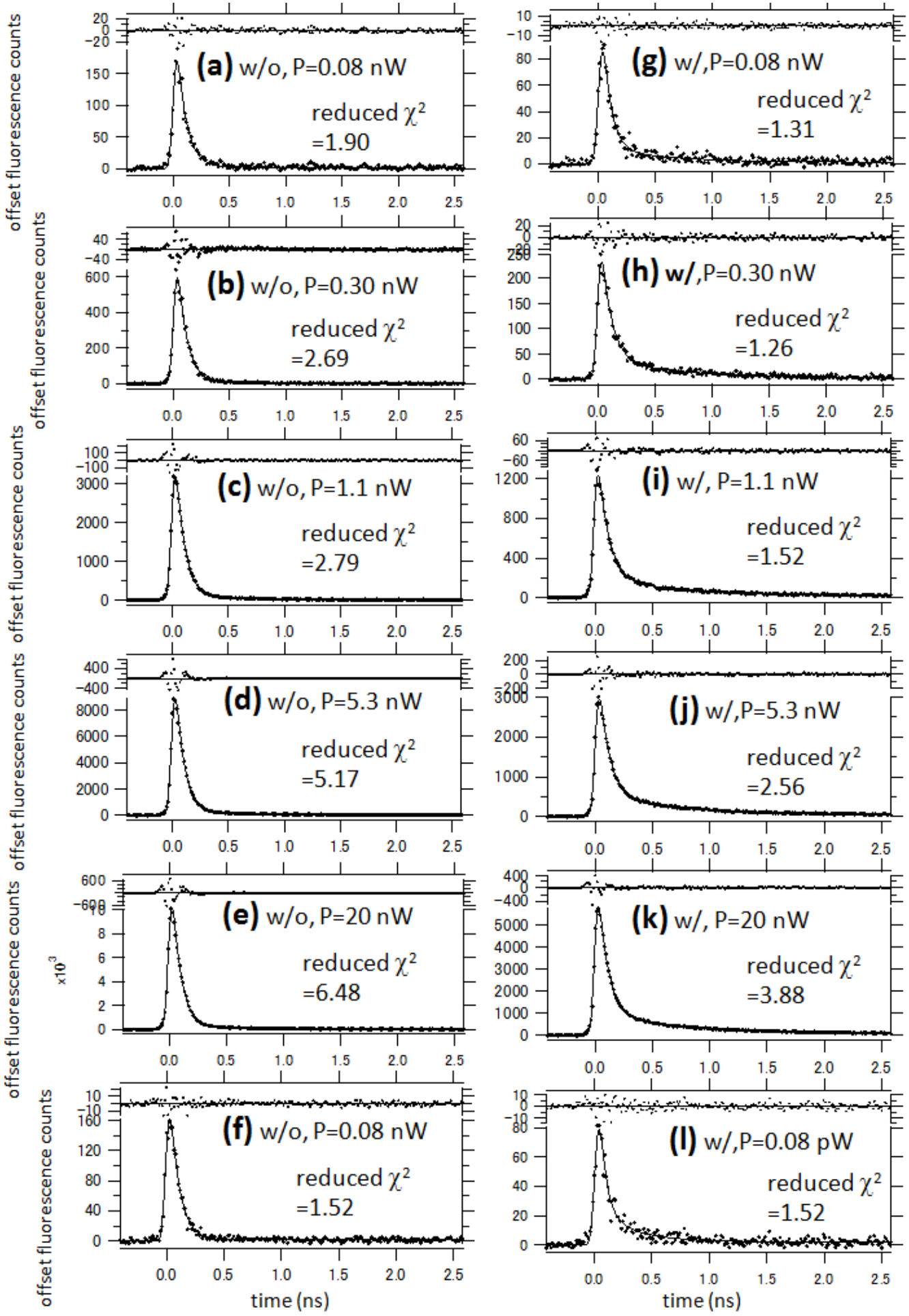

Supplemental Figure S4.

Legend for Supplemental Figure S4. Fluorescence decay profiles of selected heterocyst cells in *A. variabilis* measured at 689 nm. All heterocyst (22) that we studied with FLIM were classified into two subgroups by the fluorescence lifetime based on the single-cell single exponential curve fitting. Sum of fluorescence decay profiles of 17 heterocysts with relatively short lifetimes are shown in (a,b,c,d,e,f, symbolized by w/o (without substantial long-lived component)). Sum of fluorescence decay profiles of 5 heterocysts with relatively long lifetimes are shown in (g, h, i, j, k, l, symbolized by w/ (with substantial long-lived component)). Dots represent detected number of photons, but average photon counts in the sufficiently negative time region was subtracted. It is thus possible that artificially negative photon counts arise. Solid lines represent fitting curves made by convolution of the instrument-response function with a sum of one or two exponential functions. The parameters obtained through the curve fitting are shown in Table 2 in the main text. The plots in (a) and (e) are the same as used in Fig. 2(b) in the main text. The plots in (g) and (k) are the same as used in Fig. 2(c) in the main text. Although both the residuals and reduced chi square values indicate that more exponential components may be necessary to achieve sufficient fit to the data especially at relatively high laser powers, we are here focusing on an approximate description of the whole data sets by at most two exponential decaying components. This basic policy is consistent with the use of two-state model to reproduce open-closed status of PSII in the FLIM.

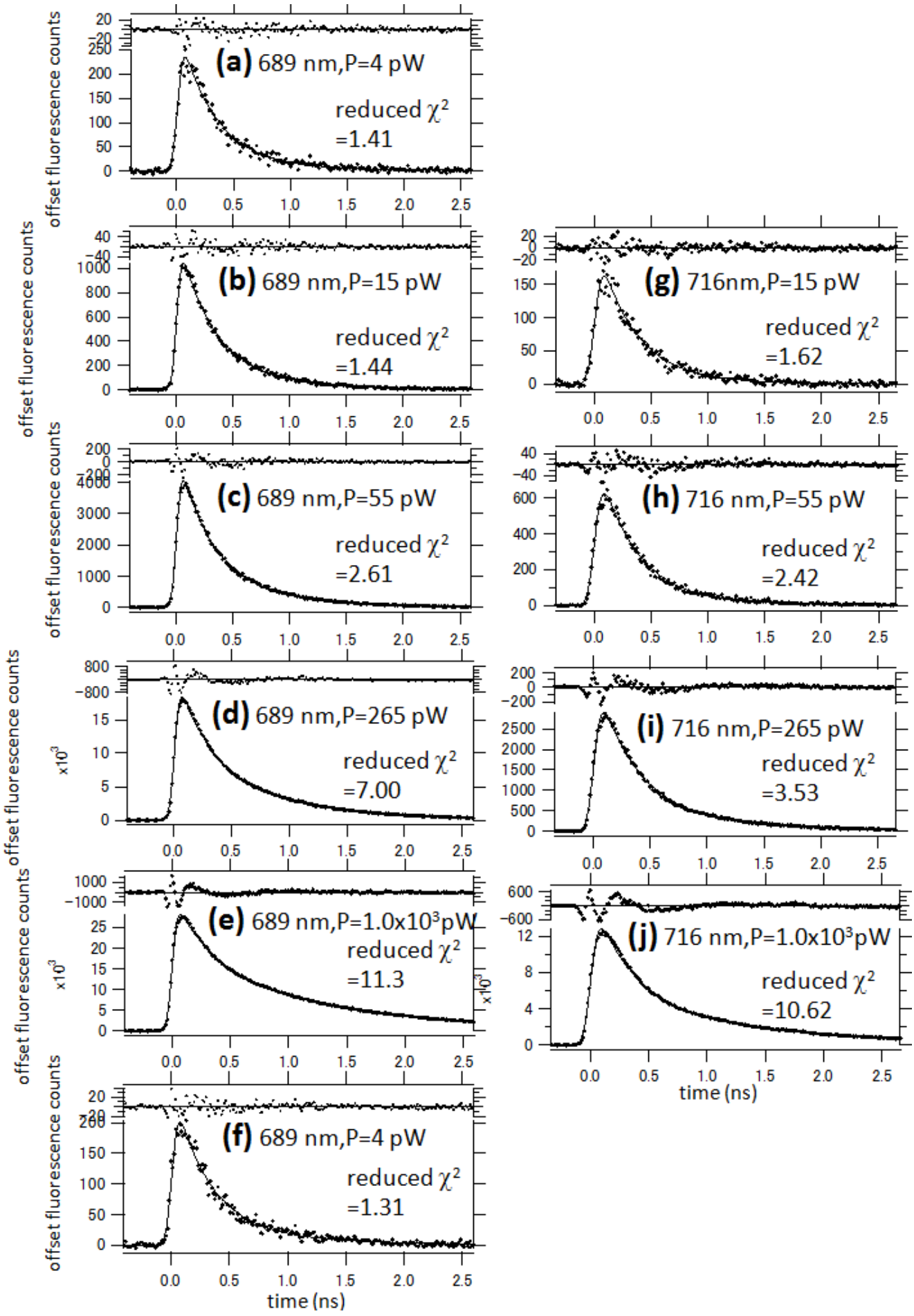

Supplemental Figure S5.

Legend for Supplemental Figure S5. Fluorescence decay profiles of *P. kessleri*. Detection wavelength range was centered at 689 nm (a, b, c, d,e,f) or 716 nm (g,h,i,j). Fluorescence photon counts from 21 cells at 1 - 3 focal planes were collected and summed. The cells were sampled 24 days after an inoculation. Dots represent detected number of photons, but average photon counts in the sufficiently negative time region was subtracted. It is thus possible that artificially negative photon counts arise. Solid lines represent fitting curves made by convolution of the instrument-response function with a sum of one or two exponential functions. The parameters obtained through the curve fitting are shown in Table S4. The plots in (a) and (e) are the same as used in Fig. 2(d) in the main text. Although both the residuals and reduced chi square values indicate that more exponential components are necessary to achieve sufficient fit to the data especially at relatively high laser powers, we are here focusing on an approximate description of the whole data sets by at most two exponential decaying components. This basic policy is consistent with the use of two-state model to reproduce open-closed status of PSII in the FLIM.

Table S2.

Parameters yielded by curve fitting of the FLIM data of vegetative cells of *A. variabilis*.

P_{laser} [nW]	λ_{fl} [nm]	τ_1[ns] (amplitude in %)	τ_2 [ns] (amplitude in %)	Average lifetime [ns]	∞ (amplitude in %)	days after inoculation
0.08	689	0.23 (97)	n.d.	0.23	(3)	90
		0.22 (100)	n.d.	0.22	(0)	24
		0.21 (96)	0.75 (4)	0.23	(0)	3
0.30		n.a.	n.a.	n.a.	n.a.	90
		0.22 (96)	0.86 (4)	0.25	(0)	24
		0.23 (96)	0.79 (4)	0.25	(0)	3
1.1		0.21 (86)	0.62 (14)	0.27	(0)	90
		0.23 (88)	0.73 (12)	0.29	(0)	24
		0.24 (80)	0.77 (20)	0.34	(0)	3
5.3		n.a.	n.a.	n.a.	n.a.	90
		0.25 (72)	0.72 (28)	0.38	(0)	24
		0.24(57)	0.80 (43)	0.48	(0)	3
20		0.23(55)	0.79(44)	0.47	(1)	90
		0.27 (70)	0.70 (30)	0.39	(0)	24
		0.24 (53)	0.73(47)	0.47	(0)	3
0.08	716	0.23 (99)	n.d.	0.23	(2)	90
		0.21 (99)	1.24(< 1)	0.21	(0)	24
		0.24 (100)	n.d.	0.24	(0)	3
0.30		n.a.	n.a.	n.a.	n.a.	90
		0.23(100)	n.d.	0.22	(0)	24
		0.22(100)	n.d.	0.22	(0)	3
1.1		0.22 (95)	0.94 (4)	0.25	(1)	90
		0.23(98)	1.31(2)	0.29	(0)	24
		0.24 (93)	0.96 (7)	0.29	(0)	3
5.3		n.a.	n.a.	n.a.	n.a.	90
		0.23 (88)	0.83 (12)	0.30	(0)	24
		0.23 (82)	0.93 (18)	0.36	(0)	3
20		0.21 (81)	0.90 (19)	0.34	(0)	90
		0.24 (87)	0.80 (13)	0.31	(0)	24
		0.23 (81)	0.88 (19)	0.36	(0)	3

P_{laser}: laser power at the sample position

λ_{fl}:center wavelength of the detected fluorescence

n.d. = not detected

n.a. = no available data

Table S3.

Parameters yielded by curve fitting of the FLIM data of heterocysts of *A. variabilis*.

P_{laser} [nW]	λ_{fl} [nm]	τ_1[ns] (amplitude in %)	τ_2 [ns] (amplitude in %)	Average lifetime [ns]	∞ (amplitude in %)	days after inoculation
0.08	689	0.096 (99)	n.d.	0.096	(1)	90
		0.087 (98)	n.d.	0.087	(2)	24
		0.078 (100)	n.d.	0.078	(0)	3
0.30		n.a.	n.a.	n.a.	n.a.	90
		0.096(99)	n.d.	0.096	(1)	24
		0.084 (100)	n.d.	0.084	(0)	3
1.1		0.082 (97)	1.11 (3)	0.11	(0)	90
		0.078 (94)	0.61(5)	0.11	(0)	24
		0.081 (98)	0.84 (2)	0.094	(0)	3
5.3		n.a.	n.a.	n.a.	n.a.	90
		0.082(95)	0.83 (5)	0.12	(0)	24
		0.080 (98)	0.88(2)	0.94	(0)	3
20		0.084 (97)	1.41 (2)	0.11	(1)	90
		0.081 (91)	0.64 (8)	0.13	(1)	24
		0.078 (98)	0.72 (2)	0.089	(0)	3
0.30	716	n.a.	n.a.	n.a.	n.a.	90
		0.15 (100)	n.d.	0.15	(0)	24
		0.14 (100)	n.d.	0.14	(0)	3
1.1		0.13(100)	n.d.	0.13	(0)	90
		0.15 (100)	n.d.	0.15	(0)	24
		0.14 (100)	n.d.	0.14	(0)	3
5.3		n.a.	n.a.	n.a.	n.a.	90
		0.14(100)	n.d.	0.14	(0)	24
		0.14 (100)	n.d.	0.14	(0)	3
20		0.14 (100)	n.d.	0.14	(0)	90
		0.14 (99)	1.78(1)	0.16	(0)	24
		0.14 (100)	n.d.	0.14	(0)	3

P_{laser}: laser power at the sample position

λ_{fl}:center wavelength of the detected fluorescence

n.d. = not detected

n.a. = no available data

Table S4.

parameters yielded by curve fitting of FLIM data of *P. kessleri*.

P_{laser} [nW]	λ_{fl} [nm]	τ_1 (ns) (amplitude in %)	τ_2 (ns) (amplitude in %)	Average lifetime (ns)	∞ (amplitude in %)	days after inoculation
4 -	689	0.28 (83)	0.62(17)	0.36	(0)	29
		0.40 (99)	n.d.	0.40	(1)	15
15		0.28 (79)	0.65 (21)	0.36	(0)	29
		n.a.	n.a.	n.a.	n.a.	15
55		0.29 (76)	0.69 (24)	0.38	(0)	29
		0.29 (66)	0.68 (34)	0.42	(0)	15
265		0.29 (61)	0.82(39)	0.50	(0)	29
		n.a.	n.a.	n.a.	n.a.	15
1.0 $\times 10^3$		0.32 (46)	1.3 (54)	0.83	(0)	29
		0.34 (48)	1.2(52)	0.77	(0)	15
15	716	0.32 (95)	0.87(5)	0.34	(0)	29
		n.a.	n.a.	n.a.	n.a.	15
55		0.34(100)	n.d.	0.34	(0)	29
		0.40(100)	n.d.	0.40	(0)	15
265		0.36 (90)	1.3(10)	0.45	(0)	29
		n.a.	n.a.	n.a.	n.a.	15
1.0 $\times 10^3$		0.37 (72)	1.5 (28)	0.68	(0)	29
		0.36(72)	1.3 (28)	0.63	(0)	15

P_{laser}: laser power at the sample position

λ_{fl}:center wavelength of the detected fluorescence

n.d. = not detected

n.a. = no available data

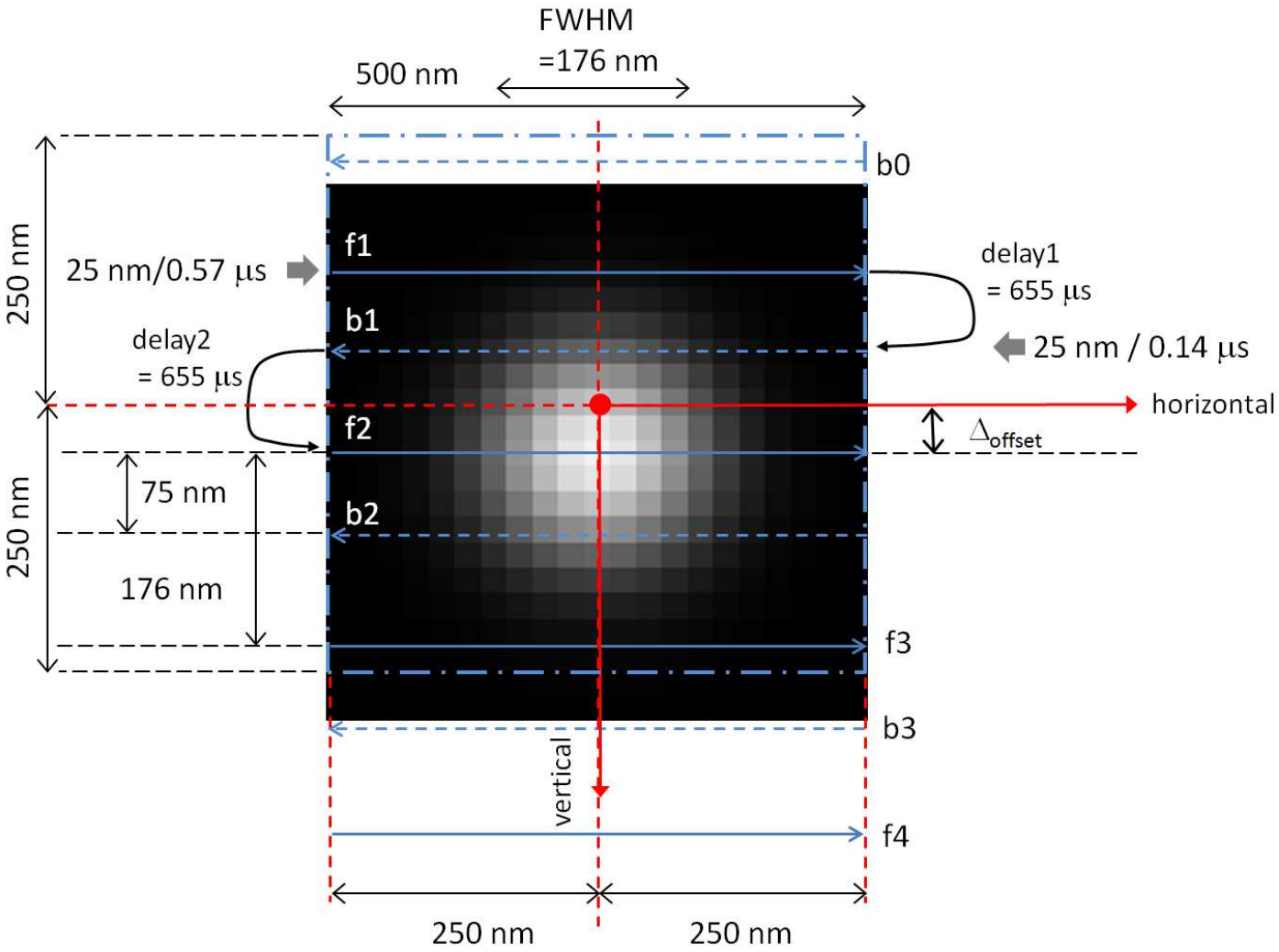

Supplemental Figure S6. Illustration of our model to reproduce the laser focus moving for FLIM image formation. The laser focus moves along the horizontal lines (light blue solid lines designated as f1,f2,f3,f4, ...) that are separated by 176 nm from each other, while time-correlated single photon counting (TCSPC) data are acquired. After each forward scan, the laser focus needs to move in the backward direction in order to be ready for the next forward scan (fly-back motion). For simplicity and averaging, the fly-back motion was assumed to be along a horizontal line that is separated from the previous forward scan by 75 nm (light blue broken lines designated as b0, b1, b2, b3, ...). Our TCSPC data were not acquired during the fly-back motion, but actinic effects by the laser in the fly-back motion was taken into account in the simulation. The forward and backward scans were performed at different speeds of 25 nm/0.57 μs and 25 nm/0.14 μs, respectively. In the simulation to reproduce FLIM data, single PSII unit is supposed to be fixed at the origin of the xy-coordinate (closed red circle). The distance between PSII and one of the horizontal lines for the forward scan (f2 in the figure) was defined to be Δ_{offset}. Simulations with Δ_{offset} of 0, 25, 50,75, 100, 125,150 nm were performed and averaged to yield the final results. The laser focus is expressed by a two-dimensional Gaussian distribution of photons with a full width at half maximum of 176 nm, when PSII is located exactly in the focus plane of the microscope objective. Excitation of PSII by the laser was assumed to be effective only when PSII resides in the square of a side length of 500 nm centered at the center of the laser focus, which is illustrated by the size of the gray-scale image showing intensity distribution of the laser. See Supplemental Text S1 for more details of the simulation.

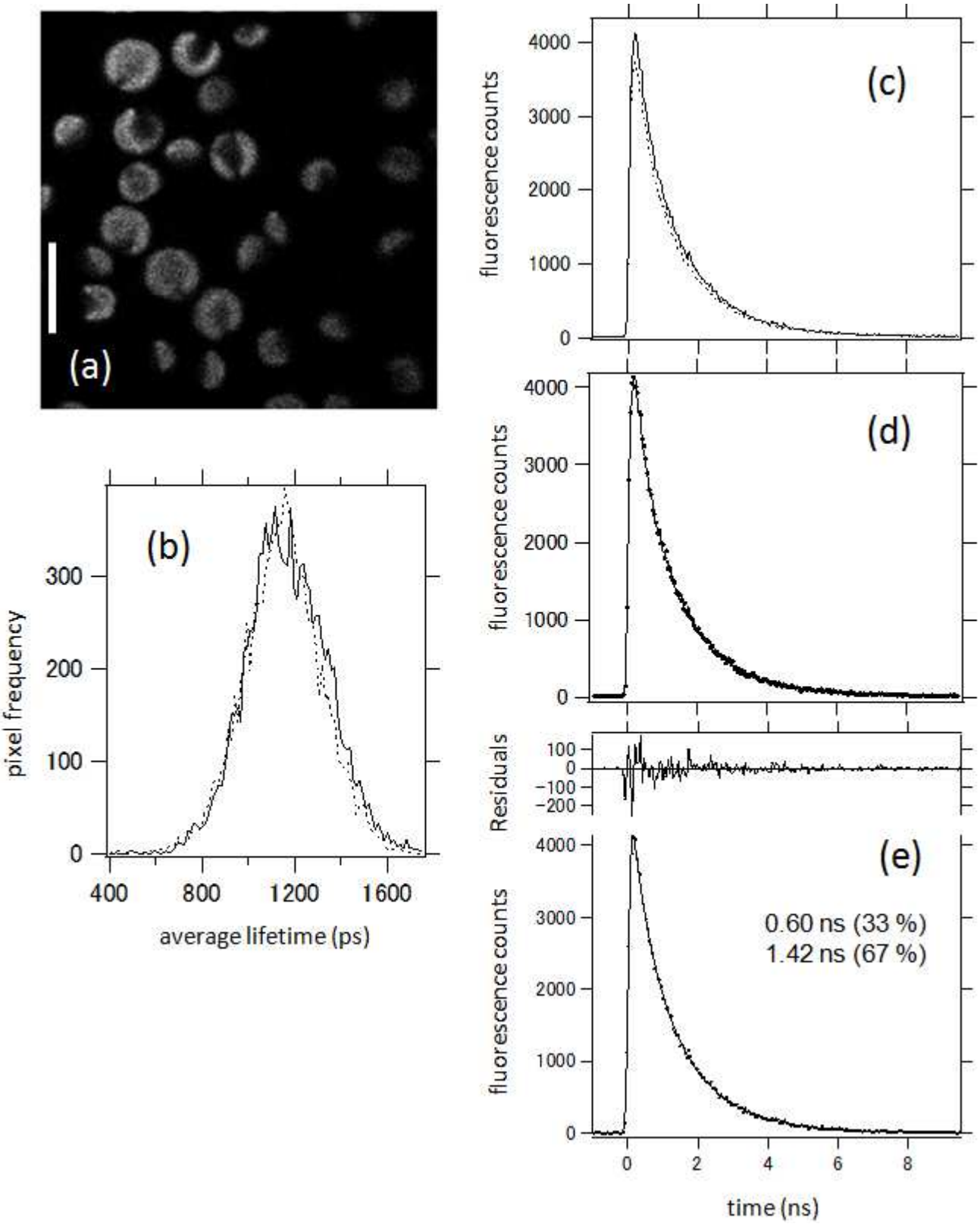

Supplemental Figure S7. FLIM data of *P. kessleri* cells with an exposure time of 4.5 s and repeated 10 times (Total exposure time was 45 s) with a relatively strong laser power (6 nW, cf. Fig. 4 in the main text). (a) Photon count-based fluorescent images obtained in the first 4.5 s. Scale bar = 10 μm. (b) Distributions of average fluorescence lifetime in the first (solid line) and last (broken line) 4.5 s. (c) Decay profiles of fluorescence of the whole image around 689 nm in the first (solid line) and last (broken line) 4.5 s without intensity normalization. Photon timing data of the whole image as in (a) were used. (d) The same plots as in (c) but with intensity normalization (solid line : first 4.5 s, dots: last 4.5 s). (e) The decay profile in the first 4.5 s (dots) fitted by a sum of two exponential functions (solid line, 1.42 ns (67%) and 0.60 ns (33%)) convoluted with the instrument-response function.

Supplemental text S1. Detailed explanation on the numerical simulation to reproduce multiexponential nature of fluorescence decay.

The simulation below is designed to estimate ratio of fluorescence photons detected from closed PSII in comparison with those from open PSII under the employed experimental conditions. First, the laser intensity profile in the focal plane was assumed to be given by a normalized two-dimensional Gaussian with the integration of 1 over the whole xy space.

$$f_{\mathrm{PSF}}(y,x)=\frac{\ln(2)}{\pi}\frac{1}{(d_{\mathrm{FWHM}}/2)^2}\exp[-\ln(2)\frac{(x-x_0)^2+(y-y_0)^2}{(d_{\mathrm{FWHM}}/2)^2},] \qquad \text{(eq. 1)}$$

where d_{FWHM} was a full width at half maximum to be equal to the so-called diffraction limit:

$$d_{\mathrm{FWHM}}=\frac{0.61\lambda}{NA}=\frac{0.61\times 0.404}{1.4}=0.176 \quad [\mu\mathrm{m}] \qquad \text{(eq. 2)}$$

λ and NA in eq.2 are wavelength of excitation laser and numerical aperture of the microscope objective, respectively. The unit length in the simulation, d_{unit}, was defined to be 25 nm when PSII is located at the exact focal plane of the microscope. Eq.1 is rewritten for the digital calculation as follows.

$$f_{\mathrm{profile}}(j_y,j_x)=\frac{\ln(2)}{\pi}\frac{1}{(d_{\mathrm{FWHM}}/d_{\mathrm{unit}}/2)^2}\exp[-\ln(2)\frac{{j_y}^2+{j_x}^2}{(d_{\mathrm{FWHM}}/d_{\mathrm{unit}}/2)^2}] \qquad \text{(eq.3)}$$

The j_y and j_x in (eq. 3) represent positions in lengths with the single unit length of 25 nm along the x and y coordinates, respectively. The normalization of (eq. 3) is approximately satisfied in a rectangular range of ±0.25 μm from the center of focus as in the following relation.

$$\sum_{j_y=-10}^{+10}\sum_{j_x=-10}^{+10} f_{\mathrm{profile}}(j_y,j_x)\approx 0.999163 \quad . \qquad \text{(eq. 4)}$$

We have thus neglected excitation photons of about 0.08 %.

Given the laser power at the sample position of P_{laser} in W (Watt), number of photons irradiated in the unit area of the simulation (25 × 25 nm) per unit time (1 s) is expressed as follows.

$$\frac{P_{\mathrm{laser}}}{(hc/\lambda)} f_{\mathrm{profile}}(j_y,j_x). \qquad \text{(eq.5)}$$

Dwell time per single pixel was 4 μs, and the size of single pixel in the sample space was 176 nm in the experimental imaging setup. It thus follows that number of photons irradiated in the unit area per single step time of the simulation (25 × 25 nm and per 4×25/176 μs) is expressed as follows.

$$\frac{P_{\mathrm{laser}}}{(hc/\lambda)} f_{\mathrm{profile}}(j_y,j_x)\frac{25}{176}\times 4\times 10^{-6} \quad . \qquad \text{(eq. 6)}$$

Although the time-correlated single photon counting (TCSPC) was performed only in the forward scan along the horizontal axis, the backward scan without TCSPC, the so-called "fly back", also affect the photochemical status of the thylakoid membrane. The time necessary for the fly back was 0.300 ms for the backward horizontal motion over the total pixel of 256, by which we assumed that number of photons irradiated by the fly back in the unit area per single step time (25 × 25 nm and per (300/256)×(25/176) μs) is given as follows.

$$\frac{P_{\text{laser}}}{(hc/\lambda)} f_{\text{profile}}(j_y, j_x) \frac{25}{176} \times \frac{300}{256} \times 10^{-6} \quad . \quad \text{(eq. 7)}$$

If total absorption cross section of the light-harvesting system for a single PSII reaction center (per PSII core monomer), σ_{PSII}, is given in the unit of cm^2 (Text S2, Table S7, S8), the excitation probability of PSII is expressed as follows, while the beam moves by 25 nm (= d_{unit}) in the forward and backward (fly back) horizontal scans.

$$p_f(j_y, j_x) = \frac{P_{\text{laser}}}{(hc/\lambda)} \frac{1}{{d_{\text{unit}}}^2} f_{\text{profile}}(j_y, j_x) \frac{25}{176} \times 4 \times 10^{-6} \sigma_{\text{PSII}} \quad , \qquad \text{(eq. 8)} \quad \text{for the forward scan,}$$

and

$$p_b(j_y, j_x) = \frac{P_{\text{laser}}}{(hc/\lambda)} \frac{1}{{d_{\text{unit}}}^2} f_{\text{profile}}(j_y, j_x) \frac{25}{176} \times \frac{300}{256} \times 10^{-6} \sigma_{\text{PSII}} \, , \qquad \text{(eq. 9) for the backward fly-back motion.}$$

where d_{unit} should be now in the unit of cm (25×10^{-7} cm). One single calculation step of the simulation in the forward scan is thus set to be different from that in the backward fly-back scan.

Time evolution of a single PSII (PSII core monomer containing only one electron transfer system) at a fixed position is calculated while the laser focus moves according to the above-mentioned manner (raster scan). Since the decay of closed PSII is reported to be multi-exponential with at least three components in both chloroplasts and cyanobacteria [1, 2], we have assumed three groups of PSII, each of which shows a single recovery time constant from closed PSII to the open state. We have assumed the same time constants as those reported for *Chlamydomonas reinhardtii* (0.23 ms (73 %), 46 ms (16 %) and 7.5 s (11%)) and *Synechocystis* sp. PCC6803 (0.22 ms (68 %), 2.9 ms (23 %) and 13 s (9%)) in the cases of *P. kessleri* and *A. variabilis*, respectively [1, 2].

Given one of the above time-constant, τ_{R}, one complete simulation can be performed to predict the ratio of fluorescence from closed PSII to that from open PSII in the FLIM data. We next calculate a weighted average of the three PSII types with the different time constants. Fluorescence from open PSII is defined to be fluorescence from PSII that is in the open state before the excitation. The closed PSII is set to be converted into open PSII with one of the exponential lifetimes. Fluorescence from closed PSII is defined to be fluorescence from PSII that was in the closed state before the excitation.

In a single step of the simulation, the excitation laser beam was set to be fixed at a position. The laser beam is set to move by 25 nm for the next calculation step, which is the unit length of the simulation. While the laser beam is fixed, single PSII unit is excited by a probability of p_{f} and p_{b} during the forward and backward scans, respectively (See eqs. 8 and 9 above). Closed PSII is set to be generated from the excited open PSII with a probability of 80 % [3] (See also section 3.2 in the main text). The time evolution of the number of closed and open PSII at the origin in the case of forward scan is given as follows ,

$$\begin{bmatrix} N_{\mathrm{open}}(t_{m+1}) \\ N_{\mathrm{closed}}(t_{m+1}) \end{bmatrix} = \begin{bmatrix} 1-0.80\,p_f(j_y(t_m), j_x(t_m)) & \{1-\exp[-(t_{m+1}-t_m)/\tau_{\mathrm{R}}]\} \\ 0.80\,p_f(j_y(t_m), j_x(t_m)) & \exp[-(t_{m+1}-t_m)/\tau_{\mathrm{R}}] \end{bmatrix} \begin{bmatrix} N_{\mathrm{open}}(t_m) \\ N_{\mathrm{closed}}(t_m) \end{bmatrix}, \qquad \text{(eq. 10)}$$

where $N_{\mathrm{open}}(t_{\mathrm{m}})$ and $N_{\mathrm{closed}}(t_{\mathrm{m}})$ are the number of open and closed PSII at the simulation time t_{m} (at the mth step) in a unit volume, respectively, j_{y} and j_{x} represent the relative location of the laser focus with respect to PSII unit and they are functions of t_{m}. ($j_{\mathrm{y}}(t_{\mathrm{m}})$ and $j_{\mathrm{x}}(t_{\mathrm{m}})$). Sum of the two types of PSII is actually constant: $N_{\mathrm{PSII}} = N_{\mathrm{open}}(t_{\mathrm{m}}) + N_{\mathrm{closed}}(t_{\mathrm{m}})$, as far as there is no net changes in the PSII concentration. The eq. 10 here is shown as eq. 3 in the main text. We here briefly describe how eq. 10 was derived. Our simulation originates from the following differential equation:

$$\begin{aligned} \frac{d}{dt}N_{\mathrm{open}}(t) &= -0.80k_{ex}N_{\mathrm{open}}(t) + \frac{1}{\tau_{\mathrm{R}}}N_{\mathrm{closed}}(t) \\ \frac{d}{dt}N_{\mathrm{closed}}(t) &= 0.80k_{ex}N_{\mathrm{open}}(t) - \frac{1}{\tau_{\mathrm{R}}}N_{\mathrm{closed}}(t) \end{aligned} \qquad \text{(eqs. 11)}$$

where k_{ex} is the rate constant of transition by optical excitation. The most common approximate conversion from the above differential equation into a difference equation for a computer numerical simulation is as follows.

$$\begin{aligned} \frac{N_{\mathrm{open}}(t_{m+1}) - N_{\mathrm{open}}(t_m)}{t_{m+1}-t_m} &\approx -0.80k_{ex}N_{\mathrm{open}}(t_m) + \frac{1}{\tau_{\mathrm{R}}}N_{\mathrm{closed}}(t_m) \\ \frac{N_{\mathrm{closed}}(t_{m+1}) - N_{\mathrm{closed}}(t_m)}{t_{m+1}-t_m} &\approx 0.80k_{ex}N_{\mathrm{open}}(t_m) - \frac{1}{\tau_{\mathrm{R}}}N_{\mathrm{closed}}(t_m) \end{aligned} \qquad \text{(eqs. 12)}$$

These are further converted into the following eqs. 13.

$$\begin{aligned} N_{\mathrm{open}}(t_{m+1}) - N_{\mathrm{open}}(t_m) &\approx -0.80k_{ex}(t_{m+1}-t_m)N_{\mathrm{open}}(t_m) + \frac{t_{m+1}-t_m}{\tau_{\mathrm{R}}}N_{\mathrm{closed}}(t_m) \\ N_{\mathrm{closed}}(t_{m+1}) - N_{\mathrm{closed}}(t_m) &\approx 0.80k_{ex}(t_{m+1}-t_m)N_{\mathrm{open}}(t_m) - \frac{t_{m+1}-t_m}{\tau_{\mathrm{R}}}N_{\mathrm{closed}}(t_m) \end{aligned} \qquad \text{(eqs. 13)}$$

The eqs.13 are equivalent to the following eq. 14, when $k_{\mathrm{ex}}(t_{\mathrm{m+1}}\text{-}t_{\mathrm{m}})$ is set to be p_{f}

$$\begin{bmatrix} N_{\mathrm{open}}(t_{m+1}) \\ N_{\mathrm{closed}}(t_{m+1}) \end{bmatrix} \approx \begin{bmatrix} 1-0.80\,p_f(j_y(t_m), j_x(t_m)) & (t_{m+1}-t_m)/\tau_{\mathrm{R}} \\ 0.80\,p_f(j_y(t_m), j_x(t_m)) & 1-(t_{m+1}-t_m)/\tau_{\mathrm{R}} \end{bmatrix} \begin{bmatrix} N_{\mathrm{open}}(t_m) \\ N_{\mathrm{closed}}(t_m) \end{bmatrix} \qquad \text{(eq. 14)}$$

It should be noted that the excitation probability depends on the distance between the center of the laser focus and PSII. On the other hand, we can predict the exact changes of the open and closed PSII when there is no optical excitation as follows.

$$N_{\text{closed}}(t_{m+1}) = N_{\text{closed}}(t_m)\exp\left[-\frac{t_{m+1}-t_m}{\tau_R}\right]$$

$$N_{\text{open}}(t_{m+1}) = N_{\text{PSII}} - N_{\text{closed}}(t_{m+1}) = \left\{N_{\text{open}}(t_m) + N_{\text{closed}}(t_m)\right\} - N_{\text{closed}}(t_m)\exp\left[-\frac{t_{m+1}-t_m}{\tau_R}\right] \quad \text{(eqs. 15)}$$

$$= N_{\text{open}}(t_m) + N_{\text{closed}}(t_m)\left\{1-\exp\left[-\frac{t_{m+1}-t_m}{\tau_R}\right]\right\}$$

The eqs. 15 can also be expressed in an analogous matrix and vector form as follows.

$$\begin{bmatrix} N_{\text{open}}(t_{m+1}) \\ N_{\text{closed}}(t_{m+1}) \end{bmatrix} = \begin{bmatrix} 1 & \{1-\exp[-(t_{m+1}-t_m)/\tau_{\text{R}}]\} \\ 0 & \exp[-(t_{m+1}-t_m)/\tau_{\text{R}}] \end{bmatrix} \begin{bmatrix} N_{\text{open}}(t_m) \\ N_{\text{closed}}(t_m) \end{bmatrix} \quad \text{(eq. 16)}$$

If we add the effects of optical excitation to the eq. 16 as in eq. 14, we obtain the following eq. 17.

$$\begin{bmatrix} N_{\text{open}}(t_{m+1}) \\ N_{\text{closed}}(t_{m+1}) \end{bmatrix} = \begin{bmatrix} 1-0.80\,p_f(j_y(t_m), j_x(t_m)) & \{1-\exp[-(t_{m+1}-t_m)/\tau_{\text{R}}]\} \\ 0.80\,p_f(j_y(t_m), j_x(t_m)) & \exp[-(t_{m+1}-t_m)/\tau_{\text{R}}] \end{bmatrix} \begin{bmatrix} N_{\text{open}}(t_m) \\ N_{\text{closed}}(t_m) \end{bmatrix} \quad \text{(eq. 17)}$$

This is actually the same as eq. 10. When $(t_{m+1}-t_m)/\tau_R$ is sufficiently small, the eq. 17 is well approximated by the eq. 14 because of the following approximate relation.

$$\exp\left[-\frac{t_{m+1}-t_m}{\tau_R}\right] \approx \left(1-\frac{t_{m+1}-t_m}{\tau_R}\right) \quad \text{(eq. 18)}$$

The eq. 17 is thus equivalent to eq. 14 when the simulation time step is sufficiently small, and the eq. 17 is more rigorous and superior to eq. 14 in the calculation step in which there is no optical excitation. It should be noted that single PSII is not exposed to laser light in most of the time during the FLIM imaging in the case of single-laser-focus-based confocal scanner. The eq. 17 was thus employed in our work.

The eq. 10 or 17 can be converted into the following expression based on probability for a single PSII if it is divided by N_{PSII}.

$$\begin{bmatrix} p_{\text{open}}(t_{m+1}) \\ p_{\text{closed}}(t_{m+1}) \end{bmatrix} = \begin{bmatrix} p_{\text{open}}(t_{m+1}) \\ 1-p_{\text{open}}(t_{m+1}) \end{bmatrix} = \begin{bmatrix} 1-0.80\,p_f(j_y(t_m), j_x(t_m)) & \{1-\exp[-(t_{m+1}-t_m)/\tau_{\text{R}}]\} \\ 0.80\,p_f(j_y(t_m), j_x(t_m)) & \exp[-(t_{m+1}-t_m)/\tau_{\text{R}}] \end{bmatrix} \begin{bmatrix} p_{\text{open}}(t_m) \\ 1-p_{\text{open}}(t_m) \end{bmatrix},$$

(eq. 19)

where $p_{\text{open}}(t_{\text{m}}) = N_{\text{open}}(t_{\text{m}})/N_{\text{PSII}}$ and $p_{\text{closed}}(t_{\text{m}}) = N_{\text{closed}}(t_{\text{m}})/N_{\text{PSII}}$. This is equal to the eq. 3 in the main text. The fluorescence counts from open and closed PSII at the simulation time t_{m} are proportional to the product between excitation probability and populations of PSII in the two states at the time t_{m}, which are proportional to the $p_{\text{open}}(t_{\text{m}})$ and $1-p_{\text{open}}(t_{\text{m}})$, respectively. The experimentally obtained fluorescence decay is made of many PSII units in cells, but this situation is equivalently expressed by a single representative PSII unit at the position (x,y,z) = (0,0,0) with full description on the probability of

open/closed status, as shown by eq. 19. It thus follows that total number of fluorescence photons from open and closed PSII are accumulated as follows.

$$F_{\text{open, accum}} \propto \sum_{s=1}^{2\text{or}3}\sum_{k=1}^{29}\sum_{i=N_{y1}}^{N_{y2}}\sum_{j=-N_x}^{+N_x} p_f\left(7i+\left\{\Delta_{\text{offset}}/25\right\}, j\right) N_{\text{PSII}} p_{\text{open}}(t_{j,i,k,s}) = N_{\text{PSII}}\sum_{s=1}^{2\text{or}3}\sum_{k=1}^{29}\sum_{i=N_{y1}}^{N_{y2}}\sum_{j=-N_x}^{+N_x} p_f\left(7i+\left\{\Delta_{\text{offset}}/25\right\}, j\right) p_{\text{open}}(t_{j,i,k,s}) \quad \text{(eq. 20)}$$

$$F_{\text{closed, accum}} \propto \sum_{s=1}^{2\text{or}3}\sum_{k=1}^{29}\sum_{i=N_{y1}}^{N_{y2}}\sum_{j=-N_x}^{+N_x} p_f\left(7i+\left\{\Delta_{\text{offset}}/25\right\}, j\right) N_{\text{PSII}}\left\{1-p_{\text{open}}(t_{j,i,k,s})\right\} = N_{\text{PSII}}\sum_{s=1}^{2\text{or}3}\sum_{k=1}^{29}\sum_{i=N_{y1}}^{N_{y2}}\sum_{j=-N_x}^{+N_x} p_f\left(7i+\left\{\Delta_{\text{offset}}/25\right\}, j\right)\left\{1-p_{\text{open}}(t_{j,i,k,s})\right\} \quad \text{(eq. 21)}$$

where the previously used index *m* is replaced with a new set of indices *j, i, k, s*. The index *j* correspond to different horizontal positions of the laser focus at a constant vertical position, *i* to different vertical positions of the laser focus in a single focal plane, *k* to different frames for accumulation in the same focal plane, and *s* to different focal planes. The parameter Δ_{offset} (varied between 0 and 175 nm, as described later) represents a relative vertical offset in nm between the origin (location of PSII) and one of the horizontal lines that are fastest scan axes of the laser. The integer coordinates, $7i+(\Delta_{\text{offset}}/25)$ and *j* corresponding to j_y and j_x in the previous notations (eq. 19 and earlier ones), indicate the relative location of the laser focus with respect to the position of PSII (origin), as shown in Fig. S6, by which probability of exciting and detecting the fluorescence from the PSII at the simulation step denoted by *j,i,k,s* is determined. It should be noted that different horizontal lines of the laser scans are separated by 176 nm, which gives the rounded integer value 7 in $p_f(7i+\{\Delta_{\text{offset}}/25\})$ in eqs 20 and 21 (because 176/25~7, when the unit length of the simulation is 25 nm at z_s=0 μm). For a simulated time of $t_{j,i,k,s}$, there is a unique position of the laser focus, (x_j, y_i, z_s). According to the size of the laser focus and confocality in the fluorescence detection , *j* and *i* are limited to the range that satisfy the following conditions (cf. eq. 4, and Supplemental Fig. S6).

$$\begin{aligned} &|x_j| \le 0.25 \quad [\mu\text{m}], \\ &|y_i| \le 0.25 \quad [\mu\text{m}], \end{aligned} \quad \text{or equivalently expressed as} \quad \begin{aligned} &|j_x| = |j| \le 10 = N_x \quad , \\ &|j_y| = \left|7i+\left\{\Delta_{offset}/25\right\}\right| \le 10, \end{aligned} \quad \text{(eq. 22)}$$

These ranges were used when the laser focus is located in the plane of z_s=0 (when PSII is located in the exact focus plane). It should be again noted that PSII unit is set to be at the origin of the xyz coordinate. In the actual experiments, the scan for the 256 horizontal positions in the imaging was carried out at 256 different vertical positions with an interval of 176 nm to form an image of 256×256 pixels (45 × 45 μm area). Due to the finite range of excitation area (eq. 22 and Supplemental Fig. S6), for PSII located at the origin, (x,y,z) = (0,0,0), horizontal laser scans in the forward direction at only two or three vertical positions can excite the PSII in a single xy scan (single frame), due to the inequality of 176×3> 2×250>176×2 in nm (N_{y2}–N_{y1}= 1 or 2 in eqs 20 and 21). It is also the case with the backward fly-back motion of the laser. The backward fly-back motion of the laser is set to be parallel with the previous horizontal line (forward scan) with a separation of 75 nm,

which is for the sake of simplicity of calculation (Supplemental Fig. S6). When the laser is moving in a single line at a constant vertical position while eq. 22 is satisfied, $t_{j+1,i,k,s} - t_{j,i,k,s}$ is set to be 4×(25/176) and 300/256×(25/176) μs in the forward and backward scans, respectively (cf. eq. 8 and 9). The time interval between one forward scan and the subsequent backward scan (e.g., between f1 and b1, or between f2 and b2 in Supplemental Fig. S6) is set to be 655 μs (delay 1), which is about half the time required for a single line in the imaging by the confocal scanner. The same time interval (655 μs) was assumed between one backward scan and the subsequent forward scan (This is designated as delay 2, e.g., between b1 and f2, or between b2 and f3 in Supplemental Fig. S6). Between two consecutive frames in the multiple frames used to improve the s/n of the image at the same focal plane, $t_{j,i,k+1,s} - t_{j,i,k,s}$ is set to be 341 ms that is the minimal time for acquiring a single image under the current settings of the scanning parameters. The total number of the frames was actually 29, by which it took about 10 s to obtain a single accumulated FLIM image (0.341×29 = 9.889).

Furthermore, FLIM images at three focal planes with a spacing of 1.0 μm were acquired in this study. Even when the laser focus and depth of PSII (z=0) is different by e.g., 1.0 μm, there is some actinic effects by the laser. Intensity profile of the laser beam at the out-of-focus position was estimated according to the Gaussian beam theory [4].

$$w_{1/2}(\Delta z) = w_{1/2}(0)\sqrt{\left\{1+\left(\frac{\lambda(\Delta z)2\ln(2)}{\pi\{w_{1/2}(0)\}^2}\right)^2\right\}} \qquad \text{(eq. 23)}$$

where full width at half maximum (FWHM) of the laser intensity profile in the plane of z=Δz, $w_{1/2}(\Delta z)$, is related to the one at the exact laser focus, $w_{1/2}(0)$ (=0.176 μm), the optical wavelength in the medium, λ (=0.404/n), and the difference in depth between PSII and the laser focus, Δz. Refractive index, n, was assumed to be 1.4, which is an intermediate value between water (1.33) and the chloroplast (>1.42),[5], although there should be wavelength dependence. In the calculation of excitation probability of PSII by such an out-of-focus laser, unit length of the calculation was enlarged proportionally to the enhancement of the FWHM of the laser intensity profile as in eq. 23. In order to save computing times without degradation in the accuracy, we have analogously magnified the following factors in the excitation probability calculation: (i) upper limit of the distance between PSII to be excited and the center of laser focus (eq. 22), (ii) single step time in the calculation, $t_{j+1,i,k,s} - t_{j,i,k,s}$. For example, when the exact laser focus and depth of PSII (z=0) is different by 1.0 μm,

$$\begin{aligned} w_{1/2}(1.0) &= w_{1/2}(0)\times 4.23 = 0.176\times 4.23 \quad [\mu m] \\ d_{unit}(1.0) &= d_{unit}(0.0)\times 4.23 = 0.025\times 4.23 \quad [\mu m] \end{aligned} \qquad \text{(eq. 24)}$$

Single step time at each focal plane, $t_{j+1,i,k,s} - t_{j,i,k,s}$, is given by $d_{unit}(1.0)$ divided by the constant laser scanning speed. The summation over the different s (different focal planes) in eqs. 20 and 21 are thus efficiently performed by adjusting the beam intensity profile, unit length, single step time and the distance limit between center of laser focus and PSII to be excited. For the CF decay profiles of *A. variabilis* at 689 nm (Fig. S2) and the consequent fitting results (Table 1 in the main text and Table S2), we have used only FLIM data at the depth of −1.0 μm, although all cells that were scanned at −1.0, 0.0 and 1.0 μm. The FLIM data at −1.0 μm was always acquired after the data collection at 0.0 (first) and 1.0 μm (second) (Table S1). The simulation curve in Fig. 4 in the main text for the case of *A. variabilis* was thus estimated to be TCSPC data collected after PSII was irradiated by out-of-focus laser at Δz=1.0 and 2.0 μm in eq. 23. For the CF decay profiles of *P. kessleri* (Supplemental Fig. 5) and the consequent fitting results (Table 3 in the main text and Table S4), we have averaged all FLIM data at the three scanning depths, which were −1.0, 0.0 and 1.0 μm. The simulation in Fig. 4 in the main text for the case of *P. kessleri* was thus estimated to be TCSPC data collected after PSII was irradiated by out-of-focus

laser at Δz=1.0 μm on average.

There remains an arbitrariness in the choice of relative vertical offset, Δ_{offset}, between the origin (location of PSII) and one of the horizontal lines for the forward scan of the laser. We have thus obtained $F_{\mathrm{open,\ accum}}(\Delta_{\mathrm{offset}})$ and $F_{\mathrm{closed,\ accum}}(\Delta_{\mathrm{offset}})$ by the above simulation with 8 different offset positions with an interval of 25 nm, which approximately spans over the whole interval between neighboring horizontal lines (25 nm×(8−1) ~176 nm). The eight sets of $F_{\mathrm{open,\ accum}}(\Delta_{\mathrm{offset}})$ and $F_{\mathrm{closed,\ accum}}(\Delta_{\mathrm{offset}})$ were averaged to obtain the $F_{\mathrm{open,\ accum}}(P_{\mathrm{laser}}, \tau_{\mathrm{R}})$ and $F_{\mathrm{closed,\ accum}}(P_{\mathrm{laser}}, \tau_{\mathrm{R}})$ at a specified laser power (P_{laser}) and recovery time (τ_{R}) (cf. Fig. S8).

Finally, one should take into account the weights of the three different time constants, $\tau_{\mathrm{R},1}$, $\tau_{\mathrm{R},2}$, $\tau_{\mathrm{R},3}$, for the recovery of open PSII from closed PSII [1],[2]. The experimentally obtained dependence of FLIM on the laser power should be compared with a weighted average as follows (cf. Fig. S8).

$$\left\langle F_{\mathrm{open,\ accum}}(P_{\mathrm{laser}})\right\rangle = \sum_{i=1}^{3} w_i F_{\mathrm{open,\ accum}}(P_{\mathrm{laser}}, \tau_{R,i})$$

$$\left\langle F_{\mathrm{closed,\ accum}}(P_{\mathrm{laser}})\right\rangle = \sum_{i=1}^{3} w_i F_{\mathrm{closed,\ accum}}(P_{\mathrm{laser}}, \tau_{R,i}) \qquad \text{(eqs. 25)}$$

Supplemental Text S2. Total absorption coefficients of PSII in *P. kessleri* and *A. variabilis*.

Total absorption coefficient of photosystem II for A. variabilis.

The pigments of PS II of *A. variabilis* was assumed to be the same as reported in the core of the PSII monomer (*Thermosynechococcus vulcanus*) [6]. 35 molecules of chlorophyll *a*, 2 molecules of pheophytin *a* and 11 molecules of β-carotene were considered. Absorption coefficients of these molecules at 404 nm (6.11×10^5 $cm^{-1}mol^{-1}dm^3$, 1.07×10^6 $cm^{-1}mol^{-1}dm^3$, and 5.59×10^5 $cm^{-1}mol^{-1}dm^3$ for chlorophyll *a*, pheophytin *a* and β-carotene, respectively) were obtained with the help of several references (Chappelle et al 1992, Watanabe et al 1984, Ustin et al 2009) [7-9]. The total absorption coefficient of PSII monomer amounts to 2.97×10^6 $cm^{-1}mol^{-1}dm^3$ (cf. Table S7).

Total absorption coefficient of photosystem II for Parachlorella kessleri.

The organization of PS II supercomplex of *P. kessleri.* was assumed to be the same as that proposed in the case of *Chlamydomonas reinhardtii* [10]. When light-harvesting ability per PSII is largest in state 1, there are three trimers of LHCII and a CP26 and CP29 per PSII monomer in the model PSII complex. The total number of pigments were largely based on a reference [11]. In addition to the above-mentioned absorption coefficients for the pigments common to cyanobacterial PSII, absorption coefficients of the other pigments at 404 nm (1.45×10^5 $cm^{-1}mol^{-1}dm^3$, 4.75×10^5 $cm^{-1}mol^{-1}dm^3$, 6.01×10^5 $cm^{-1}mol^{-1}dm^3$, and 5.69×10^5 $cm^{-1}mol^{-1}dm^3$ for Chl *b*, neoxanthin, violaxanthin, lutein) were obtained with the help of several references reporting their absorption spectra and absorption coefficients at representative peaks [7, 8, 12-14]. Given the sum of all pigments per PSII monomer (124.5 Chl *a*, 62.5 Chl *b*, 10 neoxanthin, 6.3 violaxanthin, 24.7 lutein, 11 β-carotene, 2 pheophytin molecules) , the total absorption coefficient amounts to 1.15×10^7 $cm^{-1}mol^{-1}dm^3$ (cf. Table S8).

Absorption coefficient of allophycocyanin for A. variabilis.

Extinction coefficients of the basic unit of allophycocyanin, $(\alpha\beta)_1$ (hereafter designated as monomer) at a peak absorption (2.32×10^5 $cm^{-1}mol^{-1}dm^3$, at 650 nm) was taken from the one reported for a cyanobacterium, *Synechococcus* PCC6312 [15]. According to the allophycocyanin complex reported for *Anabaena* PCC7120, *A. variabilis* and *Mastigocladus laminosus* [16], one whole allophycocyanin complex, whole core part of the phycobilisome, contains 12 trimers of a composition $(\alpha^{AP}\beta^{AP})_3$, 2 heterotrimers of a composition $(\alpha^{AP\text{-}B}\alpha_2{}^{AP}\beta_3{}^{AP})$, and 2 heterogeneous complexes of a composition $(\alpha_2{}^{AP}\beta_2{}^{AP}\beta^{16})$. Each unit of α and β contains single phycocyanobilin chromophore [17]. The total absorption coefficient of allophycocyanin complex is thus set to be 47 times (=12×3+2×3+2×3×(5/6)) that of monomer, $(\alpha\beta)_1$. The absorption coefficient of APC in a single PBS at 404 nm (6.86×10^5 $cm^{-1}mol^{-1}dm^3$) was estimated to be 0.0476 times that of the peak at 650 nm, based on the reported absorption spectrum [15] (cf. Table S7).

Absorption coefficient of phycocyanin and phycoerythrocyanin for A. variabilis.

Extinction coefficients of the basic unit of phycocyanin (PC), $(\alpha\beta)_6$ (hereafter designated as hexamer) at a peak absorption (17.92×10^5 $cm^{-1}mol^{-1}dm^3$, at 619 nm) was taken from the one reported for a cyanobacterium, *Mastigocladus laminosus* [18]. Extinction coefficients of the basic unit of phycoerythrocyanin (PEC), $(\alpha\beta)_6$ (hereafter designated as hexamer) at a peak absorption (18.42×10^5 $cm^{-1}mol^{-1}dm^3$, at 568 nm) was taken from the one reported for a cyanobacterium, *Anabaena* sp. 6411 [19]. A study based on single particle electron microscopy on *Anabaena* sp. PCC7120 showed that a single phycobilisome complex contains 8 rod structures attached to the core part [20]. Each rod contained mostly 2, sometimes 3 stacked elements. Each element had a dimension of 5-6 nm ×10 -12 nm, which well corresponds to the unit of $(\alpha\beta)_6$ [21]. Based on the proposed stoichiometry and structures in previous reports [20, 22], we have assumed that numbers of

PC hexamer and PEC hexamer in a single PBS of *A. variabilis* are 16 (=2 ×8) and 4 (=0.5 ×8), respectively. The total absorption coefficient at 404 nm by PC in a single PBS (2.29×10^{6} $cm^{-1}mol^{-1}dm^{3}$) was estimated to be 0.080 times that of the peak at 619 nm, based on the average of reported absorption spectra (cf. Table S2) [19, 23-27]. The total absorption coefficient at 404 nm by PEC in a single PBS (4.63×10^{5} $cm^{-1}mol^{-1}dm^{3}$) was estimated to be 0.063 times that of the peak at 619 nm, based on the average of reported absorption spectra (cf. Table S7) [19, 28].

Supplemental Text S3 (including a table below).

cell type	relative number of PSI in cell measured by fluorescence at sufficiently weak laser intensity	relative number of PSII in cell measured by fluorescence at sufficiently weak laser intensity	amplitude ratio of the short-lived fluorescence (< 0.3 ns)	amplitude ratio of the long-lived fluorescence (>0.5 ns)	laser power [nW]	open-closed status of PSII
vegetative	1/3	2/3	1	0	0.08	100 % open
			(1/3)+(1/2)*(2/3) =2/3	(1/2)*(2/3) =1/3	10	50 % closed
heterocyst	$1-r_2$	r_2	1	0	0.08	100 % open
			$1-0.5r_2$	$0.5r_2$	10	50 % closed

The aim of consideration in this section is to estimate contribution of PSI and PSII in the fluorescence at 689 nm, based on an assumption that contribution from PBS is negligible in the case of excitation at 404 nm. In the case of vegetative cells, the partitioning of CF at 689 nm into PSI and PSII contributions (1/3:2/3=1:2) was estimated in the section 3.2 (See also Fig. 4(a)). At 10 nW of the excitation power, 50 % of PSII is estimated to be closed by the simulation (See the broken line denoted by "PSII alone" in Fig. 4(a)). We assume that light-harvesting abilities of the dark-adapted PSII in vegetative cells (state II) and PSII in heterocysts of cyanobacterium *A. variabilis* are the same, which leads 50 % of PSII in heterocysts to be closed by the 10 nW laser. In the above table, r_2 is the ratio of PSII fluorescence in all CF at 689 nm in heterocysts. We here estimate r_2 based on the experimental and simulation results. The long-lived component attributable to photochemically active PSII is at most 4% of the total fluorescence amplitude at 689 nm even in the selected subgroup of heterocysts, because a long-lived component attributable probably to uncoupled phycobilisome seems to contribute to 8 % of the total amplitude (Table 2 in the main text). It then follows that the following relation holds:

$$1-0.5r_2 : 0.5r_2 \approx 1-0.04-0.08 : 0.04 = 0.88 : 0.04 = 22 : 1$$

$$r_2 \approx \frac{1}{11.5}$$

The PSII ratio in the fluorescence with a lifetime of shorter than 0.3 ns at 689 nm when PSII is open in heterocysts in comparison with those in vegetative cell is estimated to be as follows.

$$\frac{\dfrac{r_2}{(1-r_2)}}{\dfrac{(2/3)}{(1/3)}} \approx \frac{\dfrac{1}{11.5-1}}{2} \approx 0.048$$

Table S5 Fluorescence lifetime components resolved in studies on green algae using time-correlated single photon counting.

organism	λ_{ex} [nm] λ_{fl} [nm] W_{IRF} [ns]	lifetimes [ns] (amplitude in %)	average lifetime[a] [ns]	preillumination conditions, open-closed status or quenching status	reference
Chlorella pyrenoidosa	λ_{ex}=580 - 640 λ_{fl}>665 W_{IRF} ~0.79	0.49		dark	Beddard et al. 1979 [29]
Chlorella pyrenoidosa	λ_{ex}=620 λ_{fl}>665 W_{IRF} ~0.31	0.06 (2) 0.39 (30) 0.84(68)	0.69	open	Haehnel et al. 1982 [30]
Chlamydomonas reinhardtii	λ_{ex}=619 λ_{fl}=680 W_{IRF} ~0.13	0.086(58.6) 0.387(39.5) 1.395(0.019)	0.23	dark	Gulotty et al. 1985 [31]
Chlamydomonas reinhardtii	λ_{ex}=625 λ_{fl}=685 W_{IRF} ~0.06-0.07		0.4 1.69	open closed	Moya et al. 1986 [32]
Chlorella vulgaris	λ_{ex}=630 λ_{fl}=686 W_{IRF} ~0.13		0.345 1.59	open closed	Holzwarth et al. 1985 [33]
Scenedesmus obliquus	λ_{ex}=620 λ_{fl}=680-700 W_{IRF} ~0.12	0.085(38), 0.315(36) 0.61(25), 2.3 (0.3)	0.31	dark	Wendler and Holzwarth 1987 [34]
Chlamydomonas reinhardtii	λ_{ex} =405 λ_{fl}= 665 - 685 W_{IRF} =n.a.	0.17 (>98) 0.25 (>98)		state 1 state 2	Iwai et al 2010 [35]
Chlamydomonas reinhardtii	λ_{ex} =410 λ_{fl}= 644 - 716 W_{IRF} =0.15.	0.07 (0.51) 0.33 (0.43) 1.2 (0.06)	0.25	150 s under 600 µmol photons m^{-2} s^{-1}	Amarnath et al. 2012 [36]
Haematococcus pluvialis	λ_{ex}=850 (2hν) λ_{fl}= 650 - 720 W_{IRF} =n.a.	0.25 (92) 1.1 (8)	0.32	1 5 min under 250 µmol photons m^{-2} s^{-1}	Kristoffersen, et al. 2012 [37]
Chlorella sorokiniana	λ_{ex} =632 λ_{fl}= 660 - 750 W_{IRF} =0.11		0.24 - 0.28 1.25 - 1.45	open closed	Rizzo et al 2014 [38]

[a]For an easy comparison with our results, average amplitudes in the specified wavelength region were estimated based on the decay-associated spectra in the references.

n.a.= data not available.

Table S6 Fluorescence lifetime components resolved in several studies on cyanobacteria

organism	λ_{ex} [nm] λ_{fl} [nm][a] W_{IRF} [ns]	lifetimes [ns] (amplitude in %)	average lifetime[a] [ns]	preillumination conditions, open-closed status or quenching status	ref
Anabaena variabilis	λ_{ex} =580 λ_{fl}= 680 - 700 W_{IRF} =0.06	0.22 (85) 1.1 (9) 1.85(6)	0.40	dark-adapted	Bittersmann et al. 1988 [39]
Synechococcus 6301	λ_{ex} =670 λ_{fl}= 685 - 690 W_{IRF} =0.22	0.04 (77) 0.17 (19) 0.41 (4)	0.08	open	Mullineaux and Holzwarth 1993 [40]
Synechocystis 6803	λ_{ex} =680 λ_{fl} =690 W_{IRF} = 0.03 - 0.04	0.02 (87.5) 0.12-0.13 (9.7) 0.37-0.4 (2.6)	0.04	dark-adapted	Bittersmann and Vermaas 1991 [41]
Synechocystis 6803	λ_{ex}=407 λ_{fl}=680-700 W_{IRF} =0.08	0.04(36) 0.14(20) 0.28(36) 1.06(7) 3.32(1)	0.27	dark-adapted	Veerman et al. 2005 [42]
Synechocystis 6803	λ_{ex} =590 λ_{fl}=680-700 W_{IRF} =0.009	0.195 (~100)[b]		unquenched	Tian et al 2011 [43]
Synechocystis 6803	λ_{ex} =400 λ_{fl}=680-700 W_{IRF} ~0.009	0.025(70.5) 0.125(21.6) 0.389(6.6) 2.92(1.2)	0.107	dark	Krumova al. 2010 [44]

[a]For an easy comparison with our results, average amplitudes in the specified wavelength region were estimated based on the decay-associated spectra in the references.

[b]Rising components observed in the reference were excluded from the calculation of average fluorescence lifetime.

Supplemental Table S7 Summary of absorption coefficients and energy levels relevant to *A. variabilis*, based on an assumption that dimer of PSII is connected to phycobilisome consisting of allophycocyanin, phycocyanin and phycoerythrocyanin with the reported structure for *A. variabilis* [22]. See Text S2 for more details.

pigment molecules (approximate fluorescence peak wavelength in nm)	PSII monomer	23.5 units of allophycocyanin ($\alpha\beta$) per PSII monomer	48 units of phycocyanin ($\alpha\beta$) per PSII monomer	12 units of phycoerythrocyanin ($\alpha\beta$) per PSII monomer	total
number of Chla (685 nm)[a]	35	0	0	0	33
number of pheophytins (680 nm)[a]	2	0	0	0	2
number of carotenoid (510 nm)[a]	11	0	0	0	11
number of phycocyanobilin (approximate fluorescence peak wavelength in nm)	0	47 (660 nm)[a]	144 (645 nm)[a]	24 (620 nm)[a]	215
number of phycobiliviolin (approximate fluorescence peak wavelength in nm)	0	0	0	12 (620 nm)[a]	12
thermally equilibrated antenna size expressed by equivalent number of Chla[b]	36.2[b] (88%)	3.2[b] (8%)	1.7[b] (4 %)	0.02[b] (<0. 1%)	41.1[b] (100 %)
total absorption coefficient at 404 nm $cm^{-1}mol^{-1}dm^3$.	2.97×10^6 (63%)	3.43×10^5 (7 %)	1.15×10^6 (25 %)	2.32×10^5 (5%)	4.70×10^6 (100 %)

[a]These approximate peak wavelengths of fluorescence were taken from those in references [12, 45-47]

[b] Definition of thermally equilibrated antenna size expressed by equivalent number of Chla is given in Supplemental Text S7. Energy levels were based on approximate peaks of fluorescence spectra.

Supplemental Table S8 Summary of total absorption coefficients of PSII and energy levels of pigments relevant to *P. kessleri*., based on an assumption that PSII dimer is connected to six trimers of LHCII, one CP26 and one CP29. See Text S2 for more details.

pigment molecules (approximate fluorescence peak wavelength in nm)	number of pigment molecules in PSII monomer	number of pigment molecules in 9 LHCII units (3 trimers) per PSII monomer	number of pigment molecules in CP26 and CP29 per PSII monomer	total
Chla (685)[a]	35	72	17.5	
pheophytins (680)[a]	2	0	0	
Chlb (665)[a]	0	54	8.5	
β-carotene (530)[a]	11	0	0	
neoxanthin (510)[a]	0	9	1	
violaxanthin (510)[a]	0	4.5	0.8	
lutein (520)[a]	0	22.5	2.2	
thermally equilibrated antenna size expressed by equivalent number of Chla[b]	36.2[b] (27 %)	78.3[b] (59 %)	18.5[b] (14 %)	131.0[b] (100 %)
total absorption coefficient at 404 nm $cm^{-1}mol^{-1}dm^3$.	2.97×10^6 (26%)	7.16×10^6 (61 %)	1.52×10^6 (13%)	1.15×10^7 (100 %)

[a]These approximate peak wavelengths of fluorescence were taken from those in references or estimated based on fluorescence and absorption spectra of analogous molecules [12, 45, 47-49].

[b] Definition of thermally equilibrated antenna size expressed by equivalent number of Chla is given in Supplemental Text S7. Energy levels were based on approximate peaks of fluorescence spectra.

Supplemental text S4.

Averaged photon flux over the whole image area (45×45 μm = *A*) is given here in the case of 1 nW incident laser power of 404 nm at the sample (cf. Fig. 4 in the main text).

$$\frac{P}{\frac{hc}{\lambda}AN_A} \approx \frac{1\times10^{-9}}{\frac{6.626\times10^{-34}\times2.998\times10^{8}}{404\times10^{-9}}\times\left(45\times10^{-6}\right)^2\times6.02\times10^{23}}$$

$$\approx 1.67\times10^{-6} \quad \mathrm{mol\,m^{-2}\,s^{-1}} \quad when \quad P=1\times10^{-9} \quad [\mathrm{W}]$$

A: area of image obtained by the confocal laser-scanning microscope.

N_A: Avogadro constant

P: average laser power at the sample position

h: Plank constant

c:speed of light

λ: laser wavelength

Supplemental text S5

Excitation probability of PSII (e.g., with 200 Chla per PSII monomer) by a single pulse in the case of 1 nW incident laser power of 404 nm at the sample. This light-harvesting ability is slightly larger than the estimation of PSII for *P. kessleri* (~190 Chla)) that was employed for a simulation curve Fig. 4 in the main text.

Absorption cross section of chlorophyll is given as follows.

$$\sigma_{\mathrm{chl}} = \varepsilon 10^3 (\ln 10) N_A^{-1} \quad [\mathrm{cm^2}]$$

$$\varepsilon = 61{,}100 \qquad @\,404nm$$

ε : molar extinction coefficient (dm^3 mol^{-1} cm^{-1})=(M^{-1} cm^{-1}).

Excitation probability of PSII per single pulse is given as follows.

$$P_{ex} = N_{photons}\sigma_{\mathrm{chl}}\times200$$

$$= 6.11\times10^{4+3}(\ln10)N_A^{-1}\times200\times N_{photons}$$

$$= \frac{6.11\times10^{4+3}(\ln10)N_A^{-1}\times200\times\frac{1\times10^{-9}}{75.5\times10^{6}}\times\left(\frac{404\times10^{-9}}{6.63\times10^{-34}\times3.00\times10^{8}}\right)}{3.14\times\left(0.61\frac{404\times10^{-7}}{1.4}\right)^2}$$

$$\approx 0.005$$

where,

approximate area of the laser focus: $3.14\times\left(0.61\frac{404\times10^{-7}}{1.4}\right)^2$ (cm^2)

single pulse energy: $\frac{1\times10^{-9}}{75.5\times10^{6}}$ [J]

number of photons per single pulse: $\frac{1\times10^{-9}}{75.5\times10^{6}}\times\left(\frac{404\times10^{-9}}{6.63\times10^{-34}\times3.00\times10^{8}}\right)$

$N_{photons}$: number of photons in a single pulse per cm^2.

σ_{chl} : absorption cross section of chlorophyll at 404 nm. (cm^2)

Supplemental text S6.

The relation between CFL (chlorophyll fluorescence lifetime) and the maximum quantum yield of photosynthetic charge separation of PSII in the dark-adapted state.

In the simplest model (two-state model), PSII is assumed to exhibit only two states in terms of the fluorescence properties. One is open state that can quench singlet excited state by the primary charge separation. The other is closed state that already has charge-separated redox cofactors by which no more photosynthetic charge separation (PCS) occurs. The simulation plots in Fig. 4 were obtained by assuming this two-state model. In this case, the CFLs of the open and closed PSII is most simply defined as follows.

$$\tau_{open}=\frac{1}{k_{PCS}+k_{NPQ}+k_R+k_{NR}}$$

$$\Rightarrow\quad \tau_{closed}=\frac{1}{k_{NPQ}+k_R+k_{NR}},\qquad \text{if } k_{\mathrm{PCS}}=0\ .$$

where k_{PCS}, k_{NPQ}, k_R and k_{NR} are rate constants of photosynthetic charge separation, biologically activated quenching (so-called nonphotochemical quenching, NPQ), radiative decay and the other non-radiative decay, respectively. In the case of the CL at 689 nm of *P. kessleri* chloroplasts (cf. Table 3 in the main text),

$$\frac{\left\langle\tau_{open}\right\rangle^{-1}-\tau_{closed}{}^{-1}}{\left\langle\tau_{open}\right\rangle^{-1}}=\frac{k_{PCS}}{k_{PCS}+k_{NPQ}+k_R+k_{NR}}\approx\frac{(0.38)^{-1}-(1.42)^{-1}}{(0.38)^{-1}}\approx0.73\approx\frac{F_M-F_0}{F_M}\equiv\frac{F_V}{F_M}$$

where F_M, F_0, F_V are maximum fluorescence yield, minimal fluorescence yield and variable fluorescence yield of dark-adapted PSII in the PAM fluorometry, respectively. For *A. variabilis* in this study, use of the CFL at 689 nm (cf. Table 1 in the main text) leads to the following results.

$$\frac{k_{PCS}}{k_{PCS}+k_{NPQ}+k_R+k_{NR}}\approx\frac{(0.25)^{-1}-(0.79)^{-1}}{(0.25)^{-1}}\approx0.68$$

In the more detailed three-state model, the electron transfer system needs to be more explicitly considered. Only one example of a framework is described here [50].

The most relevant four redox cofactors are as follows.

P: primary electron donor chlorophyll (conventionally denoted P680)

I: primary electron acceptor (conventionally attributed to a pheophytin)

Q_A: secondary electron acceptor, quinone

Yz: secondary electron donor, the redox active tyrosine

Based on the above symbols,

(fully) open state: (Yz, P, I, Q_A)

semiclosed state(s) : e.g., (Yz^+, P, I, Q_A^-) , (Yz, P, I, Q_A^-)

closed state: e.g., (Yz, P, I^-, Q_A^-), (Yz, P^+, I^-, Q_A^-), (Yz, P^+, I, Q_A^-)

Only limited examples in each case are shown. The semiclosed state can be formed from the open state by single excitation of PSII. The fully closed state is formed only after open state is doubly excited.

Supplemental Text S7

Definition of thermally equilibrated antenna size expressed by equivalent number of Chla. If there is sufficient number of exchange of electronic excitation energy among all connected pigments in terms of energy transfer before the singlet excited state is lost, the probability of excitation to reside on a pigment of type *i* after the thermalization process is expressed as follows (Boltzmann factor).

$$\exp\left[-\frac{E_i - E_{\mathrm{Chla}}}{k_{\mathrm{B}}T}\right]$$

where k_B, T, E_{Chla}, E_i are Boltzmann factor, absolute temperature, energy level of Chla and energy level of the pigment of type *i*, respectively. In order to estimate total capacity of accepting excitation energy of a pigment-protein complex at a thermal equilibrium, one should estimate the number-weighted sum of the Boltzmann factor for all pigment types as follows.

$$\sum_i N_i \exp\left[-\frac{E_i - E_{\mathrm{Chla}}}{k_{\mathrm{B}}T}\right] = \sum_i N_i \exp\left[-\frac{hc}{k_{\mathrm{B}}T}\left(\frac{1}{\lambda_i} - \frac{1}{\lambda_{\mathrm{Chla}}}\right)\right]$$

where N_i, h, c, λ_{Chla}, λ_i are number of the same type of pigment, Plank's constant, speed of light, wavelengths of light coresponding to the energy levels, respectively. This formula is used for Tables S3 and S4.

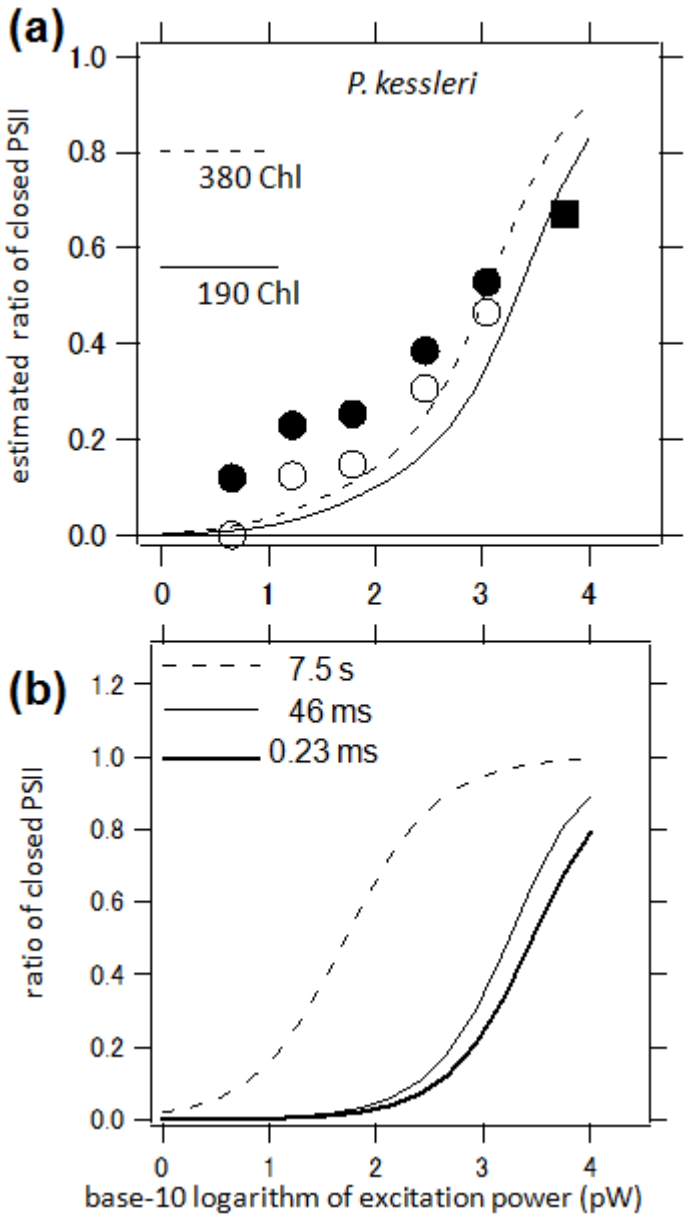

Supplemental Figure S8. Simulated ratio of long-lived fluorescence from closed PSII that is dependent on laser power. This panel is the same as the panel (b) of Fig. 4 in the main text, but it is shown here for easy comparison with the panel (b) on the same horizontal scale. (b) Simulated ratio of closed PSII that is dependent on laser power. Three plots were estimated with closed PSII converted into open PSII with a single time constant. The employed time constants are shown as a legend in the graph, which are based on a reference [2].

Reference list for the Supplemental Materials

[1] I. Vass, D. Kirilovsky, A.L. Etienne, UV-B radiation-induced donor- and acceptor-side modifications of photosystem II in the cyanobacterium Synechocystis sp PCC 6803, Biochemistry, 38 (1999) 12786-12794.

[2] A. Volgusheva, G. Kukarskikh, T. Krendeleva, A. Rubin, F. Mamedov, Hydrogen photoproduction in green algae Chlamydomonas reinhardtii under magnesium deprivation, Rsc Advances, 5 (2015) 5633-5637.

[3] S.W. Hogewoning, E. Wientjes, P. Douwstra, G. Trouwborst, W. van Ieperen, R. Croce, J. Harbinson, Photosynthetic Quantum Yield Dynamics: From Photosystems to Leaves, The Plant Cell, 24 (2012) 1921-1935.

[4] A.E. Siegman, Lasers, University Science Books, Sausalito, California, 1986.

[5] Y. Tamada, T. Murata, M. Hattori, S. Oya, Y. Hayano, Y. Kamei, M. Hasebe, Optical Property Analyses of Plant Cells for Adaptive Optics Microscopy, International Journal of Optomechatronics, 8 (2014) 89-99.

[6] Y. Umena, K. Kawakami, J.-R. Shen, N. Kamiya, Crystal structure of oxygen-evolving photosystem II at a resolution of 1.9 Å, Nature, 473 (2011) 55-60.

[7] T. Watanabe, A. Hongu, K. Honda, M. Nakazato, M. Konno, S. Saitoh, PREPARATION OF CHLOROPHYLLS AND PHEOPHYTINS BY ISOCRATIC LIQUID-CHROMATOGRAPHY, Analytical Chemistry, 56 (1984) 251-256.

[8] E.W. Chappelle, M.S. Kim, J.E. McMurtrey, RATIO ANALYSIS OF REFLECTANCE SPECTRA (RARS) - AN ALGORITHM FOR THE REMOTE ESTIMATION OF THE CONCENTRATIONS OF CHLOROPHYLL-A, CHLOROPHYLL-B, AND CAROTENOIDS IN SOYBEAN LEAVES, Remote Sensing of Environment, 39 (1992) 239-247.

[9] S.L. Ustin, A.A. Gitelson, S. Jacquemoud, M. Schaepman, G.P. Asner, J.A. Gamon, P. Zarco-Tejada, Retrieval of foliar information about plant pigment systems from high resolution spectroscopy, Remote Sensing of Environment, 113 (2009) S67-S77.

[10] B. Drop, M. Webber-Birungi, S.K.N. Yadav, A. Filipowicz-Szymanska, F. Fusetti, E.J. Boekema, R. Croce, Light-harvesting complex II (LHCII) and its supramolecular organization in Chlamydomonas reinhardtii, Biochimica Et Biophysica Acta-Bioenergetics, 1837 (2014) 63-72.

[11] S. Caffarri, T. Tibiletti, R.C. Jennings, S. Santabarbara, A Comparison Between Plant Photosystem I and Photosystem II Architecture and Functioning, Current Protein & Peptide Science, 15 (2014) 296-331.

[12] H.A. Frank, J.A. Bautista, J.S. Josue, A.J. Young, Mechanism of nonphotochemical quenching in green plants: Energies of the lowest excited singlet states of violaxanthin and zeaxanthin, Biochemistry, 39 (2000) 2831-2837.

[13] G. Britton, UV/visible spectroscopy, in: G. Britton, Liaaen-Jensen, S. and Pfander, H. (Ed.) Carotenoids: Spectroscopy, Birkhauser, Basel, 1995, pp. 13 - 62.

[14] B.H. Davies, K**ö**st H.-P., Carotenoids, in: K. H.-P. (Ed.) Handbook of Chromatography; Plant Pigments, CRC Press, Boca Raton, 1998, pp. 1-185.

[15] G. Cohen-Bazire, S. Beguin, S. Rimon, A.N. Glazer, D.M. Brown, PHYSICOCHEMICAL AND IMMUNOLOGICAL PROPERTIES OF ALLOPHYCOCYANINS, Archives of Microbiology, 111 (1977) 225-238.

[16] A. Ducret, S.A. Muller, K.N. Goldie, A. Hefti, W.A. Sidler, H. Zuber, A. Engel, Reconstitution, characterisation and mass analysis of the pentacylindrical allophycocyanin core complex from the cyanobacterium Anabaena sp. PCC 7120, Journal of Molecular Biology, 278 (1998) 369-388.

[17] B.D. Cohen-Bazire G, Phycobilisomes: Composition and Structure, in: W.B. Carr NG (Ed.) The biology of cyanobacteria, University of California Press, Berkeley, 1982, pp. 143-190.

[18] R. Fischer, S. Siebzehnrübl, H. Scheer, C-phycocyanin from Mastigocladus laminosus, in: H. Scheer, S. Schneider (Eds.) Photosynthetic Light-Harvesting Systems: Organization and Function, Walter de Gruyter,

Berlin, NewYork, 1988, pp. 71-76.
[19] D.A. Bryant, A.N. Glazer, F.A. Eiserling, Characterization and structural properties of the major biliproteins of Anabaena sp, Archives of microbiology, 110 (1976) 61-75.
[20] A. Ducret, W. Sidler, E. Wehrli, G. Frank, H. Zuber, Isolation, characterization and electron microscopy analysis of a hemidiscoidal phycobilisome type from the cyanobacterium Anabaena sp. PCC 7120, European journal of biochemistry, 236 (1996) 1010-1024.
[21] A. Marx, N. Adir, Allophycocyanin and phycocyanin crystal structures reveal facets of phycobilisome assembly, Biochimica et Biophysica Acta (BBA)-Bioenergetics, 1827 (2013) 311-318.
[22] A.N. Glazer, PHYCOBILISOMES - STRUCTURE AND DYNAMICS, Annual Review of Microbiology, 36 (1982) 173-198.
[23] A.N. Glazer, S. Fang, D.M. Brown, Spectroscopic properties of C-phycocyanin and of its α and ß subunits, Journal of Biological Chemistry, 248 (1973) 5679-5685.
[24] A.J. Tooley, Y.A. Cai, A.N. Glazer, Biosynthesis of a fluorescent cyanobacterial C-phycocyanin holo-α subunit in a heterologous host, Proceedings of the National Academy of Sciences, 98 (2001) 10560-10565.
[25] K. Minkova, A. Tchernov, M. Tchorbadjieva, S. Fournadjieva, R. Antova, M.C. Busheva, Purification of C-phycocyanin from Spirulina (Arthrospira) fusiformis, Journal of biotechnology, 102 (2003) 55-59.
[26] R. Bermejo, M.A. Felipe, E.M. Talavera, J.M. Alvarez-Pez, Expanded Bed Adsorption Chromatography for Recovery of Phycocyanins from the Microalga Spirulina Platensis, Chromatographia, 63 (2006) 59-66.
[27] D. Kumar, D.W. Dhar, S. Pabbi, N. Kumar, S. Walia, Extraction and purification of C-phycocyanin from Spirulina platensis (CCC540), Indian Journal of Plant Physiology, 19 (2014) 184-188.
[28] D.A. Bryant, Phycoerythrocyanin and phycoerythrin: properties and occurrence in cyanobacteria, Journal of general Microbiology, 128 (1982) 835-844.
[29] G. Beddard, G. Fleming, G. Porter, G. Searle, J. Synowiec, The fluorescence decay kinetics of in vivo chlorophyll measured using low intensity excitation, Biochimica et Biophysica Acta (BBA)-Bioenergetics, 545 (1979) 165-174.
[30] W. Haehnel, J.A. Nairn, P. Reisberg, K. Sauer, Picosecond fluorescence kinetics and energy transfer in chloroplasts and algae, Biochimica et Biophysica Acta (BBA)-Bioenergetics, 680 (1982) 161-173.
[31] R.J. Gulotty, L. Mets, R.S. Alberte, G.R. Fleming, Picosecond fluorescence study of photosynthetic mutants of Chlamydomonas reinhardii: origin of the fluorescence decay kinetics of chloroplasts, Photochemistry and Photobiology, 41 (1985) 487-496.
[32] I. Moya, M. Hodges, J. Briantais, G. Hervo, Evidence that the variable chlorophyll fluorescence in Chlamydomonas reinhardtii is not recombination luminescence, Photosynthesis Research, 10 (1986) 319-325.
[33] A.R. Holzwarth, J. Wendler, W. Haehnel, Time-resolved picosecond fluorescence spectra of the antenna chlorophylls in Chlorella vulgaris. Resolution of Photosystem I fluorescence, Biochimica et Biophysica Acta (BBA)-Bioenergetics, 807 (1985) 155-167.
[34] J. Wendler, A.R. Holzwarth, State transitions in the green alga Scenedesmus obliquus probed by time-resolved chlorophyll fluorescence spectroscopy and global data analysis, Biophys. J., 52 (1987) 717.
[35] M. Iwai, M. Yokono, N. Inada, J. Minagawa, Live-cell imaging of photosystem II antenna dissociation during state transitions, Proceedings of the National Academy of Sciences of the United States of America, 107 (2010) 2337-2342.
[36] K. Amarnath, J. Zaks, S.D. Park, K.K. Niyogi, G.R. Fleming, Fluorescence lifetime snapshots reveal two rapidly reversible mechanisms of photoprotection in live cells of Chlamydomonas reinhardtii, Proceedings of the

National Academy of Sciences of the United States of America, 109 (2012) 8405-8410.
[37] A.S. Kristoffersen, Ø. Svensen, N. Ssebiyonga, S.R. Erga, J.J. Stamnes, Ø. Frette, Chlorophyll a and nadph fluorescence lifetimes in the microalgae haematococcus pluvialis (chlorophyceae) under normal and astaxanthin-accumulating conditions, Applied Spectroscopy, 66 (2012) 1216-1225.
[38] F. Rizzo, G. Zucchelli, R. Jennings, S. Santabarbara, Wavelength dependence of the fluorescence emission under conditions of open and closed Photosystem II reaction centres in the green alga Chlorella sorokiniana, Biochimica et Biophysica Acta (BBA)-Bioenergetics, 1837 (2014) 726-733.
[39] E. Bittersmann, A. Holzwarth, G. Agel, W. Nultsch, PICOSECOND TIME - RESOLVED EMISSION SPECTRA OF PHOTOINHIBITED AND PHOTOBLEACHED Anabaena variabilis, Photochemistry and Photobiology, 47 (1988) 101-105.
[40] C.W. Mullineaux, A.R. Holzwarth, Effect of photosystem II reaction centre closure on fluorescence decay kinetics in a cyanobacterium, Biochimica et Biophysica Acta (BBA)-Bioenergetics, 1183 (1993) 345-351.
[41] E. Bittersmann, W. Vermaas, Fluorescence lifetime studies of cyanobacterial photosystem II mutants, Biochimica et Biophysica Acta (BBA)-Bioenergetics, 1098 (1991) 105-116.
[42] J. Veerman, F.K. Bentley, J.J. Eaton-Rye, C.W. Mullineaux, S. Vasil'ev, D. Bruce, The PsbU subunit of photosystem II stabilizes energy transfer and primary photochemistry in the phycobilisome-photosystem II assembly of Synechocystis sp. PCC 6803, Biochemistry, 44 (2005) 16939-16948.
[43] L. Tian, I.H. van Stokkum, R.B. Koehorst, A. Jongerius, D. Kirilovsky, H. van Amerongen, Site, rate, and mechanism of photoprotective quenching in cyanobacteria, Journal of the American Chemical Society, 133 (2011) 18304-18311.
[44] S.B. Krumova, S.P. Laptenok, J.W. Borst, B. Ughy, Z. Gombos, G. Ajlani, H. van Amerongen, Monitoring Photosynthesis in Individual Cells of Synechocystis sp. PCC 6803 on a Picosecond Timescale, Biophys. J., 99 (2010) 2006-2015.
[45] M. Mimuro, T. Tomo, Y. Nishimura, I. Yamazaki, K. Satoh, Identification of a photochemically inactive pheophytin molecule in the spinach D 1-D 2-cyt b 559 complex, Biochimica et Biophysica Acta (BBA)-Bioenergetics, 1232 (1995) 81-88.
[46] S. Kumazaki, M. Akari, M. Hasegawa, Transformation of Thylakoid Membranes during Differentiation from Vegetative Cell into Heterocyst Visualized by Microscopic Spectral Imaging, Plant Physiology, 161 (2013) 1321-1333.
[47] A.V. Ruban, P. Horton, A.J. Young, AGGREGATION OF HIGHER-PLANT XANTHOPHYLLS - DIFFERENCES IN ABSORPTION-SPECTRA AND IN THE DEPENDENCY ON SOLVENT POLARITY, Journal of Photochemistry and Photobiology B-Biology, 21 (1993) 229-234.
[48] D. Kosumi, M. Fujiwara, R. Fujii, R.J. Cogdell, H. Hashimoto, M. Yoshizawa, The dependence of the ultrafast relaxation kinetics of the S2 and S1 states in ß-carotene homologs and lycopene on conjugation length studied by femtosecond time-resolved absorption and Kerr-gate fluorescence spectroscopies, The Journal of chemical physics, 130 (2009) 214506.
[49] H.K. Lichtenthaler, [34] Chlorophylls and carotenoids: Pigments of photosynthetic biomembranes, Methods in enzymology, (1987) 350-382.
[50] W.J. Vredenberg, A three-state model for energy trapping and chlorophyll fluorescence in photosystem II incorporating radical pair recombination, Biophys. J., 79 (2000) 26-38.